Sensor Processing for Localization with Applications to Safety

Ehsan Ul Haq

Submitted in partial fulfilment of the requirements of the degree of

Doctor of Philosophy

Department of Electrical and Electronic Engineering
THE UNIVERSITY OF MELBOURNE

June 2018

Abstract

Heavy industries such as construction, mining and transport typically have dangerous work environments, where injuries and fatalities are rampant despite all the rules and regulations. Such mishaps are largely due to human negligence and improper monitoring of the work place. Injuries are also more likely when man and machine operate together. To ensure safety, a framework is needed capable of tracking moving objects around a user with centimeter accuracy. The sensor should be small enough to be easily incorporated in workers safety equipment, and robust against all the random movements of the user and the objects in the surrounding area. This thesis addresses the issues in developing a framework of a low cost smart helmet for workers in dangerous work environments. The techniques developed for safety helmets are also directly applicable to light-weight navigation systems needed for tiny drones. At its core, we have developed a framework and algorithms using simple and cheap continuous wave (CW) Doppler radars to obtain the precise location of static and dynamic obstacles around a user. CW Doppler radars only provide relative radial velocity, so the first issue is to determine the conditions under which the position of a target is observable. We have also designed, compared and analyzed different nonlinear trackers to determine which works better under certain scenarios. We explore how instantaneous frequency measurements can be obtained from rate of phase change in returned waves of CW radars. To this end, we performed various simulations with different order models and results showed that we can successfully localize walls with sub-centimeter accuracy. Moreover, we show that random human head movements and walking do not pose much threat to estimation accuracy and can be easily handled through added noise in the system.

Declaration

This is to certify that

1. the thesis comprises only my original work towards the PhD,
2. due acknowledgement has been made in the text to all other material used,
3. the thesis is less than 100,000 words in length, exclusive of tables, maps, bibliographies and appendices.

Ehsan Ul Haq, June 2018

Preface

This dissertation is submitted in partial fulfillment of the requirements for the degree of Doctor of Philosophy at University of Melbourne. The research described in here was carried by me under the supervision of Professor Robin John Evans, Professor Terry Caelli and Professor Peter Farrell in the Department of Electrical and Electronics Engineering, University of Melbourne.

The idea of a system to help improve workers safety by reducing number of injuries and fatalities first came to mind from couple of news articles mentioned by Prof. Terry Caelli. From there, I started to look into the statistics of injuries in dangerous work environments in Australia. To our dismay this number is huge and owing to the fact that these are ever growing industries, one can only imaging it getting bigger. Our research showed that only little research has been done regarding construction workers' safety and most of the research was in preliminary stages.

Research, algorithms and simulation results mentioned in chapters 3-5 are done in collaboration with Prof. Rob Evans. All simulations results reported in this thesis are programmed in Matlab®.

Ehsan Ul Haq
August 2017

Acknowledgements

For a long time, I have been looking forward to this moment when I could formally acknowledge in writing the people without whom this doctoral journey would have neither started nor finished.

I wish to express my gratitude to Professor Robin John Evans for his guidance, help and inspiration in my work. During my PhD, he patiently guided me through intriguing discussions on various aspects of research problems. I am also ever grateful to him that, besides academic ventures, he has been a great mentor in helping me through the non-stated hurdles of the PhD journey, like integrating in Australian society and feeling welcomed away from home.

I must mention Prof. Darko Musicki, who introduced me to the world of research and later recommended me to Prof Rob Evans and the University of Melbourne. Though he is not among us today, his patience, calmness, and confidence with an issue was exemplary. If he ever became aware of a difficulty I had, instead of turning me away, he would spend many hours taking me from A to B to C. I will continue to honor him by doing the same.

I am also thankful to Professor Terry Caelli, who nudged me gently along this research problem at the start and also to Professor Peter Farell who helped intermittently along the way. Thank you all for teaching me everything I know in this field. To my father M. Rafique, Who would have been more happy and proud than I can imagine. I feel honored to own that without his discipline, I could not have achieved this. May his soul rest in peace! I would also like to thank my mother for all the restless nights and the prayers that she puts up for me. She worked on me consistently for years and enabled me to reach where I am today. I would like to express my ever-increasing indebtedness and gratitude to my mentor-for-life, Dr Abdul Rashid Kausar. Thank you for believing in me, listening

to me and taking a chance with me when most doubted my words and actions. Thank you for being a wonderful teacher through all these years.

To my dearest wife, Maya, who motivated me and kept my spirits high whenever I doubted myself. I am ever indebted to her for all those moments I missed - the meals and the precious times when we could have been together but I was debugging simulations. I love you and I am free now to take you to all those promised places and to do everything together. Plus, thank you for giving me the most beautiful gift - our daughter Efa (AKA Tuni). She has been both my stress reliever and a constant reminder that I need to deliver in time. To my family members Salman Ahmed, M. Waseem, Humera Waseem, Javaria Rafique and Dr. Shafique Ur Rehman for supporting me and keeping me free from various obligations all these years. This PhD came at a very crucial point in my life and you kept me going. To my sister Attiya for teaching me in those early school days and secretly helping out with homework.

To my best friend Hasan A. Nasir and all the unsung colleagues at the University of Melbourne with whom I shared such important moments though this journey. Thank you for your continuous support, understanding and collaborations.

To my father, M. Rafique.

Contents

List of Figures

Chapter 1
Introduction

1.1 Problem Statement and Motivation

Autonomous collision avoidance and navigation is a classic problem that is still an active area of research because of endless opportunities and applications in numerous fields. One such example is industrial production lines, where computer-guided vehicles are developed for the automatic flow of materials. Similarly, unmanned surveillance vehicles are being developed that are capable of navigating themselves while securing a marked area. Drones are ubiquitous, from recording high definition videos to rescue missions and urban parcel deliveries. Sensors required for flight control of these drones must be cheap and accurate, as well as robust enough to survive harsh environments. Though they seem disparate, all these applications require semi or full autonomous navigation of a machine with collision avoidance at its core. Research in recent decades has amassed plethora of literature on this topic. However, following fundamental requirements of an effective collision avoidance system still needs a feasible solution:

- Localization precision of sub centimeters;
- Low power consumption;
- Robust in both indoor and outdoor environments;
- Low cost of deployment, maintenance and operation;
- Compatible with equipment or systems already in use;
- User friendly.

Heavy industries such as construction, mining and transport employ a huge percentage of a countrys workforce. These are dangerous work environments, where injuries and fatalities are common despite strict regulations. Such accidents are largely due to human error, negligence and improper monitoring of work place environments. This is exacerbated by tighter deadlines and escalating project costs, meaning employees often have to work long hours resulting in stress and fatigue, which in turn increases the likelihood of injuries. Although governments typically regulate site safety inspections, it is simply too expensive and impractical to ensure continuous monitoring and safety by human resources on site.

Australian federal and state governments have been collecting and managing work related injuries and fatalities statistics for the past 10-15 years. Their latest findings were published in May 2016 [1] - containing work related injuries and claims statistics from 2000 to 2014. These records reported about 12.5 million injured workers. Out of these about 4.3% injuries occurred in last two years of record keeping . This means even after rigorous monitoring, control and management, accidents are rampant in industry. Due to their injuries about 7% of all injured workers changed their jobs. Measuring in number of persons, there were about 43 per 1000 workers who experienced a work related injury in the last 12 months. Although it decreased from 53 persons per 1000 workers in 2009-2010, this decline is clearly very small over a period of 4 years. Of all the Australian states, Tasmania had the highest injury rate with 66 per 1000 workers in 1 year. The occupations with the highest number of work related injuries or illnesses are:

- Machinery operators and drivers - 88 per 1000 employees;
- Community and personal service workers - 73 per 1000 employees;
- Technicians and trades workers - 72 per 1000 employees;
- Laborers - 66 per 1000 employees.

On the other hand, the industries with the highest work-related injuries are:

- Manufacturing;

- Transport, postal and warehousing;
- Agriculture, forestry and fishing;
- Construction.

Of all the 323,700 injured workers, 31% were 'Technicians and trade workers', 20% were in Manufacturing, 18% were 'Machinery operators and drivers' and 16% were in construction.

Of the 531,800 injured workers, about 20% (106,200) sustained their injury or illness by **'Hitting: being hit or cut by an object or vehicle'** and 13% (68,200) through **'Fall on the same level'**.

The work-related injury statistics provided above do not include the number of people who die each year from work-related injuries. As these statistics are more serious they are recorded separately. This includes fatalities resulting from a work related activity and also as a side-effect of someone elses work activity. In the 13 years from 2003 to 2015, when government started to maintain records, 3,207 workers lost their lives in work related activities. About two thirds of these worker fatalities involved vehicles. For example, in 2015 alone, 115 out of 195 (59%) fatalities involved a vehicle collision. Another important finding from these statistics is that 76% of bystander fatalities (workers fatality as a result of someone elses work-related activity) were due to a vehicle collision or a moving object.

In terms of effecting the project time lines, 61% of the 531,800 injured workers took some time off work and 15% were no longer working in the job in which the injury or illness occurred. A particularly alarming fact is that median compensation payments have increased by 71% since 2000-01.

These statistics show that each year most fatalities occur within **Transport, Warehousing, Agriculture, Fishing, Construction and Mining** industries. In all industries, workers operate in close proximity to heavy machinery within confined spaces. In 2015 alone, these industries accounted for **47% fatalities**.

A key element in success in any rescue or crisis intervention is the availability of an accurate and updated map of the area. Such situational awareness can be used to map

previously unknown areas or update the a-priori map of a place destroyed by natural calamity. For rescue workers who lose their orientation due to fire or smoke, such real-time maps could guide them to a safer location. But the successful utilization of such a system lies in its miniaturization and its smooth integration with equipment already in use. The feedback from such a system must also be subtle and user friendly to avoid burdening the user.

A hard hat, being light weight and sturdy, is a key uniform element for workers in unsafe fields. It is designed to protect the head from injuries in case of a mishap. Our idea is to make these helmets smart enough to sense the surroundings and alarm the user of possible dangers. This requires any sensor which goes on the helmet to be small, adding only negligible weight, and robust enough to withstand rugged environments.

Recent advances in microelectronics and signal processing have provided us with very small, low cost and high performance Doppler radars. Our idea is to research the problems associated with placing these Doppler radars on a helmet to detect moving objects in the surroundings. For example, if the helmet detects a potentially approaching construction vehicle from the left side, it could alert the user by beeping in the left ear. Similarly, if the helmet detects something dangerous on the right side it alerts the user by beeping in the right ear. However, this approach has a number of intrinsic research issues that must be addressed before this technology can be a viable option.

It must be noted that another important application of such technology is in robots and UAVs. With advancements everyday it is clear that such autonomous machines will infiltrate every aspect of human life. Basic ability to self navigate and avoid collisions in complex and dynamic environments is essential for these machines. Any such collision avoidance system should be light so as to add only minimal weight. Current technologies rely mostly on vision sensors, which comparatively consume more power, and are heavy and delicate.

1.2 Research Objectives

The objective of this research is to develop a smart system with the following properties:

1. The ability to detect and track moving objects around a user with high accuracy;
2. Light enough to add negligible weight to the user;
3. Ability to withstand rough and rugged environments like construction;
4. Low power consumption;
5. Performance is unaffected by random human movements;
6. Ability to alert the user of imminent danger.

1.3 Organization and Contributions of Thesis

In this thesis we have tackled the issues of designing a low-cost, lightweight and efficient safety system for workers. At its core we have developed algorithms and system architecture using simple and cheap continuous wave (CW) Doppler radars to obtain the precise location of static and dynamic obstacles around a user. This thesis is composed of six chapters as follows.

- Chapter 1 explains the background to the research problem, its motivation and objectives.
- Chapter 2 contains a detailed review of previous approaches to similar problems of localization. It also contains a detailed theoretical background of the techniques used in our research. It primarily introduces the role of estimation theory in tracking a target. Additionally, we identify the conditions which make a target observable from an observers point of view. These observability conditions later form the basis of our trackers.
- Chapter 3 discusses the design of various trackers based on the identified observability conditions. Given the high non-linear nature of the problem, it also contains detailed simulation results to show the efficiency as well as limitations in different scenarios.

- Chapter 4 then tackles the issue of indoor localization. It discusses the design of simulation scenarios for indoor environments and associated difficulties in target state estimation. Then it details the design and simulation results of state estimation filters.

- Chapter 5 discusses the design and challenges of building a smart helmet. It introduces the idea of how instantaneous frequency measurements can be obtained from rate of phase change in returned waves of a continuous wave radar. It also discusses the design of estimation algorithms based on such measurements. Since these trackers are iterative, they need a reasonable starting point. Another contribution of this chapter is the proposal of a new initialization strategy for these iterative trackers. Simulations show significant improvement in convergence time with this new initialization methodology.

- Chapter 6 discusses the results of our research, conclusions drawn from it and directions for future work.

Chapter 2

Literature Review and Theoretical Background

2.1 Introduction

Simple localization of targets/objects around a mobile user/platform is a highly desirable feature, having fundamental applications in numerous, seemingly diverse areas. The aerospace industry, for example, has an incessant demand for light weight sensors for locating targets around a plane. With recent advancements, drones and quadcopters are ubiquitous. With their small size factor, the demand of light weight localizing sensors is at its peak. This is because these flying machines have to satisfy strict weight, size and computational requirements which limit the use of traditional navigational methods. To improve safety in congested work environments like construction and mining, one needs light weight sensors that can be simply integrated into equipment already worn, increasing situational awareness.

Doppler radars are simple and cheap sensors that provide valuable information by measuring Doppler shift of transmitted and reflected radio signals. With recent advancements in microelectronics, frequency measurements can easily be obtained with high accuracy through cheap Doppler radars. However, given the simplicity of the sensor, Doppler-only tracking is a complex problem.

In this chapter, we first present the literature review and discuss existing approaches used by researchers for indoor localization. In the next section, we formulate the problem mathematically according to our situation. Then we briefly discuss the theory of target tracking and estimation. Next, we review the fundamental issue of target observabil-

ity from the frequency only measurements. The last section of the chapter contains key points and conclusions drawn from the literature review, on the basis of which we would design and develop target trackers.

2.2 Existing Approaches

Determining the relative position of an entity in an indoor environment is an integral task of navigational applications and numerous building services. A plethora of literature can be found covering different aspects of this problem [2] [3]. Solutions and systems being developed offer a wide range of accuracy. In some applications, like controlling the lights in a room, it is enough to get a rough estimate as to where a person is located. However, for safety application such as collision avoidance, one needs localization precision of a few centimeters.

Radio Frequency Identification (RFID) technology uses electromagnetic waves to detect, identify and track objects. These systems are composed of RFID readers which read the electromagnetic waves generated by tags attached to objects. Depending on the requirements, tags can be active or passive. Active RFID tags provide a detection range of tens of meters, whereas passive tags can only be detected within 1-2 meters of a reader. One popular and obvious approach for indoor tracking is to attach a tag to each entity to be tracked. The authors in [4] developed an inexpensive solution based on this idea using off-the-shelf components. By analyzing the strength of radio signals received they were able to localize objects in 3 dimensions. Their system was composed of several base stations measuring the strength of signal received from an active tag attached to the target. Then a central server collects this information and estimates the position of the target through triangulation. The authors claim to have achieved an accuracy of around 3 m. Besides poor accuracy, the system also takes about 10-20 seconds to get one measurement. A similar solution was offered as LANDMARC [5], which also uses active RFID tags. However, to reduce the number of readers, the authors used the idea of reference tags. These are fixed tags at known locations and are referenced for system calibration. It is reported that the maximum range error is less than 2 m.

Researchers have also proposed the Ultra Wide Band (UWB) active tags based system for indoor localization. These systems employ ultrashort pulses with low duty cycle. Besides being low powered, they can be used in close proximity to other RF equipment because each uses a different signal and radio spectrum. UWB systems use the Time of Arrival (ToA) and Angle of Arrival (AoA) characteristics of these short pulses to achieve very high accuracy. Several systems based on UWB technology have been presented in the literature. For example, Ubisense [6] is a commercially available UWB based localization system. It uses active tags that transmits UWB signals to networked receivers. It then employs both Time Difference of Arrival (TDOA) and AoA to estimate a tag's position. Just like cellular networks, it divides an area to be monitored into sensor cells, with each cell having four or more readers. High deployment and maintenance costs are the main drawbacks of this approach.

To reduce costs, scientists have also proposed localizing systems based on wireless local area networks (WLANs). These use Received Signal Strength (RSS) at different receivers to determine the target's location. The RADAR localization system [7], proposed by Bahl et al., uses a variant of k-nearest-neighbors algorithm with empirical measurement of signal strength at access points to determine a user's position. Its accuracy is reported to be between 2-3 m. Given the practicality and cost effectiveness of the system, the authors have proposed another variant to improve accuracy [8] using a Viterbi-algorithm-like approach. Horus systems [9] localize objects using probabilistic modeling of signal propagation. Different experiments were performed to show that an accuracy of about 2 m is possible in more than 90% of cases. In [10], the authors developed a grid-based approach with Bayesian filtering to localize objects within 1.5 m. The commercially available Ekahau system also uses WLAN to track electronic devices such as tags and laptops. It works by correlating received signal strength with space information [11]. However, this system has its own drawbacks like requiring a large number of access points to cover blind spots in buildings, hence increasing overall costs. [12] presents a Through-Wall Imaging (TWI) technique, which uses UWB pulses to detect static and dynamic objects through the walls of a building. It has gained much interest among law enforcing agencies. Using multiple frequencies, it is possible to obtain very high resolu-

tion images of the objects [12, 13]. In [14] Y.K. Cho et al. tracked indoor mobile assets in construction using a UWB wireless network system and also demonstrated that statistical modeling of errors can significantly improve tracking. On the other hand, 1.5 cm accuracy was reported by [15] for 2D localization, but within a very small area of about 2x2m. Similarly, J. Teizer et al. [16] tried to estimate 3D location of building resources in complex construction environments. In [17], T. Cheng et al. continued their research on evaluating the capabilities of commercially available Radio Frequency ID based systems in measuring construction site dynamics. From experimentation on real job sites, they reported the accuracy of a UWB system for tracking mobile resources within 2 meters.

A WiFi based active localization solution is offered by Intel Place Lab [18]. In this framework, each WiFi enabled device is assigned a unique ID when it connects to an access point. Then the device is localized by triangulation using different access points closer to the device. This system can provide accuracy of only up to 20 m and it reduces even further when there are fewer access points. Its main advantage is that clients do not require any additional hardware, and companion software is available online free of charge.

AeroScout [19] is a company that provides indoor localization solutions using WiFi signals from active tags attached to objects. Depending on room size and environment to be monitored, it estimates the tag's position using either Time Difference of Arrival (TDOA) or Received Signal Strength Indicator (RSSI). The deployment cost can be made relatively low by using the already existent wireless infrastructure. The feasibility of a WiFi based tracking and positioning system for construction sites is studied in [20]. In their research, they tracked the approximate location of labor within 5 m of error, using Received-Signal-Strength-Information. Hazard prone areas such as those where tools, materials, or objects could fall down or from above are a major threat to human safety. [21] developed a prototype using Ultra Wide Band technology to determine if a worker is in the close proximity of a predefined potentially dangerous area.

A relatively high accuracy of about 9 cm is reported by AT&T's Active Bats Systems [22]. However, once again, high deployment cost, difficulties in scalability and adjustment are its main drawbacks. It works by sending ultrasonic messages to receivers

mounted on ceilings at every square meter. Then the system computes a user's location using Time of Flight (TOF) based triangulation. Further research has also been done in discarding measurements arising from multipath reflections of same the message. However, the high initial cost has limited its application and development.

Regarding safety at work, many researchers have approached the problem in two steps. First, a detailed analysis of previous accidents and injuries is performed, where all accident precursors and near-misses are identified and documented. In the second step, a framework is proposed that tries to eliminate the precursors and related behaviors. S. Chae et al.[23] performed a detailed analysis of various construction site related injuries and accidents. They collected previous work-injury data and built a database in order to identify the major causes of accidents. The crux of the research was that accidents usually occur for one of the following reasons:

1. Work procedures not set;
2. Circumstances and environment not checked;
3. Restricted areas not maintained;
4. Safety training not provided or enforced.

The authors then developed a Fault Tree Analysis model from the accidents database and postulated that a collision avoidance system (see below for more details) should have following three functions:

1. Provide adequate time for emergency avoidance response;
2. Ensure adequate information for situation (task and environment) awareness;
3. Ensure adequate ways of guaranteeing and confirming workers' attention in situ.

Based on this approach, the authors then proposed a collision avoidance system using active RFID tags. They estimated the working area of different machines and laborers on-site wearing these tags. The system then issues warnings whenever working areas of two entities overlap. Real construction site experiments were performed to measure and report the feasibility of the system.

In [24] H. Yang et al. adopted a similar two-step approach and identified the following three accident precursors:

1. Unauthorized persons or machines in hazardous areas;
2. Lack of regular site, machine and material inspections;
3. Untrained workers not following the right procedures.

In order to minimize these accident precursors, they designed an integrated ZigBee RFID based sensor network structure.

J. Teizer et al. [25] argued that research on safety in construction is mostly reactive; i.e., based on data that is being reported after a fatal accident. They emphasize the need for pro-active systems that work, on near-miss and close-call events. To achieve this, they developed a RFID Active Tags based solution. In their approach they attached an Equipment Protection Unit (EPU) on all heavy machines and handed a Personal Protection Unit (PPU) to workers on foot. Whenever a PPU was in proximity of an EPU a warning message was issued.

Safety is also highly correlated with ease of access to workers bio data such as their training, authorization and time on job etc. It is also related to quick access to information about machines such as their inspection schedule, time on job, repair work done, etc. [26–28]. RFID based access management solutions were presented by [23–25]. They managed an active database of workers that would grant access to machines and restricted areas to authorized personnel only.

Blind spot measurements show that equipment operators need visual aid because of their limited field-of-view. Teizer et al. [29–31] discovered that incidents occur mostly because of *the collision of heavy machinery with workers in the blind spots of the machines*. They used an automatic laser-based tool to measure the blind spot of different construction machines. Figure 2.1 shows the result of their research [30].

Imaging and Vision techniques have mostly been applied in estimating the difference between as-planned and as-built infrastructure - to automatically detect defects in construction, for analyzing project time lines and for modelling in augmented reality [32–37].

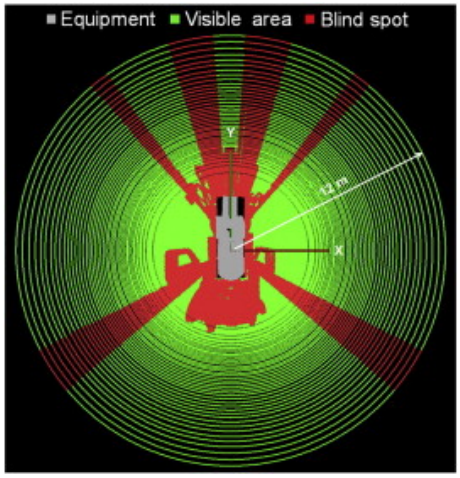

Figure 2.1: Blindspot map of a fork lifter

Yang et al. [38] explored two systems, a vision based system and an ultra-wide band based system, to automatically extract the trajectory of interacting workforce. This information was then proposed to be used for task scheduling, production analysis and progress evaluation.

Many site supervisors monitor video streams coming live from construction sites to evaluate the quality and safety of work. Simultaneously monitoring tens of cameras, if not impossible, would require huge resources. Memarzadeh et al. [39] marked potential candidates in video streams for location of workers and equipment in 2D, using Histogram of Oriented Gradiant and Hue-Saturation Colour Descriptors. To reduce costs, some have experimented with video cameras to track and detect construction site entities. M. Park et al. [40] developed a method using background subtraction, histogram of oriented gradients (HOG), and HSV color histogram to automate the classification of workers from non-workers. According to [41], about 80-90% of accidents are due to the workers' unsafe behaviour. So authors proposed a vision-based framework to detect such behaviors. In the first trials, they used it to determine unsafe ladder climbing postures. A similar approach was also researched by [42, 43]. In [44], the authors integrated real time data obtained from a crane into a 3D model located off site, enabling off site supervision for safe operations. Others have also experimented with various vision-based algorithms, already tried in different fields, to evaluate their efficacy in construction-related

tasks [45–48]. There has also been some focus on developing algorithms that work on live video streams from construction sites, for pose extraction, blob tracking and classification. A major purpose of this type of resarch is to monitor the productivity of workers [49].

In [50, 51], the authors reported working on utilizing information in BIM to enhance safety-related scheduling and planning activities on construction sites. They also elaborated on the opportunities of promoting safety with better communications through use of BIM between different parties, such as contractors, safety specialists, healthcare personnel, etc. The target is to improve occupational safety by embedding safety solutions in BIM for safer construction planning and scheduling, and better communications and management of site tasks.

In [52], researchers from MIT Media lab developed a system that infers safety conditions at construction sites. They developed wearable sensors that measure levels of dangerous gases, noise, light quality, altitude and motion. Similar research is also carried out for the safety of mine workers in [53, 54]. LukoWicz et al. used microphones and accelerometers mounted on the users body to classify tasks like sawing, hammering and turning screws [55, 56].

In [53, 57–59], the authors have tried to improve safety conditions by integrating miniature positioning devices and communication instruments in compulsory safety equipment worn by all the workers on site; for example, hard hats, jackets, belts, etc. Using the 3-axis accelerometer and gyroscope sensors of a smart phone [60], R. Dzeng et al. developed and compared three algorithms to evaluate how well a smart phone can be used to determine falls and fall portents.

The safety of workers is of foremost important. However, technological developments have mostly been directed towards the tracking and management of valuable assets. Much research is being conducted in scheduling labor or optimizing timely delivery of prefabricated parts, expensive machinery, construction tools and material, etc. [61–67].

2.2.1 What is missing?

The Australian government is promoting a culture aimed at ensuring every worker returns home safely - every day. To facilitate this, governments and companies are inviting innovative solutions to safety issues at dangerous work sites. Realizing the importance of safety, practitioners around the globe have already started integrating automated techniques, equipment and procedure into their projects. Tools like Building Information Modelling (BIM), introduced to support architects and engineers in designing buildings, are now increasingly used in project planning, scheduling, cost reductions, clash detections, energy analysis, resource-savings, progress tracking, etc. What is missing is how we can best use this vast amount of prior knowledge to determine potential safety loopholes - in situ, in real time. Little effort has been made in integrating real time site statistics with such BIM knowledge bases. The BIM model is meant to work in a collaborative environment where architects, engineers, contractors, sub-contractors, decision makers, and all other members of the team can coordinate and share information. With improved real time information about site safety statistics in BIM, the scope for mistakes can be reduced to a large extent.

The objective of this research is to develop a framework for workers safety through efficient use of real time sensed information. Sensing for safety at construction sites is quite different from apparently similar areas like vehicle or pedestrian collision detection on roads.

Current solutions also mostly rely on RFID, WIFI, Ultra Wide Band or computer vision. However, the requirement of attaching a separate tag to each entity usually in thousands - would limit the applicability of such solutions in large, complex and dynamic construction environments. If only a handful of site entities remain untagged such systems can be quite unreliable, and even dangerous themselves. Besides this, RFID has only been able to triangulate the position of objects within a 2-5 meter radius, or up to 1 meter with Ultra Wide Band based systems.

Recent developments in radar miniaturization has produced radar-on-a-chip, costing less than $5 each, making this very attractive for our applications. For example, The Occupational Health and Safety (OHS) Act 2004 places duties on various parties to ensure

safety, such as compliance for the prevention of falls. Nevertheless, injuries due to falls account for more than 1/3rd of all injuries [21, 60]. Surrounding a fall prone area with a warning tape or scaffolding is not enough. On the other hand, manually monitoring for safe distance of workers from such pitfalls 24/7 is also infeasible. Therefore, automatic techniques based on radar tracking of objects around hazard prone areas could be devised, ensuring safety compliance is met in such situations.

Statistics also show that approximately 1/3rd of fatalities or injuries at construction sites are the result of collision with large hydraulic machines or excavators [23, 25–27]. In the case of cranes, for example, radar could be placed on a crane head, tracking workers in its surroundings. The crane operator would be updated continuously if there is a worker or another machine in his blind spots. At the same time, workers can be warned about the position of cranes in their surroundings.

The OHS Act also demands that particular safety equipment, such as hard hats, must be worn by all workers at all times. Research could be done to place the radar-on-a-chip (with RFID personal identification) on hard hats, that continuously provides each identified worker with information about their surroundings. Additionally, if hard hats are not worn a person-specific signal could be generated to remind the individual to wear his hat, etc. Safety compliance checking can also be integrated into the system, including situation-aware helmets that guarantee a crane load is never closer than 10m from a construction worker. Similarly, a warning can be issued if a worker is approaching a prohibited area or is working under suspended loads.

Investing in smarter technology could save thousands of dollars spent each year in compensating workers claims. At the same time, sensing for safety could also ensure timely completion of projects by saving the time spent in remunerating serious accidents.

2.3 Mathematical Problem Formulation

In this section, we mathematically & formally formulate our problem of tracking a target from an observer. To keep things simple, initially we assume that there's only one target and observer. Consider a target T moving along a trajectory $\bar{r}_T(t)$ and emitting a signal of

frequency f_o, as shown in Fig. 2.2. Initially this frequency is assumed unknown in order to arrive at a more general result.

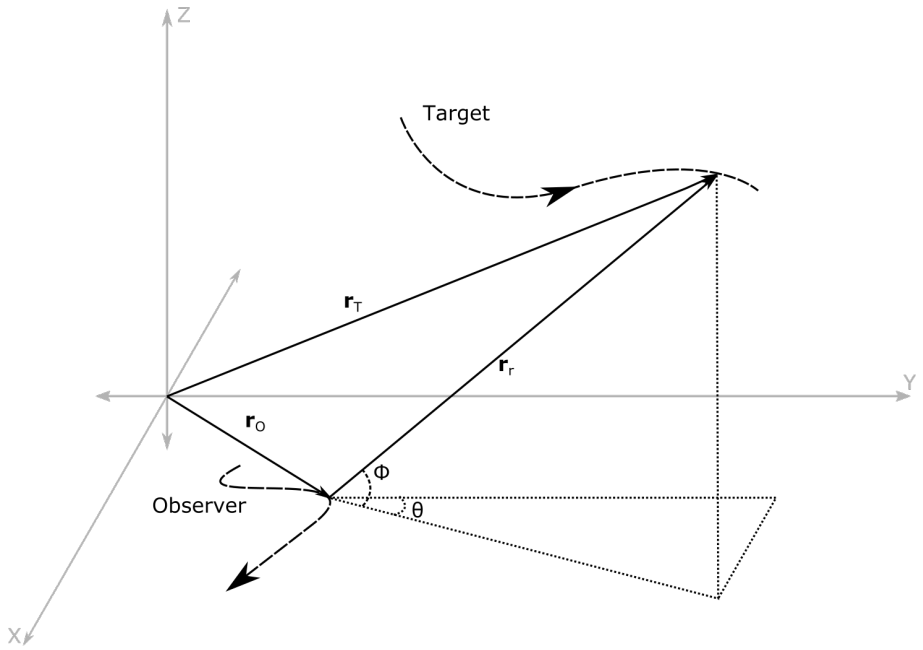

Figure 2.2: Observer and target's geometry for observability analysis

An observer moving along trajectory $\bar{r}_O(t)$ makes bearing and frequency measurements of the target and tries to estimate its state. We can obtain the following relation from the geometry in Fig. 2.2.

$$\bar{r}_T(t) = \bar{r}(t) + \bar{r}_O(t) \tag{2.1}$$

In this work, three measurements sets are considered, namely: bearings-only, frequency-only and bearing-frequency measurements together. The bearings (θ) and frequency (f) measurements satisfy following relationships,

$$\theta = tan^{-1}\frac{\bar{r}_y(t)}{\bar{r}_x(t)} \tag{2.2}$$

$$f(t) = f_o - \frac{f_o \bar{v}_r(t)}{c} \tag{2.3}$$

$$= f_o\left(1 - \frac{\bar{v}(t).\bar{r}(t)}{c\,|\bar{r}(t)|}\right) \tag{2.4}$$

$$= f_o \left(1 - \frac{|\dot{\bar{r}}(t)|}{c}\right) \tag{2.5}$$

where

- $\bar{r}(t)$ is the relative position vector
- $|\bar{r}(t)|$ is norm of $\bar{r}(t)$
- $|\dot{\bar{r}}(t)| = \frac{d}{dt}\left(|\bar{r}(t)|\right)$
- $\bar{r}_x$ and $\bar{r}_y$ are X and Y components of $\bar{r}(t)$
- $\bar{v}(t)$ is the relative velocity vector
- c is signal's velocity

2.4 Bayesian Filtering & Estimation

The task at hand of estimating a target's state, can be recast into a Probabilistic state estimation problem of nonlinear system with additive noise [68–70]. It is the problem of inferring the hidden parameters of a system in an optimal manner using available noisy measurements. We will describe our discrete-time nonlinear system as a dynamic state space model. The hidden system state $X[k]$ evolves over time as partially observed Markov process. It's initial probability density is given as $p(X_0)$ and conditional probability density is represented as $p(X[k]|X[k-1])$. Observations or measurements are independent and follow the probability density $p(Z[k]|X[k])$

Then dynamic state space model of the problem is described by following set of difference equations,

$$\text{Process Equation:} \qquad X[k] = f(X[k-1], U[k-1]) + v[k-1] \tag{2.6}$$

$$\text{Measurement Equations:} \qquad Z[k] = h(X[k], U[k]) + w[k] \tag{2.7}$$

where, $X[k] \in \mathbb{R}$ denotes state of dynamic system at time instant k, $f : \mathbb{R}^{n_x} \times \mathbb{R}^{n_u} \rightarrow \mathbb{R}_{n_x}$ and $h : \mathbb{R}^{n_x} \times \mathbb{R}^{n_u} \rightarrow \mathbb{R}_{n_z}$ are nonlinear known functions, U[k] is the known control

input and Z[k] represents measurement vector. v[k] and w[k] are independent process and measurement noise sequences, with zero mean and covariances $Q_{vv}[k]$ and $R_{ww}[k]$, respectively. The state transition probability $p(X[k]\big|X[k-1])$ is specified by f and process noise distribution $p(v[k-1])$. On the other hand, observation likelihood $p(y[k]\big|x[k])$ is defined by observation function h and observation noise distribution $p(w[k])$. This dynamic state space model of the system with known process and observation noise statistics and initial system distributions, gives us a probabilistic model of how the system evolves over time. It also gives us a framework as how one can estimate the hidden states or parameters of the system.

The optimal way to recursively update the posterior density $p(x[k]\big|x[k-1])$ as new observations arrive is given by recursive Bayesian estimation. In this domain, the estimation problem is designed to recursively build confidence in the system state at time k, using all measurements until time k $Z_{1:k}$. Here $Z_{1:k}$ denotes set of measurements history from time 1 up till k, $Z_{1:k} = \{Z[1], Z[2], \ldots, Z[k]\}$. To initiate the recursion, an initial estimate about posterior density of system state is assumed. This initial guess depends upon factors such as geometry of the problem at hand, allowable variances in the quantities to be estimated, etc. Once this prior initial PDF $p(X_0\big|Z_0)$ is available, then as new measurements arrive at each instant, posterior PDF $p(X[k]\big|Z_{1:k})$ is calculated in two steps: prediction and update.

- **Prediction Step**: It involves predicting posterior density of the state at time 'k' based on information up till time 'k-1' using system model (2.6) and Chapman-Kolmogorov equation as,

$$p(X[k]\big|Z_{1:k-1}) = \int_{\mathbb{R}^{nx}} p(X[k]\big|X[k-1]) \times p(X[k-1]\big|Z_{1:k-1})\, dX[k-1] \tag{2.8}$$

  where, the probablistic model of state transition $p(X[k]\big|X[k-1])$ is calculated from system equation (2.6) and known statistics of process noise $v[k]$.

- **Time Update Step** It involves updating the posterior density at time 'k' with mea-

surements at 'k' using Bayes' rule as,

$$p(X[k]|Z_{1:k}) = \frac{p(X[k]|Z_{1:k-1})\ p(Z[k]|X[k])}{\gamma[k]} \tag{2.9}$$

where γ is a normalizing constant that depends upon the liklehood $p(Z[k]|X[k])$ defined by measurement model and known statistics of measurement noise $w[k]$. It's value is obtained as,

$$\gamma[k] = p(Z[k]|Z_{1:k-1}) = \int_{\mathbb{R}^{n_x}} p(X[k]|Z_{1:k-1})\ p(Z[k]|X[k])\ dX[k] \tag{2.10}$$

This recursive Bayesian filtering solution as presented above provides an optimal solution to nonlinear filtering problem. Problem with above approach is that multidimensional integrals in (2.9) and (2.10) are quite complex and intractable. As a result optimal solution can't be guaranteed in all situations.

If system dynamics are linear with Gaussian noise, then the optimal closed-form recursive solution is given by Kalman Filter [68]. However, in case of most real-world systems, which are nonlinear and non-Gaussian, these multi-dimensional integrals are intractable and one has to resort to suboptimal approximate solutions.

Depending upon how non-linearity is being handled different approaches have been proposed in the literature. These approximate methods make some form of simplifying assumptions about either the form of probability density functions or system dynamics. One route to designing such filters is to fix the posterior density to take some *a priori* form such as Gaussian, leading us to methods like Extended Kalman Filter (EKF) [71], Unscented Kalman Filter (UKF) [72,73], Quadrature Kalman Filter (QKF) [74] and Cubature Kalman Filter (CKF) [75]. These filters maintain and update only first and second order moments of the probability densities. These filters appear more attractive to researchers for being computationally less expensive.

Another approach to handle non-linearities is through Sequential Monte Carlo (SMC) methods. In these algorithms no *a priori* assumption is made about posterior PDF. They are used for estimation of any nonlinear and non-Gaussian systems. These methods approximate the integrals with finite sums, where summation is done with sequential im-

portance sampling of weighted sums picked from a proposed PDF that approximates the true posterior PDF. Particle filters [76] with their numerous variants fall under this category. However although these are more accurate but they also suffer from high complexity compared to Gaussian approximate methods.

After the breakthrough introduction of Kalman filter for linear systems, the most obvious extension to nonlinear systems was to approximate the nonlinear equations through Taylor series expansion around the current estimate of the system state. This formed the basis of Extended Kalman Filter (EKF) [71]. Among all the suboptimal methods that's been developed in last 50 years or so, EKF is probably most widely used in nonlinear estimation.

2.4.1 Extended Kalman Filter (EKF)

EKF is based on linearization of nonlinear functions f() and h() in (2.6) and (2.7). Moreover, $p(X[k]|Z_{1:k})$ is assumed to be Gaussian($\mathcal{N}$).

$$p(X[k-1]|Z_{1:k-1}) \approx \mathcal{N}(X[k-1]; \hat{X}[k-1|k-1]; P[k-1|k-1]) \tag{2.11}$$

$$p(X[k]|Z_{1:k-1}) \approx \mathcal{N}(X[k]; \hat{X}[k|k-1]; P[k|k-1]) \tag{2.12}$$

$$p(X[k]|Z_{1:k}) \approx \mathcal{N}(X[k]; \hat{X}[k|k]; P[k|k]) \tag{2.13}$$

Prediction

$$\hat{X}[k|k-1] = f[\hat{X}[k-1|k-1]] + U[k-1] \tag{2.14}$$

$$P[k|k-1] = FP[k-1|k-1]F^T + Q_{vv}[k-1] \tag{2.15}$$

Innovation

$$e[k] = Z[k] - h[X[k|\hat{k}-1]] \tag{2.16}$$

$$R_{ee}[k] = HP[k1|k-1]H^T + R_{ww}[k] \tag{2.17}$$

Gain

$$K[k] = P[k|k-1]\ H^T\ R_{ee}^{-1}[k] \tag{2.18}$$

Update

$$\hat{X}[k|k] = \hat{X}[k|k-1] + K[k]\ e[k] \tag{2.19}$$

$$P[k|k] = [I - K[k]\ H]\ P[k|k-1] \tag{2.20}$$

In above algorithm, F and H represents Jacobians of nonlinear functions f() and h() respectively and are defined as,

$$F = \left.\frac{df(X)}{dX}\right|_{X=\hat{X}[k-1|k-1]} \tag{2.21}$$

$$H = \left.\frac{dh(X)}{dX}\right|_{X=\hat{X}[k|k-1]} \tag{2.22}$$

EKF algorithm linearizes using only first derivative in Taylor series expansion of f() and h(). Although there are variants of Extended Kalman filter which uses higher derivatives in linearization, however, nominal improvement given the additional complexity has rendered them obsolete.

Although EKF has been successfully applied in many research and commercial nonlinear systems, unfortunately it is based on a suboptimal implementation of Bayesian estimation. This often leads to divergence of filter i.e. where filter fails to generate a consistent estimate of estimation error covariance [73]. These and other short comings of EKF have paved way to a number of variants of approximate Gaussian filters that are derivativeless and based on deterministic sampling methods for propogation of mean & covariance of Gaussian PDFs through nonlinear systems.

2.4.2 Unscented Kalman Filter (UKF)

Another approach to handle nonlinearities in system dynamics is through statistical linearization, giving us the well celebrated Unscented Kalman filter. It works by deterministically selecting a set of points that could approximate $p(X[k]|Z_{1:k})$. These points are then propogated through the original non linear function f() and h(). These propogated points are then used to approximate the parameters of posterior PDF. As with EKF, UKF also assumes that all probabilities are Gaussian (2.11), (2.12) and (2.13).

State's Sigma Points and Weights

$$\chi_o = \hat{X}[k|k] \tag{2.23}$$

$$\chi_i = \hat{X}[k|k] + \left(\sqrt{(N_\chi + \kappa)P[k|k]}\right)_i \tag{2.24}$$

$$\chi_{i+N_x} = \hat{X}[k|k] - \left(\sqrt{(N_\chi + \kappa)P[k|k]}\right)_i \tag{2.25}$$

$$\tag{2.26}$$

$$W_o = \frac{\kappa}{N_\chi + \kappa} \tag{2.27}$$

$$W_i = \frac{1}{2(N_\chi + \kappa)} = W_{i+N_\chi} \tag{2.28}$$

$$\tag{2.29}$$

State Prediction

$$\chi_i[k+1|k] = f[\chi_i[k|k]] + U[k] \tag{2.30}$$

$$\hat{X}[k+1|k] = \sum_{i=0}^{2N_x} W_i \chi_i[k+1|k] \tag{2.31}$$

$$\tilde{\chi}_i[k+1|k] = \chi_i[k+1|k] - \hat{X}[k+1|k] \tag{2.32}$$

$$P[k+1|k] = \sum_{i=0}^{2N_\chi} W_i \tilde{\chi}_i[k+1|k]\tilde{\chi}_i^T[k+1|k] + Q_{vv}[k] \tag{2.33}$$

Measurements' Sigma Points and Weights

$$\hat{\chi}_i[k+1|k] = \{\chi_i[k+1|k],\ \chi_i[k+1|k] + \kappa\sqrt{R_{vv}[k]},\ \chi_i[k+1|k] - \kappa\sqrt{R_{vv}[k]}\} \tag{2.34}$$

Measurement Prediction

$$\mathcal{Z}_i[k+1|k] = h[\hat{\chi}_i[k+1|k]] \tag{2.35}$$

$$\hat{Z}[k+1|k] = \sum_{i=0}^{2N_\chi} W_i \mathcal{Z}_i[k+1|k] \tag{2.36}$$

Residual Prediction

$$\xi[k+1|k] = \mathcal{Z}_i[k+1|k] - \hat{Z}[k+1|k] \tag{2.37}$$

$$R_{\xi\xi}[k+1|k] = \sum_{i=0}^{2N_\chi} W_i \xi_i[k+1|k]\xi_i^T[k+1|k] + R_{ww}[k+1] \tag{2.38}$$

$$\tag{2.39}$$

Gain

$$R_{\tilde{\chi}\xi}[k+1|k] = \sum_{i=0}^{2N_\chi} W_i \tilde{\chi}_i[k+1|k]\xi_i^T[k+1|k] \tag{2.40}$$

$$\mathcal{K}[k+1] = R_{\tilde{\chi}\xi}[k+1|k]R_{\xi\xi}^{-1}[k+1|k] \tag{2.41}$$

State Update

$$e[k+1] = Z[k+1] - \hat{Z}[k+1|k] \tag{2.42}$$

$$\hat{X}[k+1|k+1] = \hat{X}[k+1|k+1] + \mathcal{K}[k+1]e(t) \tag{2.43}$$

$$P[k+1|k+1] = P[k+1|k] - \mathcal{K}[k+1]R_{\xi\xi}[k+1|k]\mathcal{K}^T[k+1] \tag{2.44}$$

2.4.3 Cubature Kalman Filter (CKF)

CKF numerically computes multivariate integrals using a so-called spherical-radical cubature rule [75]. Using Gaussian approximations, a set of cubature points and weights are selected to represent the prior PDF. These cubature points are then propagated through nonlinear functions to approximate the parameters of posterior PDF. Main feature of CKF is that it's complexity is claimed to increase linearly with system dimensionality. Main steps of algorithm are as follows,

State's Cubature Points

$$P[k|k] = S[k|k]S^T[k|k] \tag{2.45}$$

$$\chi_i[k|k] = S[k|k]\xi_i + \hat{X}[k|k] \qquad i = 1 \dots 2N_\chi \tag{2.46}$$

State's Prediction

$$\chi_i[k+1|k] = f[\chi_i[k|k], U[k]] \qquad i = 1 \dots 2N_\chi \tag{2.47}$$

$$\hat{X}[k+1|k] = \frac{1}{m}\sum_{i=1}^{2N_x} \chi_i[k+1|k] \tag{2.48}$$

$$P[k+1|k] = \frac{1}{m}\sum_{i=1}^{2N_\chi} \chi_i[k+1|k]\chi_i^T[k+1|k] + \hat{X}[k+1|k]\hat{X}^T[k+1|k] + Q_{vv}[k] \tag{2.49}$$

Measurement's Cubature Points

$$P[k+1|k] = S[k+1|k]S^T[k+1|k] \tag{2.50}$$

$$\chi_i[k+1|k] = S[k+1|k]\xi_i + \hat{X}[k+1|k] \qquad i = 1 \dots 2N_\chi \tag{2.51}$$

Measurement Prediction

$$\mathcal{Z}_i[k+1|k] = h[\chi_i[k|k], U[k]] \qquad i = 1 \dots 2N_\chi \tag{2.52}$$

$$\hat{z}[k+1|k] = \frac{1}{m}\sum_{i=1}^{2N_x} \mathcal{Z}_i[k+1|k] \tag{2.53}$$

$$P[k+1|k] = \frac{1}{m}\sum_{i=1}^{2N_\chi} \chi_i[k+1|k]\chi_i^T[k+1|k] + \hat{X}[k+1|k]\hat{X}^T[k+1|k] + Q_{vv}[k] \tag{2.54}$$

Gain

$$P_{zz}[k+1|k] = \frac{1}{m}\sum_{1}^{2N_\chi} \mathcal{Z}[k+1|k]\mathcal{Z}[k+1|k] - \hat{z}[k+1|k]\hat{z}^T[k+1|k] \tag{2.55}$$

$$P_{xz}[k+1|k] = \sum_{1}^{2N_\chi} \omega_i \left(\chi_i[k+1|k]\mathcal{Z}^T[k+1|k] - \hat{x}[k+1|k]\hat{z}^T[k+1|k]\right) \tag{2.56}$$

$$\mathcal{K}[k+1] = P_{xz}[k+1|k]P_{zz}^{-1}[k+1|k] \tag{2.57}$$

State Update

$$\hat{x}[k+1|k+1] = \hat{x}[k+1|k] + \mathcal{K}[k+1]\left(z[k+1] - \hat{z}[k+1|k]\right) \tag{2.58}$$

$$P[k+1|k+1] = P[k+1|k] - \mathcal{K}[k+1]P[k+1|k]\mathcal{K}^T[k+1] \tag{2.59}$$

Now problem at hand is to determine under what conditions a unique tracking solution could be guaranteed. Target state $\bar{r}_T(t)$ is considered observable over time interval $[t_o, t_f]$ if and only if it can be uniquely determined in that interval. If it is not unique then it's called unobservable.

2.5 Target Motion Analysis

Passive target tracking and localization is a widely studied estimation problem, commonly known as Target Motion Analysis (TMA). The conventional approach to the prob-

lem considers a single observer that monitors the movements of a target, subsequently estimating its position and velocity. Depending upon the nature of target's dynamics and resulting measurements, the system could be linear or non-linear. In case of the bearing and frequency (Doppler) measurements, the measurement equations are nonlinear. Therefore, a unique tracking solution is not always guaranteed. In practice, precise knowledge of such conditions is required under which a unique solution could be guaranteed. In this work, we consider the observability of target's state from bearing and Doppler shifted frequency measurement.

Observability deals with the issue that whether state of a dynamic system can be uniquely determined from its outputs. A given dynamic system is considered observable if its state can be uniquely determined from its model, inputs and outputs. If the system state is not uniquely determinable then system is said to be unobservable.

2.5.1 Observability Analysis with Linear Measurements

The notion of observability, though first introduced by Kalman [77, 78], goes back to method of least squares [79]. A system of equations can be recast in matrix form as,

$$\begin{bmatrix} h_{11} & h_{12} & \dots & h_{1n} \\ h_{21} & h_{22} & \dots & h_{2n} \\ \vdots & \vdots & \ddots & \vdots \\ h_{n1} & h_{n2} & \dots & h_{nn} \end{bmatrix} \begin{bmatrix} x_1 \\ x_2 \\ \vdots \\ x_n \end{bmatrix} = \begin{bmatrix} z_1 \\ z_2 \\ \vdots \\ z_n \end{bmatrix} \tag{2.60}$$

$$Hx = z \tag{2.61}$$

Once we have the above system of linear equations, we could consider the problem of finding an estimate $\hat{x}$ such that it minimizes the square of estimated measurement error,

$$\epsilon^2(x) = [H\hat{x} - z]^2 \tag{2.62}$$

This function will achieve its minimum where all its derivative with respect to $\hat{x}$ are

zero. Taking such derivative and equating to zero we obtain,

$$2H^T[H\hat{x} - z] = 0 \tag{2.63}$$

$$2H^T H\hat{x} - 2H^T z = 0 \tag{2.64}$$

$$H^T H\hat{x} = H^T z \tag{2.65}$$

Solving for $\hat{x}$, we obtain,

$$\hat{x} = [H^T H]^{-1}[H^T z] \tag{2.66}$$

Equation 2.66 has a unique solution provided that the matrix $[H^T H]$ is invertible or nonsingular. This matrix is known as ***Gramian matrix*** '$\mathcal{G}$'. If the determinant of Gramian matrix is zero, then it means that column vectors of H are linearly dependent. Therefore, $\hat{x}$ can not be uniquely specified. Conversely, if determinant is nonzero then $\hat{x}$ can be uniquely determined.

Observability of a set of unknown variables expressed as equations with some given constraints deals with the issue that whether value of unknown variables can be uniquely determined or not. If the constraint equations are linear in the unknown variables then Gramian matrix must be full rank i.e. nonsingular, for the system to be observable [79,80]

2.5.2 Observability Analysis with Nonlinear Measurements

Target motion analysis is a widely investigated topic; for example in avionics for tracking planes and missiles, in robotics & machine vision for tracking people & objects of interest, in underwater environments for tracking submarines & sea fauna, etc. In all these applications, the uniqueness of tracking solution from measurements must be guaranteed.

Tremendous work has been done regarding the observability analysis of systems with nonlinear bearing and frequency measurements. Observability is essentially a property of the given system model. We start by assuming a finite dimensional models for target and observer dynamics. A single observer then makes bearing and/or frequency

measurements about target and subsequently tries to estimate its state (position, velocity, etc.). A number of different approaches have been utilized to obtain various solutions for this observability problem. For analysis with bearings-only measurements, one of the widely used method is to transform nonlinear measurements into some linear form, which then enables the use of theorems from linear systems' theory for observability analysis [81,82]. This approach however, leads to complicated nonlinear differential equation which requires tedious mathematics to obtain a solution. Moreover, results obtained from this technique are also quite cumbersome to be interpreted for real life. An elegant approach proposed by [83–85] avoids analyzing the observability matrix altogether. It develops the uniqueness criterion for two-dimensional first-order [86], three dimensional second-order [87] and general three dimensional Nth order target dynamics case by using simple linear theory approach and geometric analysis.

When only frequency measurements are available, to the best of our knowledge, no one has yet been able to recast them into linear form [85]. For a constant velocity model, [88] derives some observability conditions for Doppler tracking. Although it provides good geometrical insights about when the solution is unique up to a rotation and reflection in observer's coordinate system, however, results and discussions are only limited to a fixed velocity target.

For combined set of bearings and frequency measurements, nonlinear equations are recast into linear form, leading to necessary and sufficient observability conditions for two-dimensional first-order dynamics case [89] and Nth-order dynamics case [83–85].

Given the nonlinearity and Nth order dynamics nature of our problem, we adopt the observability criterion developed in [85], where no restriction is imposed on observer and target's motion. In this work, author first determines the set of all the trajectories that are compatible with the given bearing and frequency measurements. Then using results from linear algebra necessary and sufficient conditions are subsequently derived that would reduce this set to a unique tracking solution. Conditions derived using this method are straight forward to be interpreted physically.

2.5.3 Observability Criteria For Bearing & Frequency Measurements

First without applying any restriction on target's motion, we analyze the transformations that would produce target trajectories compatible with measurements' history. Next, observability analysis for constrained target motions (constant velocity, constant acceleration, etc.) can easily be carried out, as it would be a subset of unconstrained motions.

Consider an arbitrary target trajectory $\bar{r}'_T(t)$ compatible with measurements obtained. That is, trajectories $\bar{r}_T(t)$ and $\bar{r}'_T(t)$ would generate same bearing measurements history,

$$\theta(t) = \theta(t)'$$

where primed variables indicate quantities associated with trajectory $\bar{r}'_T(t)$. It is necessary and sufficient for trajectories $\bar{r}'_T(t)$ to lead to same measurements history as $\bar{r}_T(t)$ if and only if Line Of Sight (LOS) angle remains constant at all times. Thus

$$\bar{r}'_T(t) = \kappa(t)\bar{r}(t) + \bar{r}_O(t) \tag{2.67}$$

where $\kappa(t)$ is an arbitrary scalar function greater than zero.

On the other hand if only frequency measurements are available, then for trajectories $\bar{r}'_T(t)$ to lead to same measurements history as $\bar{r}_T(t)$, we have

$$\begin{gathered} f(t) = f'(t) \\ f_o\left(1 - \frac{\bar{v}(t).\bar{r}(t)}{c\,|\bar{r}(t)|}\right) = f'_o\left(1 - \frac{\bar{v}'(t).\bar{r}'(t)}{c\,|\bar{r}'(t)|}\right) \end{gathered} \tag{2.68}$$

where, as before, primed variables indicates quantities associated with trajectory $\bar{r}'_T(t)$. Rearranging above equation we obtain

$$\begin{gathered} \frac{f_o c\,|\bar{r}(t)| - f_o(\bar{v}(t).\bar{r}(t))}{c\,|\bar{r}(t)|} = \frac{f'_o c\,|\bar{r}'(t)| - f'_o(\bar{v}'(t).\bar{r}'(t))}{c\,|\bar{r}'(t)|} \\ f_o c\frac{|\bar{r}(t)|}{|\bar{r}(t)|} - f_o\left(\bar{v}(t).\frac{\bar{r}(t)}{|\bar{r}(t)|}\right) = f'_o c\frac{|\bar{r}'(t)|}{|\bar{r}'(t)|} - f'_o\left(\bar{v}'(t).\frac{\bar{r}'(t)}{|\bar{r}'(t)|}\right) \\ f_o c - f_o\,|\dot{\bar{r}}(t)| = f'_o c - f'_o\left|\dot{\bar{r}}(t)\right| \end{gathered}$$

$$c(f_o - f_o') = f_o \left|\dot{\bar{r}}(t)\right| - f_o' \left|\dot{\bar{r}}(t)\right| \tag{2.69}$$

Integrating from t_o to t we obtain,

$$\int_{t_o}^{t} c(f_o - f_o')dt = \int_{t_o}^{t} \left(f_o \left|\dot{\bar{r}}(t)\right| - f_o' \left|\dot{\bar{r}}(t)\right|\right) dt$$
$$c(f_o - f_o')(t - t_o') = f_o \left(|\bar{r}(t)| - \bar{r}_o\right) - f_o' \left(\left|\bar{r}'(t)\right| - \bar{r}_o'\right)$$

Rearranging above equation we can obtain,

$$\left|\bar{r}'(t)\right| = \beta \left|\bar{r}(t)\right| + \alpha + c(1-\beta)(t - t_o) \tag{2.70}$$

where

$$\alpha = r_o' - \beta r_o \tag{2.71}$$
$$\beta = \frac{f_o}{f_o'} \tag{2.72}$$

This means that if $\bar{r}(t)$ satisfies 2.70, trajectories $\bar{r}_T(t)$ and $\bar{r'}_T(t)$ can't be distinguished form each other on the basis of frequency measurements alone. Using Eq. 2.67 and Eq. 2.70, we can obtain the set of compatible trajectories as,

$$\bar{r'}_T(t) = D(t) \left[\beta + \frac{\alpha + c(1-\beta)(t - t_o)}{|\bar{r}(t)|}\right] \bar{r}(t) + \bar{r}_O(t) \tag{2.73}$$

Here D(t) is an arbitrary orthogonal transformation. In case if the signal frequency is known then $f_o = f_o'$ or $\beta = 1$. Putting this β value in Eq. 2.73 yields,

$$\bar{r'}_T(t) = D(t) \left[1 + \frac{\alpha}{|\bar{r}(t)|}\right] \bar{r}(t) + \bar{r}_O(t) \tag{2.74}$$

This means that even in known frequency case there are compatible trajectories, parameterized by α, which produces same frequency measurements history.

Considering both bearing and frequency measurements, compatible trajectories must belong to intersection of two sets of trajectories as defined by equations (2.67) and (2.73). With additional bearing measurements at hand, the ambiguity of orthogonal transforma-

tion in (2.73) is removed. Therefore, in this case it is necessary and sufficient for $\bar{r}_T(t)$ to lead to same measurement history as $\bar{r}'_T(t)$ if following relation is satisfied,

$$\bar{r'}_T(t) = \left[\beta + \frac{\alpha + c(1-\beta)(t-t_o)}{|\bar{r}(t)|}\right]\bar{r}(t) + \bar{r}_O(t) \tag{2.75}$$

Equations (2.67), (2.73) and (2.75) show that true trajectory is always embedded in a set of compatible trajectories with no restrictions being applied on target/observer dynamics. This also shows that question of observability would only make sense for constrained motion cases, revealing special conditions that could effect target's observability.

2.5.4 Nth-Order Dynamics Model

By modeling the system as Nth order dynamics, [81–83] avoided analyzing the observability matrix. This formulation enables direct derivation of observability conditions. In similar fashion, we model target and observer states as Nth order dynamics over the observation interval $[t_o, t_f]$ as

$$\bar{r}_T(t) = \sum_{i=0}^{N} \frac{\bar{r}^i_T(t_o)}{i!}(t-t_o)^i \tag{2.76}$$

$$\bar{r}_O(t) = \sum_{i=0}^{M} \frac{\bar{r}^i_O(t_o)}{i!}(t-t_o)^i \tag{2.77}$$

where $\bar{r}^i$ represents the ith time derivative. This restriction of finite order dynamics thus reduces the set of compatible trajectories in (2.67), (2.73) and (2.75). Furthermore, since $\bar{r}_T(t)$ is an N degree vector polynomial, $\bar{r}'_T(t)$ must also be a N degree vector polynomial. If system is observable then set of compatible trajectories shrinks to only one trajectory and $\bar{r}'_T(t) = \bar{r}_T(t)$.

To simplify further analysis, let's represent class of Nth order vector polynomials as,

$$P_N = \sum_{i=0}^{N} \bar{a}_i(t-t_o)^i = A\bar{t} \tag{2.78}$$

$$\bar{a}_i = \frac{\bar{r}_T^i(t_o)}{i!} \tag{2.79}$$

where $A = [\bar{a}_o, \bar{a}_1, \ldots, \bar{a}_N]$ is an arbitrary 3x(N+1) matrix of coefficients independent of t and $\bar{t} = \left[1, (t-t_o), (t-t_o)^2, \ldots, (t-t_o)^N\right]^T$.

2.5.5 Observability Analysis for Bearings-only Measurements

Subtracting Eq. (2.1) and (2.67) to remove observer motion, we get,

$$\bar{r}'_T(t) - \bar{r}_T(t) = (\kappa(t) - 1)\bar{r}(t) \tag{2.80}$$

When $\kappa = 1$, we get true target motion as in eq (2.67). However, since we are interested in compatible target trajectories that are different from (2.67), let $\kappa \neq 1$. Rearranging above equation to obtain,

$$\begin{aligned} \bar{r}(t) &= \frac{1}{(\kappa(t) - 1)}(\bar{r}'_T(t) - \bar{r}_T(t)) \\ \bar{r}(t) &= K_b(t)\ A\bar{t} \end{aligned} \tag{2.81}$$

where $K_b = (\kappa - 1)^{-1}$. Since $\bar{r}_T \in P_N$ and $\bar{r}'_T \in P_N$, their difference must also be in P_N, i.e. $(\bar{r}'_T(t) - \bar{r}_T(t)) \in P_N$. Thus $(\bar{r}'_T(t) - \bar{r}_T(t))$ must be of the form $A\bar{t}$ as in Eq. (2.78). Eq. (2.81) is therefore the necessary and sufficient condition of unobservability in class of Nth-order dynamics targets.

For $K_b(t) = 1$, Eq (2.81) establishes the well known fact that in absence of maneuver, target is not observable. Note that in general maneuvering means existence of one or more non-zero derivatives of order higher than the order of target model dynamics to be estimated. However, only those maneuvers that satisfy Eq (2.81) are allowed. As another example, consider the case of estimating the position of a stationary target from a constant velocity moving observer. As long as, observer moves along a constant LOS trajectory, target remains unobservable. This can be verified by selecting $A = (\mathbf{1_r}, \mathbf{0_3}, \ldots, \mathbf{0}_3)$, where $\mathbf{0_3}$ is a three-dimensional null vector and $\mathbf{1_r} = \frac{\bar{r}(t)}{|\bar{r}(t)|}$ is a constant unit vector in direction

of LOS. Choosing $K_b(t) = |\bar{r}(t)|$, (2.81) becomes,

$$\bar{r}(t) = |\bar{r}(t)| \begin{bmatrix} \frac{\bar{r}_x(t)}{|\bar{r}(t)|} & 0 \\ \frac{\bar{r}_y(t)}{|\bar{r}(t)|} & 0 \\ \frac{\bar{r}_z(t)}{|\bar{r}(t)|} & 0 \end{bmatrix} \begin{bmatrix} 1 \\ t \end{bmatrix}$$

$$\bar{r}(t) = \begin{bmatrix} \bar{r}_x(t) & 0 \\ \bar{r}_y(t) & 0 \\ \bar{r}_z(t) & 0 \end{bmatrix} \begin{bmatrix} 1 \\ t \end{bmatrix} \tag{2.82}$$

2.5.6 Observability Condition

With bearings only measurements, target state is observable if and only if LOS angle between observer and target does not remain constant. This means either target or observer must maneuver.

2.5.7 Observability Analysis for Frequency-only Measurements

Similarly, as in previous section, subtracting Eq. (2.1) and (2.73) to eliminate the observer motion vector, we obtain,

$$\begin{aligned} \bar{r}'_T(t) - \bar{r}_T(t) &= D(t) \left[\beta + \frac{\alpha + c(1-\beta)(t-t_o)}{|\bar{r}(t)|} \right] \bar{r}(t) + \bar{r}_O(t) - \bar{r}(t) - \bar{r}_O(t) \\ &= \left[D(t) \left[\beta + \frac{\alpha + c(1-\beta)(t-t_o)}{|\bar{r}(t)|} \right] - I \right] \bar{r}(t) \end{aligned}$$

As before, $(\bar{r}'_T(t) - \bar{r}_T(t)) \in P_N$. Thus $(\bar{r}'_T(t) - \bar{r}_T(t))$ must be of the form $A\bar{t}$ as in Eq. (2.78). Hence above equation becomes,

$$A\bar{t} = \left[D(t) \left[\beta + \frac{\alpha + c(1-\beta)(t-t_o)}{|\bar{r}(t)|} \right] - I \right] \bar{r}(t) \tag{2.83}$$

Rearranging above equation, we can write

$$\bar{r}(t) = \left[D(t) \left[\beta + \frac{\alpha + c(1-\beta)(t-t_o)}{|\bar{r}(t)|} \right] - I \right]^{-1} A\bar{t} \tag{2.84}$$

$$= K_f(t)\ A\bar{t} \tag{2.85}$$

where,

$$K_f(t) = \left[D(t) \left[\beta + \frac{\alpha + c(1-\beta)(t-t_o)}{|\bar{r}(t)|} \right] - I \right]^{-1}$$

For $A \neq 0$, Eq. (2.84) is the necessary and sufficient condition for unobservability with frequency measurements, i.e. as long as relative distance satisfies (2.84), Nth-order target dynamics remain unobservable.

2.5.8 Constant Line of Sight Targets

In this case it is sufficient to show that for constant LOS targets there always exists an Nth-order target trajectory $\bar{r}'_T(t) \neq \bar{r}_T(t)$ which is compatible with the frequency measurements. For example, one such compatible trajectory can be obtained by selecting $D(t) = I, \beta = 1$ and $\alpha \neq 0$ and $A = (\mathbf{1_r}, \mathbf{0_3}, \ldots, \mathbf{0}_3)$, in Eq. (2.73) as,

$$\begin{aligned} \bar{r'}_T(t) &= \bar{r}(t) + \alpha\ \frac{\bar{r}(t)}{|\bar{r}(t)|} + \bar{r}_O(t) \\ &= \bar{r}(t) + \alpha\bar{\mathbf{1}}_\mathbf{r} + \bar{r}_O(t) \\ &= \bar{r}_T(t) + \alpha\bar{\mathbf{1}}_\mathbf{r} \end{aligned} \tag{2.86}$$

where $\mathbf{1_r}$ is a unit vector along $\bar{r}(t)$.

2.5.9 Non-Constant LOS Targets

As constant LOS results in unobservability in any case, therefore, we now assume that relative motion between target and observer is not along a constant LOS. Furthermore, these motions are confined to vector polynomial of order N and M, as shown in Eq. (2.76)

and (2.77). Then as stated before, relative motion is also a vector polynomial, given as,

$$\bar{r}(t) = \sum_{i=0}^{L} \frac{\bar{r}^i(t_o)}{i!}(t - t_o)^i \tag{2.87}$$

where

$$L = max(M, N) \tag{2.88}$$

$$\bar{r}^i(t_o) = \bar{r}^i_T(t_o) - \bar{r}^i_O(t_o); \tag{2.89}$$

Let us now investigate the degree of norm of relative motion vector $\bar{r}(t)$. As discussed previously that in case of unobservability, the norms of relative distances, $|\bar{r}'(t)|$ and $|\bar{r}(t)|$, are functionally related by Eq. (2.70). Note that $|\bar{r}(t)|^2 = (r_x(t)^2 + r_y(t)^2 + r_z(t)^2)$ is a polynomial of degree 2L. Squaring both sides of Eq. (2.70) and rearranging to obtain

$$|\bar{r}'(t)|^2 - \beta^2 |\bar{r}(t)|^2 - [\alpha + c(1-\beta)(t-t_o)]^2 = 2\beta |\bar{r}(t)| [\alpha + c(1-\beta)(t-t_o)] \tag{2.90}$$

Left hand side of above equation consists of two polynomials of degree 2L and a polynomial of degree 1. As left hand side of Eq (2.90) is a polynomial therefore right hand side must also be a polynomial. This right hand side consists of a product of $|\bar{r}(t)|$ and a polynomial. Using a simplified notation, Eq (2.90) can be written as,

$$P_{2L} = |\bar{r}(t)| P_1 \tag{2.91}$$

where P_x denotes a polynomial of degree x. Rearranging yields

$$|\bar{r}(t)| = \frac{P_{2L}}{P_1} \text{ for } \alpha \neq 0 \text{ and } \beta \neq 1 \tag{2.92}$$

Squaring boths sides of above equation,

$$|\bar{r}(t)|^2 = \frac{P^2_{2L}}{P^2_1} \tag{2.93}$$

However, since $|\bar{r}(t)|^2$ is a polynomial therefore it implies that P^2_1 divides P^2_{2m} without

a remainder. Moreover, factorizing above equation as follows,

$$|\bar{r}(t)|^2 = \frac{P_{2L}P_{2L}}{P_1P_1} \tag{2.94}$$

further implies that P_1 divides P_{2m} without a remainder as well. Consequently, Eq. (2.92) implies that $|\bar{r}(t)|$ is a polynomial. However, $|\bar{r}(t)|$ can be a polynomial if and only if $\bar{\mathbf{1}}_r = \frac{\bar{r}(t)}{|\bar{r}(t)|}$ is **constant**. To prove this, consider the definition,

$$\bar{r}(t) = |\bar{r}(t)|\bar{\mathbf{1}}_r \tag{2.95}$$

From above equation it's clear that degree of $\bar{r}(t)$ would equal $|\bar{r}(t)|$ if and only if $\bar{\mathbf{1}}_r$ is constant. On the contrary if it would have at least one degree higher than zero, then this would render a contradiction in equality of Eq. (2.95).

However, for unobservability LOS can't be constant. Hence, if $|\bar{r}(t)|$ is not a polynomial then the only way that the left hand side of Eq. (2.90) can still be a polynomial is if

$$\begin{aligned} \alpha &= 0 \\ \beta &= 1 \end{aligned} \tag{2.96}$$

Inserting (2.96) in (2.72), we can thus obtain that,

$$f_o' = f_o \tag{2.97}$$

$$|\bar{r}'(t)| = |\bar{r}(t)| \tag{2.98}$$

and also ,

$$D(t)\left[\beta + \frac{\alpha + c(1-\beta)(t-t_o)}{|\bar{r}(t)|}\right] = D(t) \tag{2.99}$$

This means that with frequency only measurements as long as LOS is not constant we can observe target uptill it's relative distance from observer. Thus target state ambiguity can only result from the dot product in definition Eq. (2.4). Moreover, Eq. (2.83) now

becomes,

$$[D(t) - I]\bar{r}(t) = A\bar{t} \tag{2.100}$$

Now, since $\bar{r}(t)$ and $A\bar{t}$ are vector polynomials, $D(t)\bar{r}(t)$ must also be a vector polynomial. However, it's shown in Apendix B of [85] that under this condition the time dependent orthogonal transformation $D(t)$ becomes a constant orthogonal transformation D.

$$\begin{aligned}(D - I)\bar{r}(t) &= A\bar{t} \\ \bar{r}(t) &= (D - I)^{-1}A\bar{t}\end{aligned} \tag{2.101}$$

This implies that, *in case of finite order dynamics, target state is unobservable with frequency measurements alone if and only if relative distance $\bar{r}(t)$ satisfies Eq.* (2.101). Here $A\bar{t} \in P_N$ and N being degree of target dynamics polynomial. Hence as long as relative distance is of order of target dynamics then target state is unobservable.

The set of compatible target trajectories can be obtained from Eq. (2.73) by putting $\alpha = 0$ and $\beta = 1$ as,

$$\bar{r}'_T(t) = D\bar{r}(t) + \bar{r}_O(t) \tag{2.102}$$

As stated before, for frequency only measurements, when LOS is not constant then set of trajectories, compatible with measurement history, arises because of the ambiguity associated with direction or dot product. This means if besides frequency, we have additional angle measurements this ambiguity could be resolved. We shall investigate this point in next section.

Next logical question at this point would be how to make target observable. Let's investigate (2.101) further to find out how can observability be achieved. Using Eq. (2.78) and vector polynomial definition of $\bar{r}(t)$ (2.87) in Eq (2.101)

$$(D - I)\sum_{i=0}^{L}\frac{\bar{r}^i(t_o)}{i!}(t - t_o)^i = \sum_{i=0}^{N}\bar{a}_i(t - t_o)^i \tag{2.103}$$

where $L = max(M, N)$. Depending upon the degree of observer's motion following cases should be considered.

Observer's Motion is of Lower Order Than Target's Motion ($M \leq N$)

In this case, $L = N$. Selecting $(D - I)\bar{r}(t_o) = \bar{a}_i$, (2.103) trivially can be satisfied by any orthogonal transformation D. Therefore, if observer motion is of a dynamics order less than or equal to that of target $M < N$ then target state is unobservable. The set of compatible trajectories is given by (2.102) and target state can only be determined up to rotations and reflections in the observer's coordinate system.

Observer's Motion is of Higher Order Than Target's Motion ($M > N$)

In this case, $L = M$. Now condition (2.103) could only be met if and only if all the derivatives higher than N are zero,

$$(D - I)\bar{r}^i(t_o) = 0 \forall i > N \tag{2.104}$$

Using (2.89)

$$(D - I)[\bar{r}^i_T(t_o) - \bar{r}^i_O(t_o)] = 0 \forall i > N \tag{2.105}$$

However, by assumption $\bar{r}^i_T(t_o) = 0 \forall i > N$,

$$\begin{aligned} (D - I)\bar{r}^i_O(t_o) &= 0 \forall i > N \\ D\bar{r}^i_O(t_o) &= \bar{r}^i_O(t_o) \end{aligned} \tag{2.106}$$

Condition (2.106) is fulfilled if and only if all initial non-zero vectors $\bar{r}^i_O(t_o) \forall (i > N)$ are parallel to each other and D is a rotation R about one of them.

At this point, two subclasses $M = N + 1$ and $M > N + 1$ should be distinguished. If $M = N + 1$ then condition (2.106) can always be satisfied. This means that target state is unobservable if observer motion is of order $M = N + 1$. On the other hand, if

$M \geq N+1$ then according to condition (2.106) target state is unobservable if and only if all initial observer state derivatives ($\bar{r}_O^i \forall (i > N)$) are parallel to each other. Conversely stated, target state is observable if and only if there exits at least two initial observer state derivatives which are not parallel to each other ($\bar{r}_O^{i1} \neq 0$ and $\bar{r}_O^{i2} \neq 0$ for $(i1, i2 > N)$). In case of unobservability the set of compatible trajectories is given by,

$$\bar{r}'_T(t) = R\bar{r}(t) + \bar{r}_O(t) \tag{2.107}$$

where R is rotation about $\bar{r}_O^i(t_o)$ with $i > N$. This means that target state can only be determined up to a rotation of $\bar{r}(t)$ about the direction of parallel non-zero vectors $\bar{r}_O^i(t_o)$.

2.5.10 Observability Condition

With only frequency measurements, target state is observable if and only if,

- LOS angle between observer and target does not remain constant. This means either target or observer must maneuver.
- Dynamics order of Observer's motion is of two or more degrees higher than target's motion. Moreover, at least two of these higher derivatives must not be parallel to each other.

2.5.11 Observability Analysis With Bearings & Frequency Measurements

Equipped with the results for angle-only and frequency-only measurements, observability analysis when both sets are available simultaneously is a trivial task. As mentioned earlier, that with frequency measurements when LOS angles are changing then only ambiguity is in orthogonal transformation D(t). However, now with additional angle measurements D(t) becomes identity transformation. Therefore, updating Eq. (2.83)) we obtain,

$$A\bar{t} = \left[\beta + \frac{\alpha + c(1-\beta)(t-t_o)}{|\bar{r}(t)|} - 1\right]\bar{r}(t) \tag{2.108}$$

where $A\bar{t} \in P_N$ as before. Rearranging above equation as,

$$\bar{r}(t) = \left[\beta + \frac{\alpha + c(1-\beta)(t-t_o)}{|\bar{r}(t)|} - 1\right]^{-1} A\bar{t} \tag{2.109}$$

$$= K_{bf}\ A\bar{t} \tag{2.110}$$

where,

$$K_{bf} = \left[\beta + \frac{\alpha + c(1-\beta)(t-t_o)}{|\bar{r}(t)|} - 1\right]^{-1}$$

for $A \neq 0$, this is the necessary and sufficient condition for unobservability of Nth-order dynamics. As a target is unobservable for constant LOS with angle-only and frequency-only measurements, consequently it would be unobservable with angle & frequency measurements together. When LOS is not constant then as shown earlier, the operator K_{bf} becomes unity and hence set of compatible trajectories Eq. (2.75) becomes,

$$\bar{r}'_T(t) = \bar{r}(t) + \bar{r}_O(t)$$
$$\bar{r}'_T(t) = \bar{r}_T(t)$$

That is all trajectories shrink to one original trajectory and hence target state is observable.

2.5.12 Observability Conditions

With both angle and frequency measurements, target state is observable if and only if LOS angle between observer and target does not remain constant. Unlike previous two cases, observer does not require higher degree dynamics or maneuvers. Infact observability is guaranteed even for stationary observer.

Chapter 3
Target Tracking with Doppler Radars

3.1 Introduction

Problem in indoor localization problems are inherently different from those encountered in the outdoor localization. In the latter case, there's been a lot of development in GPS based positioning and navigation. A GPS can track the position of a user with high accuracy. However, its signals are only accessible in outdoor environments - limiting their indoor applications. Despite the plethora of research regarding indoor navigation systems, a feasible and economical solution is still missing. In previous chapter, we have derived the observability conditions for the Doppler measurements. These conditions, when met, guarantee us a unique solution to the estimation problem. In this chapter, we discuss the development of Doppler frequency measurements based target localization system. We discuss the formulation of the target's state estimation as a Kalman filtering problem. Hereby, we design different trackers, catering various indoor scenarios and comparing them.

3.2 Target State Estimation

Consider an observer/user moving around in a small confined room. The observer would be possibly surrounded by people, objects and walls. Now, relative to this observer everything else is a target. Our aim is to localize and track everything surrounding the observer. However, to keep things simple and to establish a base framework, we first assume the case of one observer and one target contained in a small area. Then design a

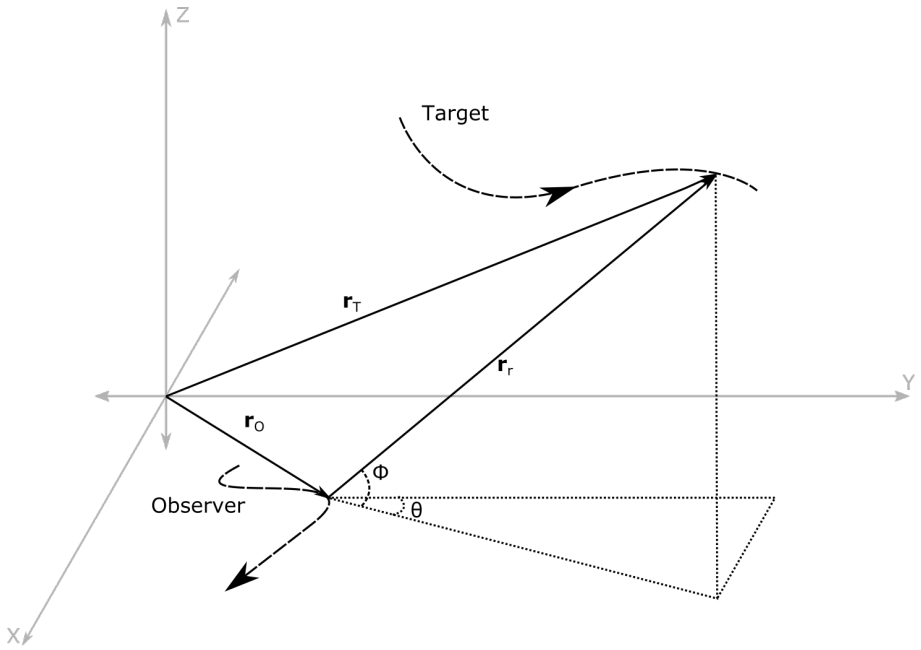

Figure 3.1: Observer and target's geometry for observability analysis

framework for localization in 2 dimensions (2D). Thereafter, extension for 3D scenarios is straightforward study. Furthermore, it is assumed that observer is focusing on target at all times - getting its bearings and Doppler measurements. To this end, consider the observer target geometry shown in Fig 2.2.

Although we are mainly concerned with building a Doppler-only tracker, however, at the same time we would also develop and consider Bearings-only and Bearings-Doppler trackers for sense of completion, comparisons and further developments in later chapters.

3.2.1 Problem Formulation

In this section, we mathematically formulate the problem of tracking a target from an observer. We use the same observer-target geometry as before and shown in Fig. 2.2, duplicated in Fig 3.1 for ease. Consider a target T moving along a trajectory $\bar{r}_T(t)$ and emitting a signal of frequency f_o.

An observer moving along trajectory $\bar{r}_O(t)$ makes bearing and frequency measurements of the target and tries to estimate its state. We can obtain the following relation from the geometry in Fig. 2.2.

$$\bar{R}_T(t) = \bar{R}(t) + \bar{R}_O(t) \tag{3.1}$$

In this work, three measurements sets are considered, namely: bearings-only, frequency-only and bearing-frequency measurements together. The bearings (θ) and Doppler frequency (f_d) measurements [90] satisfy following relationships,

$$\theta = tan^{-1}\frac{R_y(t)}{R_x(t)} \tag{3.2}$$

$$\bar{V}_R = \frac{\lambda f_d}{2} \tag{3.3}$$

where

- R_x and R_y are X and Y components of $\bar{r}(t)$
- V_R is the radial velocity vector
- λ is signal's wavelength
- f_d is Doppler frequency

Radial velocity can also be expressed as

$$\bar{V}_R = |\bar{V}|\cos(\theta_R) \tag{3.4}$$

$$\bar{V}_R = \frac{R_x\bar{V}_x + R_y\bar{V}_y}{\sqrt{R_x^2 + R_y^2}} = \frac{\bar{V}.\bar{R}}{|\bar{R}|} \tag{3.5}$$

where

- θ_R is the angle between radial direction and velocity vector.

3.2.2 CASE-1: Single Stationary Target & Maneuvering Observer

In this first scenario, consider a point-like stationary target and a dynamic observer in a $(5 \times 5)m^2$ area. Target is located at coordinates $x = 5m$ and $y = 5m$. For the target to be observable we need to meet following criterion:

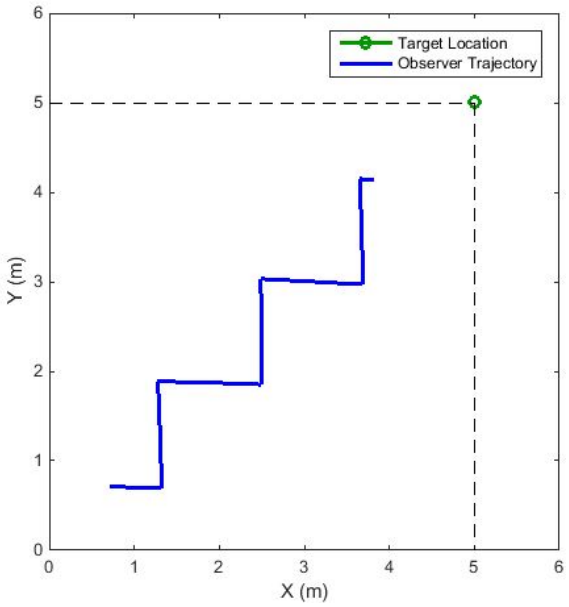

Figure 3.2: Simulation scenario of a stationary target at (5,5) and moving observer (blue track)

- **Bearings-Only Measurements:** LOS angle should not remain constant.
- **Dopper-Only measurements:** LOS angle between them should not be constant and Observer's dynamics should be at least two degrees higher than target's motion.
- **Bearing & Doppler Measurements:** LOS angle should not remain constant

Consider now that observer starts at coordinates $x = 1m$, $y = 1m$ and moves with velocity 10 km/h (2.8 m/s). Although observer moves with constant velocity, however, it exhibits 90^o maneuvers from time to time [91], as follows,

- From 90^o to 0^o at time $t = (20 + 200^k)Tsec, k = [0, 1, 2, ...]$
- From 0^o to 90^o at time $t = (100 + 200^k)Tsec, k = [0, 1, 2, ...]$

where T is sampling time. The target-observer geometry for this scenario is shown in Fig 3.2.

Let $X_T[k]$ and $X_O[k]$ denote target's and observer's state at time instant k. Position

and velocity components in $X_T[k]$ and $X_O[k]$ are arranged as,

$$X_O[k] = \begin{bmatrix} \text{x position} \\ \text{x velocity} \\ \text{y position} \\ \text{y velocity} \end{bmatrix} = \begin{bmatrix} x \\ V_x \\ y \\ v_y \end{bmatrix} \tag{3.6}$$

For constant velocity scenario, observer's dynamics can be modeled as a **Constant Velocity model** [92], also known as **Piecewise-Constant White Acceleration model** [70]. It assumes that the target moves with constant velocity where small perturbations in velocity being modeled as independent acceleration noise. It is given as,

$$X_O[k+1] = FX_O[k] + U[k] + Gv[k] \tag{3.7}$$

where, F is state transition matrix defined as,

$$F = \begin{bmatrix} 1 & T & 0 & 0 \\ 0 & 1 & 0 & 0 \\ 0 & 0 & 1 & T \\ 0 & 0 & 0 & 1 \end{bmatrix} \tag{3.8}$$

U[k] is the deterministic input vector, which accounts for the effect of observer accelerations. U[k] is deterministic since we assume that we have the knowledge of observer state X_O at every instant of time. The Gain matrix G is

$$G = \begin{bmatrix} \frac{T^2}{2} & 0 \\ T & 0 \\ 0 & \frac{T^2}{2} \\ 0 & T \end{bmatrix} \tag{3.9}$$

v(k) is zero-mean white Gaussian process noise with variance σ_v. The covariance of

process noise multiplied by gain G is given as,

$$Q = E[Gv(k)v(k)G'] \tag{3.10}$$

$$= \sigma_v^2 GG' \tag{3.11}$$

$$= \sigma_v^2 \begin{bmatrix} \frac{T^4}{4} & \frac{T^3}{2} & 0 & 0 \\ \frac{T^3}{2} & T^2 & 0 & 0 \\ 0 & 0 & \frac{T^4}{4} & \frac{T^3}{2} \\ 0 & 0 & \frac{T^3}{2} & T^2 \end{bmatrix} \tag{3.12}$$

We can now introduce the relative state vector as,

$$X[k] = X_T - X_O \tag{3.13}$$

The corresponding state equation for relative state vector is,

$$X[k+1] = FX[k] - U[k] + Gv[k] \tag{3.14}$$

Measurement vector Z[k] is related to state X[k] through nonlinear function h() as,

$$Z[k] = h(X[k]) + w(k) \tag{3.15}$$

where $w(k)$ is zero mean white Gaussian observation noise with variance σ_w. h(.) is a nonlinear function of the state, whose value depends upon the measurements being considered.

- For bearings only measurements, angle θ is measured counter-clockwise from positive X-axis.

$$h(x[k]) = \theta = tan^{-1}\left(\frac{R_y(t)}{R_x(t)}\right) \tag{3.16}$$

- For Doppler or relative velocity (V_R) only measurements,

$$h(x[k]) = \bar{V_R} = \frac{R_x \bar{V}_x + R_y \bar{V}_y}{\sqrt{R_x^2 + R_y^2}} \tag{3.17}$$

- For bearings and velocity (V_R) measurements together,

$$h(x[k]) = [\theta, V_R]^T \tag{3.18}$$

  where superscript T means transpose.

Covariance matrix R_{ww} of measurement noise is given by $\sigma_w^2 I$, where I is the identity matrix whose size depends upon h(x[k]), σ_w is standard deviation of measurement noise.

The optimal Bayesian solution to the problem formulated would require computing posterior density $p(x[k]|z[k])$. However, the optimal solution for this problem cannot be obtained because measurement equation is nonlinear (4.6). Therefore, we will have to suffice for suboptimal solutions and use filters developed for nonlinear systems as described earlier, i.e EKF, UKF, & CKF, etc.

In general, for reliable performance of non-linear filters, proper initialization is very critical [69,70,93]. Thus some *a priori* knowledge of target's range and speed is quite helpful. At this stage, suppose we have some *a priori* knowledge of the mean of initial range as μ_r and its variance σ_r^2. Also, suppose that mean of relative velocity is less than s_{max} with variance σ_v^2. With these assumptions, the state and its covariance can be initialized as

$$X[\hat{0}|0] = [\mu_r, 0, \mu_r, 0] \tag{3.19}$$

$$P[0|0] = diag[\sigma_r^2, \sigma_v^2, \sigma_r^2, \sigma_v^2] \tag{3.20}$$

Performance comparisons are based on a set of Monte-Carlo (MC) runs [93–95]. All metrics are computed after M MC runs. Let r_i and $\hat{r}_i$ denote the true and estimated ranges at *ith* MC run. Then the performance metrics used in our analysis are Root-Mean-Square (RMS) error and number of divergent tracks in M MC runs. A track is classified

as divergent if at any time, the estimated position error of the target exceeds a preset threshold. The threshold is set depending upon the geometry of the problem at hand. RMS position error is only computed for non-divergent tracks.

Considering the geometry of our scenario and constraints of observer and target dynamics, all filters are initialized with an initial range of 5m. Standard deviations of range and velocity are chosen to be $\sigma_r = 3m$ and $\sigma_v = 1.673m/s^2$. Standard deviation for process noise is $\sigma_v = 0.5m/s^2$, whereas, for bearing and Doppler measurements it is chosen to be $\sigma_\theta = 1^o$ and $\sigma_{V_r} = 0.5m/s$.

3.2.3 Simulation Results

We used Extended Kalman filter to obtain the solution for nonlinear filter equations designed above. Figure 3.3 shows the tracking results for three different trackers designed above, namely: Bearings-Only, Doppler-Only and Bearing-Doppler trackers. All of these results were obtained after 1000 MC runs and excluding the divergent tracks. Each run simulates 2.5 seconds of the scenario, allowing the observer to finish about 6 maneuvers. As mentioned earlier a track is considered divergent if its RMS position error exceeds a certain threshold. For this simulation, divergence threshold was set at 20 m.

After 1000 MC runs, we found out that, on average EKF converged about 85% of all the runs. It can be seen from Figure 3.3a that for Bearing-only tracker, RMS position error decreases with each maneuver, reaching to just about 1 m in 2.5 seconds. For Doppler-only measurements, RMS position error apparently also decreases continuously from its initial value to about 1 m in about 2.5 seconds. As expected, when both Bearings and Doppler measurements were taken into account, filter's RMS error converged much faster, reaching to 1 m in about 1 second. This error dropped even further, reaching below 500 cm in 2.5 seconds as shown in Figure 3.3c. Figure 3.3 also shows RMS velocity error for the three cases discussed.

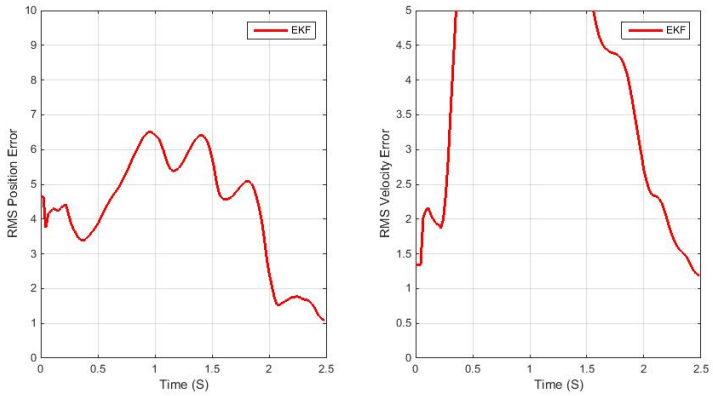

(a) Bearings-Only Tracking

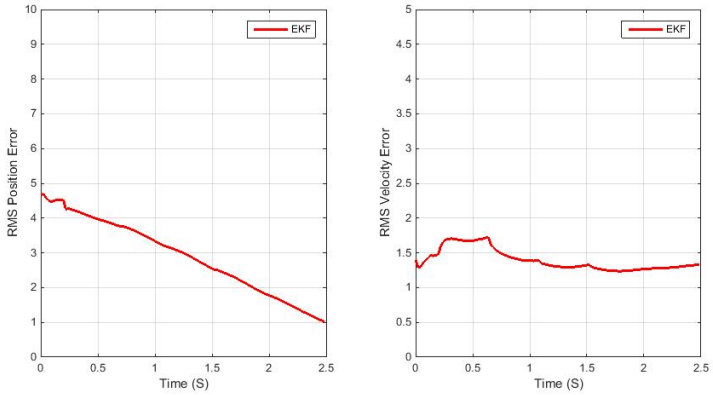

(b) Doppler-Only Tracking

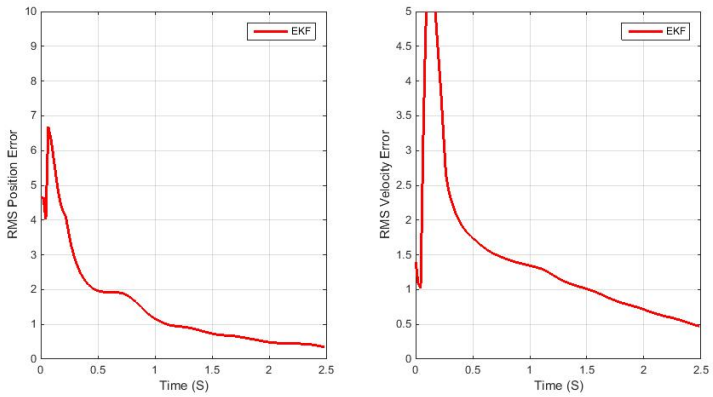

(c) Bearings-Doppler Tracking

Figure 3.3: Position & velocity error comparisons for different EKF trackers

3.2.4 Non-linear Kalman Filters' Comparisons

As mentioned earlier, Kalman filter gives us the optimal solution if underlying statistics are Gaussian and system is linear. However, in case of nonlinear system, one has to resort to approximate solutions. Since its inception nearly 40 years ago, Extended Kalman Filter has been everybody's go-to option for nonlinear systems. However, its inaccuracies in estimating system statistics cannot be overstated. Extended Kalman Filter works by linearizing the nonlinear state space equations using first-order truncation of Taylor series. However, this approximation would be only useful if all the second order and higher derivatives are effectively zero [72, 73]. If it is not the case, then resulting statistics which are linearly calculated would not be accurate. One major drawback with EKF is that during linearization process, it fails to take into account that X is a random variable. It ignores the probabilistic spread of X modeled as covariance P_{XX}, and linearizes it around a single point. This introduces large errors in later stages and effects the consistency of the filter. Posterior mean and covariance calculated by the filter doesn't represent the actual scenario and more than often filter ends up diverging.

To overcome these and other shortcomings of EKF, researchers have developed numerous approximations of Kalman filter for nonlinear systems. These algorithms are closely related as how they handle multi-modal integrals in Bayes formula. Instead of linearizing the nonlinear equations these algorithms depends upon deterministic sampling methods for the propagation of Gaussian random variables through nonlinear systems. Unscented Kalman Filter (UKF) [73] uses *scaled unscented transformation* to compute the points that can capture the current statistics of Gaussian Random Variables. Then it uses these points through the nonlinear systems thus avoiding the requirement of Taylor Series truncation. In more recent developments, Cubature Kalman Filter (CKF) was introduced as a more robust and stable version to handle the multi-model Bayes integrals. Underlying idea is same as that of Unscented Kalman Filter, however, it uses Cubature rules to handle the integrals.

In this section, we implemented and compared Extended Kalman Filter with Unscented Kalman Filter and Cubature Kalman Filter. These results are obtained after 1000 MC runs and excluding the divergent tracks. As before, a track is considered as divergent

if RMS position errors becomes greater than 20 m at any time.

Figure 3.4 shows the comparison results of the three Gaussian approximate filters. From Fig 3.4a, we can see that both UKF and CKF can localize a target within few cm in about 2 seconds. Same is the case for Doppler-only filter as shown in Figure 3.4b. However, we have even better results with Bearing-Doppler filter, where error reduces to less than 1 m in about 1 second as shown in Figure 3.4c. This error keeps on reducing, reaching less than 100 cms in 2.5 seconds. RMS Position and velocity error comparisons in Fig. 3.4(a), (b) and (c) clearly shows that error becomes smaller after each maneuver and reaching almost a steady value after about 3 maneuvers. Out of 1000 MC runs, EKF diverged about 200 times whereas UKF and CKF diverged about 4 and 5 times, respectively. As expected, both UKF and CKF performed consistently better than EKF.

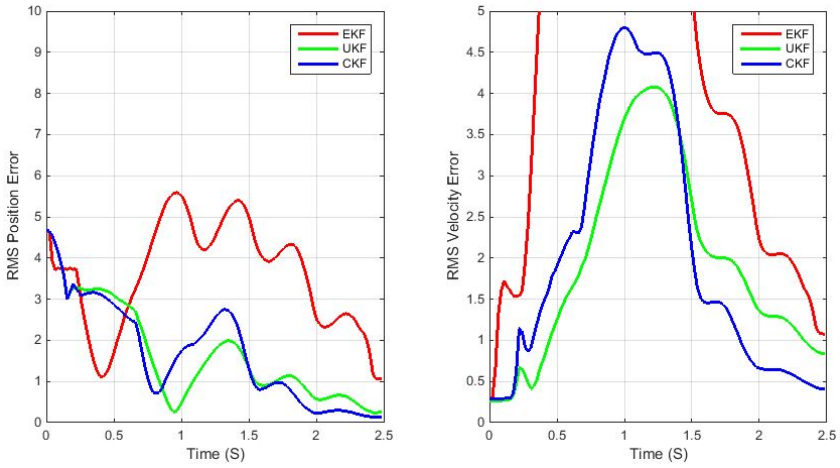

(a) Bearings-Only Tracking

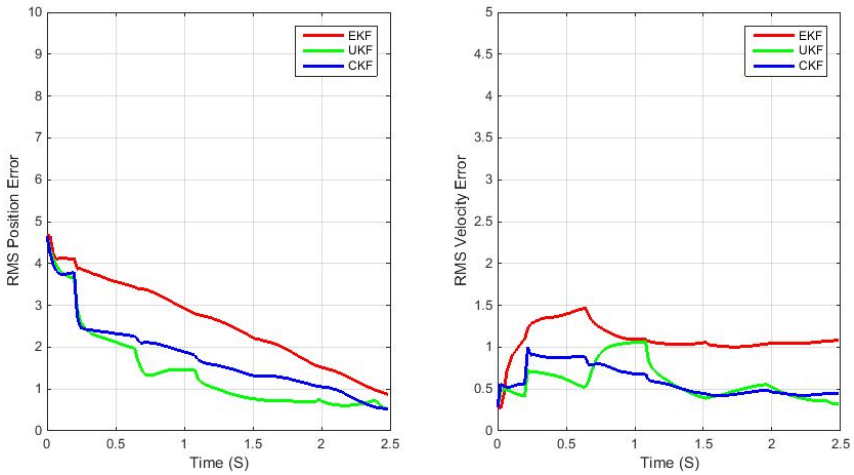

(b) Doppler-Only Tracking

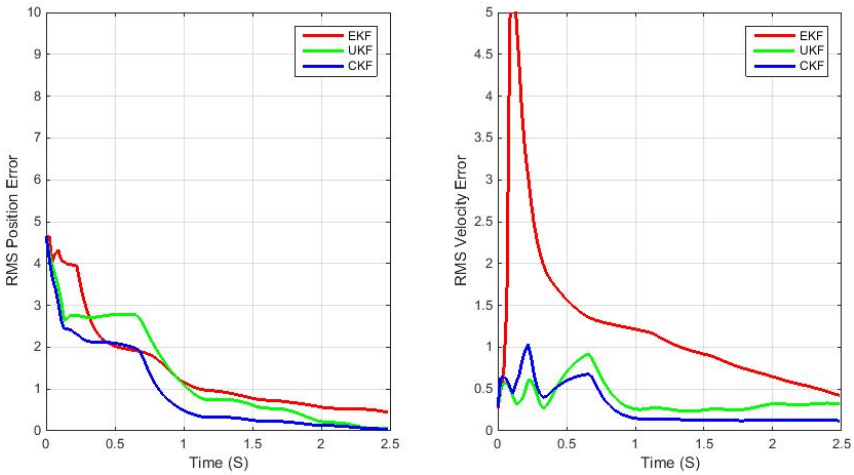

(c) Bearings-Doppler Tracking

Figure 3.4: Position & velocity error comparisons for different Gaussian approximate filters

3.2.5 CASE-2: Single Stationary Target and Circular Moving Observer

In the last section, we observed that target's localization gets better with each 90^o maneuver. However, such abrupt maneuvers are unrealistic in real life where observer's dynamics are constrained and limited. Therefore, in this second simulation scenario, the observer now moves on a circular trajectory while taking measurements of the target. Target is again assumed to be stationary at coordinates (5,5). Target-Observer track geometry in this case is shown in Fig 3.5.

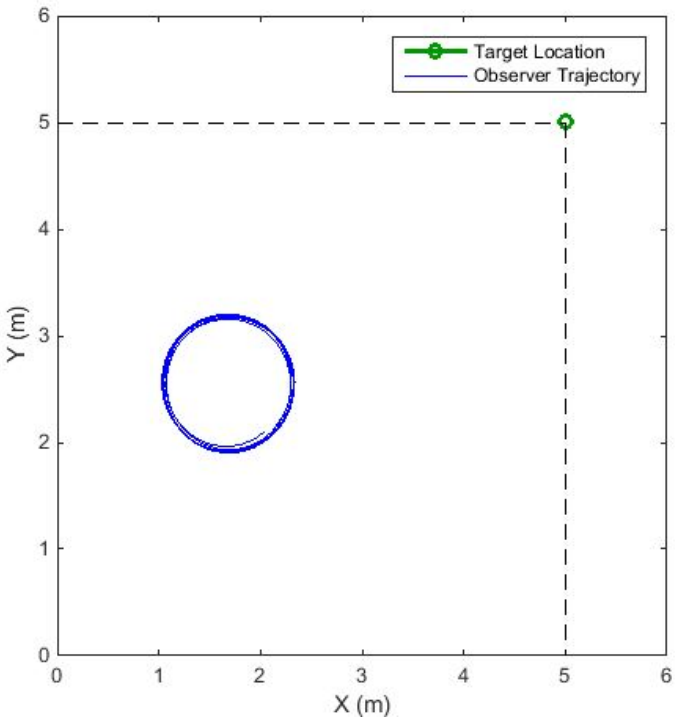

Figure 3.5: Simulation scenario of a stationary target at (5,5) and moving observer (blue track)

In this case, observer's motion is better modeled as **coordinated turn model** [92, 96, 97]. We assume that observer moves with a known constant speed and turn rate (ω). In case of known turn rate, state vector remains the same as in (3.6). The state transition

matrix in Eq. (3.7) now becomes,

$$F = \begin{bmatrix} 1 & \frac{\sin(\omega T)}{\omega} & 0 & -\frac{1-cos(\omega T)}{\omega} \\ 0 & \cos(\omega T) & 0 & -\sin(\omega T) \\ 0 & \frac{1-cos(\omega T)}{\omega} & 1 & \frac{\sin(\omega T)}{\omega} \\ 0 & \sin(\omega T) & 0 & \cos(\omega T) \end{bmatrix} \tag{3.21}$$

and covariance matrix Q (3.10) now becomes,

$$Q = \begin{bmatrix} \frac{2(\omega T-\sin(\omega T))}{\omega^3} & \frac{1-\cos(\omega T)}{\omega^2} & 0 & \frac{\omega T-\sin(\omega T)}{\omega^2} \\ \frac{1-\cos(\omega T)}{\omega^2} & T & -\frac{\omega T-\sin(\omega T)}{\omega^2} & 0 \\ 0 & -\frac{\omega T-\sin(\omega T)}{\omega^2} & \frac{2(\omega T-\sin(\omega T))}{\omega^3} & \frac{1-\cos(\omega T)}{\omega^2} \\ \frac{\omega T-\sin(\omega T)}{\omega^2} & 0 & \frac{1-\cos(\omega T)}{\omega^2} & T \end{bmatrix} \tag{3.22}$$

Remaining algorithm and settings remain same as in previous section.

3.2.6 Simulation Results

For a stationary target, an observer moving on a circular path meets all the observability conditions mentioned earlier for Bearings-only, Doppler-only and Bearings-Doppler measurements, therefore, target's state will be observable. Figure 3.6 illustrates the tracking results for different filters considered. As before, results are obtained by averaging 1000 MC runs. As expected, UKF and CKF shows very promising behavior by localizing position within few centimeters in less than half a second. Extended Kalman Filter, on the other hand, showed quite poor performance in this scenario for all three measurement sets. Out of 1000 MC runs, EKF diverged about 200 times, whereas, UKF and CKF did not diverge at all.

Unlike linear filters, the nonlinear ones are quite sensitive to initial conditions. In our case, filters with Doppler-Only measurements are quite sensitive to the initial velocity values. However, filters based on Bearings-Doppler measurements together, perform much better even with improper initialization.

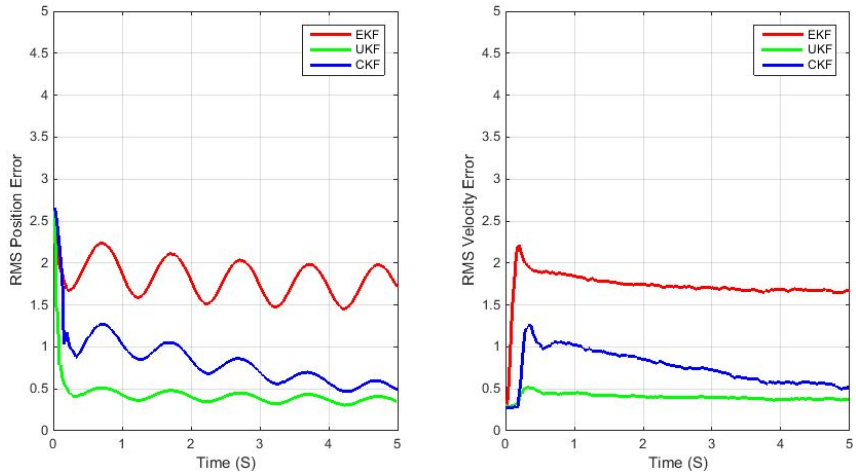

(a) Bearings-Only Tracking

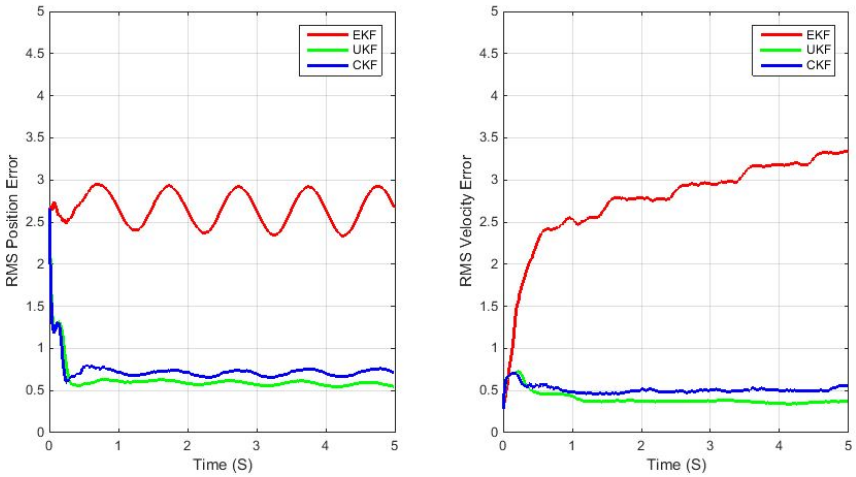

(b) Doppler-Only Tracking

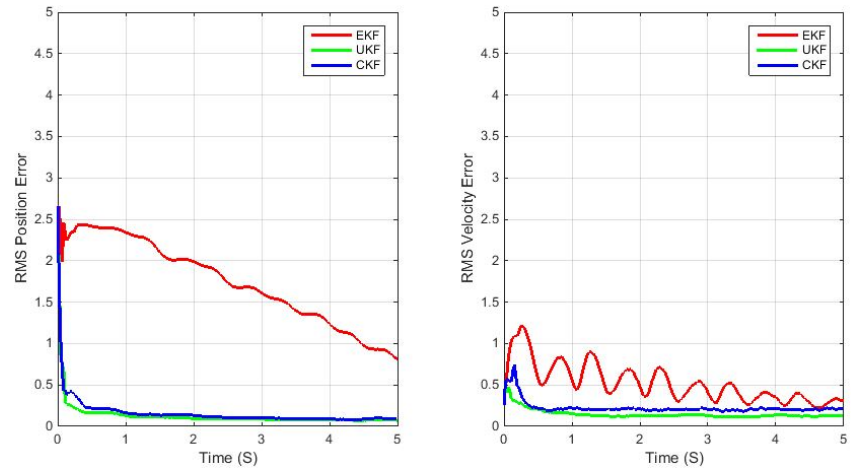

(c) Bearings-Doppler Tracking

Figure 3.6: Position & velocity error comparisons for different CT trackers

3.2.7 CASE-3: Multiple Stationary Targets & Maneuvering Observer

In previous section, we assumed one observer and one target in a small area of 5×5 m. With observer moving on a circular path, to meet the observability criteria, we were able to localize the single target within approximately 500 cm radius. In this next step, we would move one step forward by trying to localize randomly scattered multiple targets. The observer moves on a circular path and targets are all assumed to be in an area of 7×7 m. To keep things simple at this stage, it is further assumed that observer can detect targets and obtain their angle and/or frequency measurements. The observer-targets geometry for this scenario is shown in Figure 3.7,

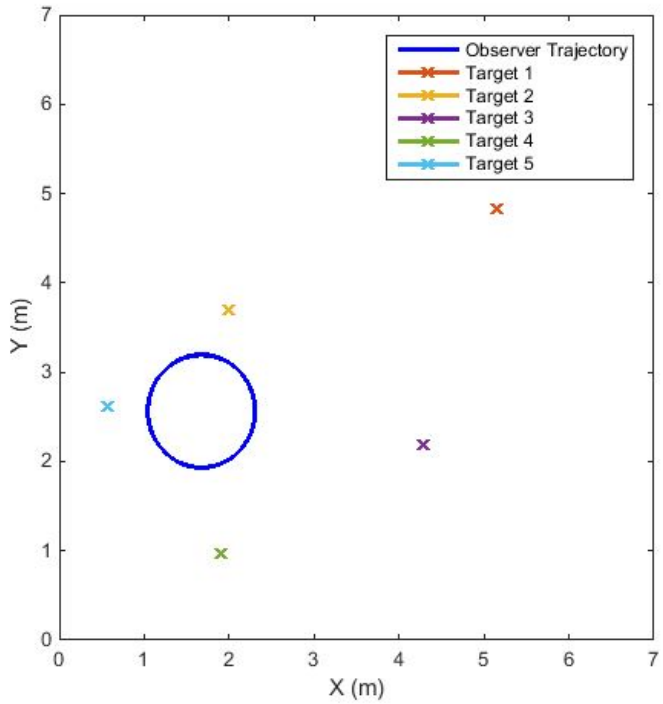

Figure 3.7: Simulation scenario of a single moving observer (blue track) and multiple targets (Crosses) around observer

As shown in the figure, blue circle indicates the path of the observer moving in anti-clockwise direction. Five crosses in the figure indicates the locations of the targets around observer. As before, all the targets are assumed to be stationary, whereas observer moves with a constant velocity of 2.8 m/s. Observer's motion is modeled using Coordinated turn model as given in Eq. 3.21 and 3.22. Whole simulation lasts for 2.5 seconds and

results are averaged after 1000 MC runs. A track is considered as divergent if its RMS position error exceeds a threshold of 10 m. Divergent tracks are not considered in final error computations but number of divergent tracks is recorded.

Although, we are mainly interested in Doppler based trackers but we would consider and compare all Bearing and Doppler filters for sense of completion and for further developments in next chapters. As we showed in previous sections that out of all Gaussian approximate filters, Unscented Kalman Filter (UKF) gives us most promising results, in terms of lower localization errors and divergent tracks. Therefore, in this section we only considered tracking results for Unscented Kalman Filter only.

Figure 3.8 contains the RMS position and velocity error results averaged after 1000 MC runs. From figures it is clear that observer has been able to successfully localize all targets, since it is meeting all the observability requirements. With bearings only measurements, RMS errors are bit high and targets were localized within 1.5 m radius. From Figure 3.8a it appears that filter converged to a steady state within 0.5 seconds but for some targets error remained more than 1 m. Figure 3.8b contains RMS errors for Doppler only case. This simulation shows very promising results, as for all targets filter was able to localize them within 50 cm radius in about 2.5 seconds. Also velocity errors are smaller than compared to Bearings only case. Finally Figure 3.8c contains the simulation errors for filter taking into account both Bearing and Doppler measurements. As with single target case, we have been able to localize all targets with very high accuracy in very short amount of time. As shown in the Figure 3.8c localization error reduces to less than 50 cm in about .75 seconds. Then this error continues to fall, reaching less than 20 cm for all targets in about 1 s.

From these and previous experiments, simulations and comparisons, we can conclude that it is possible to achieve high precision localization with Doppler only measurements. Moreover, this accuracy increases even further when we also start taking Bearing measurements into account besides Doppler measurements. This proves the efficacy of this Doppler only tracking technique. In next chapter, we would look into how these results can be exploited to our original problem of achieving inexpensive indoor localization.

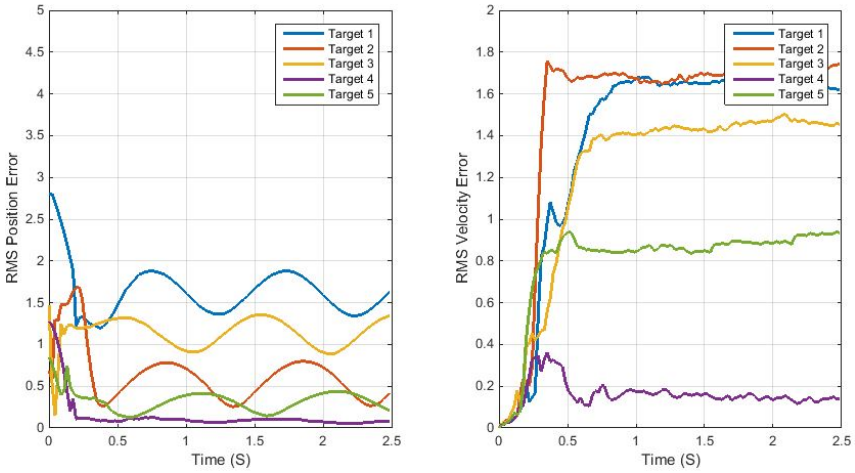

(a) Bearings-Only Tracking

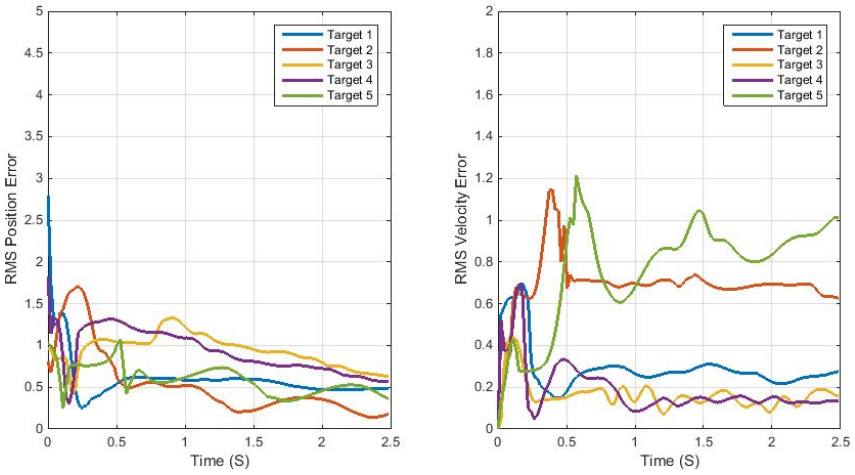

(b) Doppler-Only Tracking

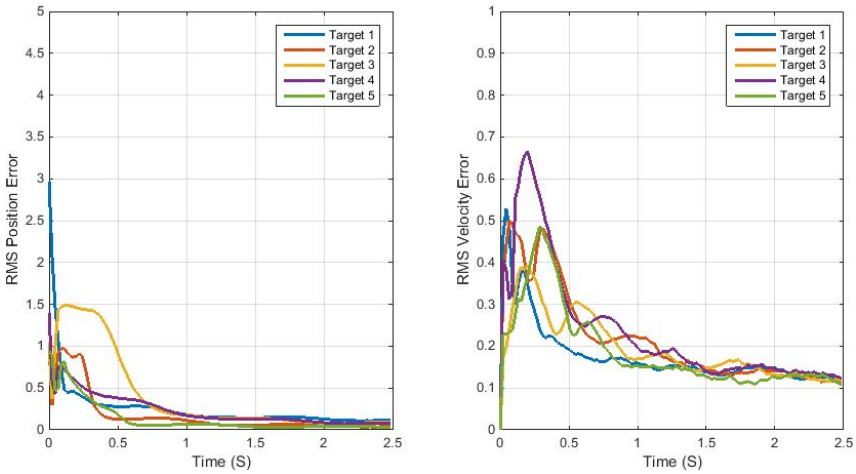

(c) Bearings-Doppler Tracking

Figure 3.8: Position & velocity error comparisons for different CT trackers

Chapter 4
Indoor Localization with Doppler Radar

4.1 Introduction

In previous chapters, we have focused our attention in finding the observability conditions based on Doppler-only and Bearing-Doppler measurements. Then formulated our problem in terms of Kalman Filter framework and tried to localize point-like targets. While localizing such targets, we assumed that radar can focus on them for all times during the localization process. In this chapter, we design systems and algorithms to localize walls and objects around a user. We start by mathematically formulating the problem and then figure out a solution to it. Once a frame work is defined, we discuss different scenarios of locating walls and doors in a generic room and measuring the performance of our algorithms.

4.2 Indoor Localization With a Doppler Radar

Assume a Continuous Wave (CW) Doppler radar is located inside a room with an area of 5×5 m. There's nothing inside the room and just four walls surrounding the observer. Based on available measurements and observability criteria, we want to find distance of surrounding walls from the observer. Once all the walls around observer are localized with high precision, further decisions like collision avoidance for inattentive worker or route-planning for robots/drones can be made. This scenario is depicted in Fig 4.1, where arrowhead shows the antenna direction in which beam is focused at any time instant.

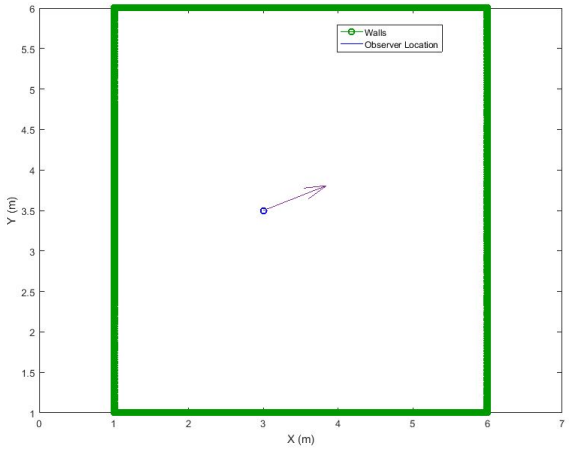

Figure 4.1: Observer and target's geometry for observability analysis

As shown before in Fig 2.2, observer moving along trajectory $\bar{r}_O(t)$ makes bearing (θ) (2.2) and frequency (f) (2.4) measurements of the target and tries to estimate its state. In order to localize walls, using only the frequency measurements, observer has to move around in a specialized manner, such that observability conditions are met. In previous chapter, we noticed that abrupt 90^0 maneuvers are not feasible in real world. However, we also showed that if observer moves in a circular pattern then all the observability conditions for bearing & frequency measurements are met. Therefore, in current scenario, let's assume that our CW Doppler radar is fixed on top of drone/UAV, which flies around in the room in a circular pattern. As drone flies around, the CW radar keeps on taking Doppler measurements. Figure 4.2 shows this scenario of a CW radar mounted drone flying in a 5×5 m room. Figure 4.3a shows the corresponding true range profile of walls from radar with respect to time, depending upon current position of radar in the room. Similarly, Fig 5.6 and 5.6 shows the Doppler velocity and bearing measurements obtained.

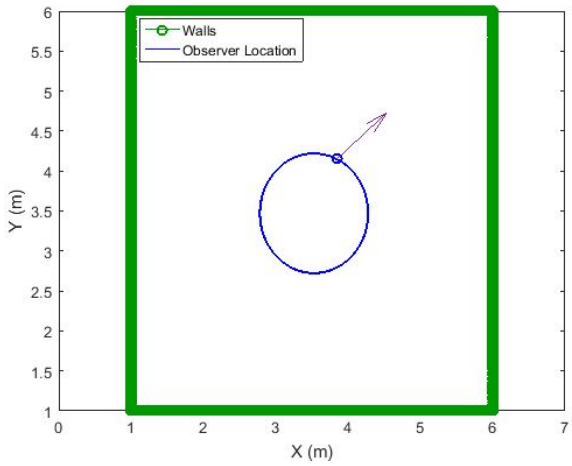

Figure 4.2: Example of drone with Doppler radar flying in circular pattern inside a 5×5 m room

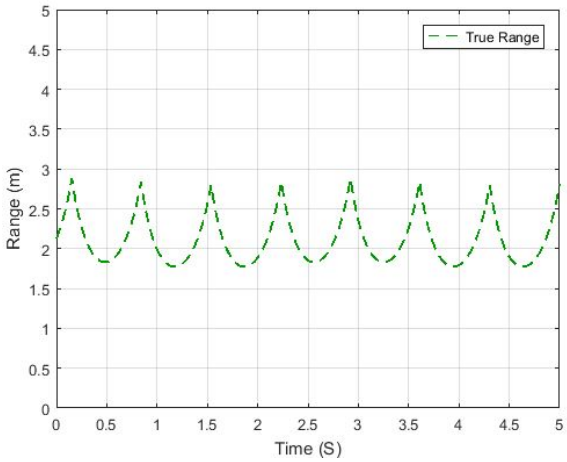

(a) True range of walls from radar as drone flies around

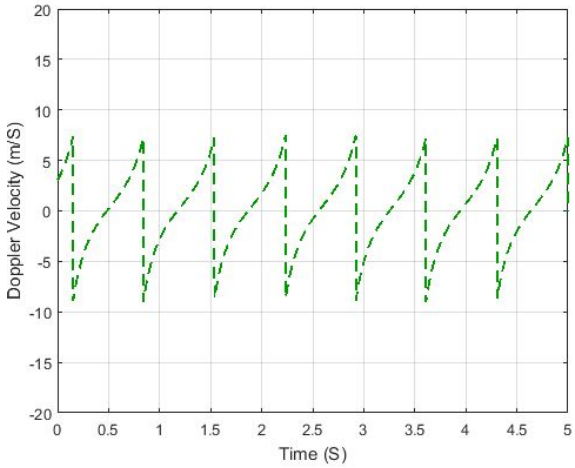

(b) Doppler velocity measurements

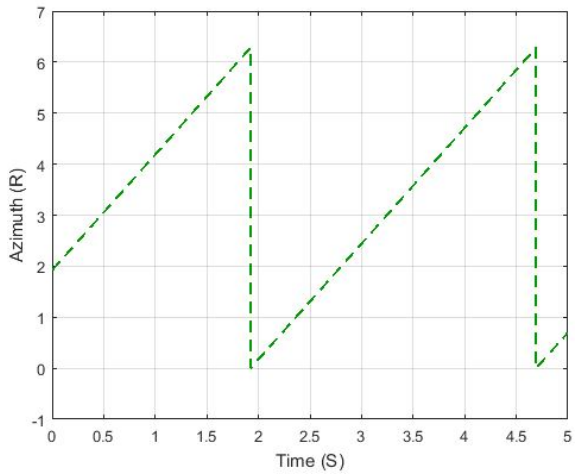

(c) Bearing measurements

Figure 4.3: True range profile, Doppler velocity and bearing measurements obtained as radar flies around in circular pattern inside a 5×5 m room

Looking at Fig 4.3a, we realize that target being tracked is highly non linear. To track such targets, we could incorporate higher derivatives in system's state space model such as '**acceleration** $= \frac{d^2\bar{r}(t)}{dt^2}$' [70, 92] or '**jerk** $= \frac{d^3\bar{r}(t)}{dt^3}$' [92, 98, 99]. One commonly used model for maneuvering targets is **Wiener-sequence acceleration model**. It assumes that target moves with some acceleration, where increments in this acceleration are modeled as independent white noise process. The state space model for this case therefore can be written as,

$$X[k+1] = F_a X[k] + G_a v[k] \tag{4.1}$$

where, F_a is state transition matrix. It is defined as,

$$F_a = \begin{bmatrix} F_{aa} & 0_{3\times3} & 0_{3\times3} \\ 0_{3\times3} & F_{aa} & 0_{3\times3} \\ 0_{3\times3} & 0_{3\times3} & F_{aa} \end{bmatrix}, \qquad F_{aa} = \begin{bmatrix} 1 & T & \frac{T^2}{2} \\ 0 & 1 & T \\ 0 & 0 & 1 \end{bmatrix} \tag{4.2}$$

where $0_{n\times m}$ is a $n \times m$ matrix of all zeros. The Gain matrix G_a is

$$G_a = \begin{bmatrix} G_{aa} & 0_{3\times1} \\ 0_{3\times1} & G_{aa} \end{bmatrix} \qquad G_{aa} = \begin{bmatrix} \frac{T^2}{2} \\ T \\ 1 \end{bmatrix} \tag{4.3}$$

v(k) is zero-mean white Gaussian process noise with variance σ_v. The covariance of process noise multiplied by gain G is given as,

$$\begin{aligned} Q_a &= E[G_a v(k) v(k) G_a'] \\ &= \sigma_v^2 G_a G_a' \\ &= \sigma_v^2 \begin{bmatrix} Q_{aa} & 0_{3\times3} & 0_{3\times3} \\ 0_{3\times3} & Q_{aa} & 0_{3\times3} \\ 0_{3\times3} & 0_{3\times3} & Q_{aa} \end{bmatrix} \end{aligned} \tag{4.4}$$

$$Q_{aa} = \begin{bmatrix} \frac{T^4}{4} & \frac{T^3}{2} & \frac{T^2}{2} \\ \frac{T^3}{2} & \frac{T^2}{2} & T \\ \frac{T^2}{2} & T & 1 \end{bmatrix} \tag{4.5}$$

Note that, as observer (radar) moves around, its line of sight angle keeps on changing. Moreover, because of radar's circular movement, the relative motion between the two also meets the required observability criteria. Therefore, we should be able to uniquely estimate target's range.

As before, measurement vector Z[k] is related to state X[k] through nonlinear function h() as,

$$Z[k] = h(X[k]) + w(k) \tag{4.6}$$

where $w(k)$ is zero mean white Gaussian observation noise with variance σ_w. h(.) is a nonlinear function of the state, whose value depends upon the measurements being considered.

- For Doppler or velocity (V_R) only measurements,

$$h(x[k]) = [\bar{V}_R] \tag{4.7}$$

- For bearings and velocity (V_R) measurements together,

$$h(x[k]) = [\theta, \bar{V}_R]^T \tag{4.8}$$

  where superscript T means transpose.

Covariance matrix R_{ww} of measurement noise is given by $\sigma_w^2 I$, where I is the identity matrix whose size depends upon h(x[k]), σ_w is standard deviation of measurement noise.

As before, the optimal Bayesian solution to the problem formulated would require computing posterior density $p(x[k]|z[k])$. However, the optimal solution for this problem cannot be obtained because measurement equation is nonlinear (4.6). Therefore, we will

have to suffice for suboptimal solutions and use filters developed for nonlinear systems as described earlier, i.e EKF, UKF, & CKF, etc. As shown in previous chapters that UKF consistently performed better, therefore we have used Unscented Kalman filter to track this accelerated target, first using Doppler measurements only and then using Bearing-Doppler measurements.

For simulations, we consider a generic room of 5×5 m with an observer randomly located at some point inside the room. The observer moves around in a circular path and takes Bearing and Doppler measurements. This scenario is depicted in Figure 4.4. Blue circular line shows observer's trajectory and arrow head shows the direction in which observer is looking at the moment. Note that Bearing measurements in this case would be the direction in which observer is currently looking or pointing. As walls are surrounding observer from all sides, so we would only consider that portion of wall as target which is in front of observer antenna at any given moment.

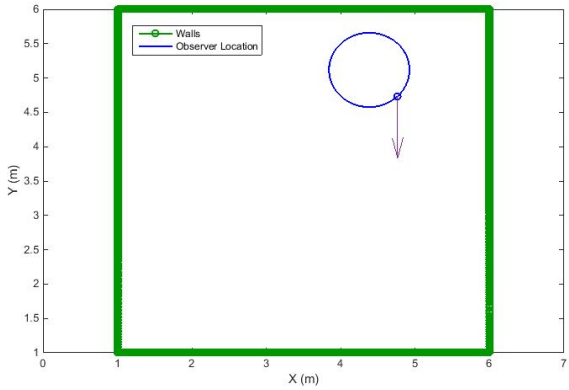

Figure 4.4: Randomly located Observer's trajectory inside a 5×5 m room

For an observer moving on a circular path and with changing Line of Sight (LOS) angle, it meets the basic observability requirement of both Doppler-Only and Bearing-Doppler case. Figure 4.5 contains the localization results for filter with Doppler-only measurements, whereas, Figure 4.6 contains results for filter with Bearing-Doppler measurements. Results are obtained after 1000 Monte-Carlo runs. Both filters converge to within few centimeters range error in only couple of seconds. Moreover, Bearing-Doppler filter converges faster than Doppler-only filter, as well as it has lower localization RMS errors. Although range error shoots a bit around corners but it also quickly reduces as

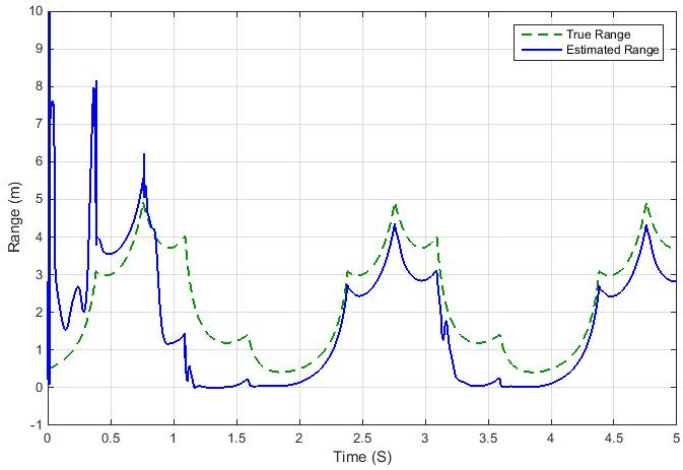

(a) Estimated range compared to true range

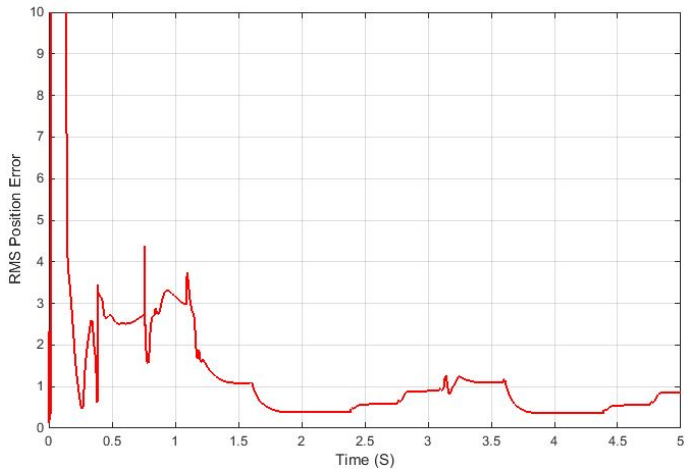

(b) RMS Position Error

Figure 4.5: Dynamic observer & static wall-targets: Error Comparisons for Constant Acceleration Doppler-only filter

new measurements arrive.

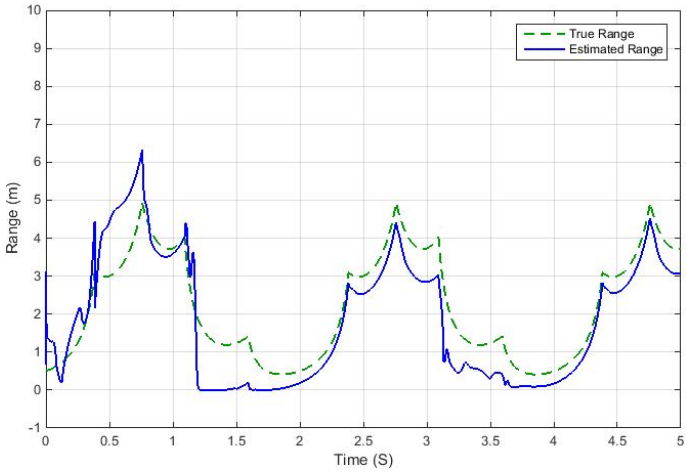

(a) Estimated range compared to true range

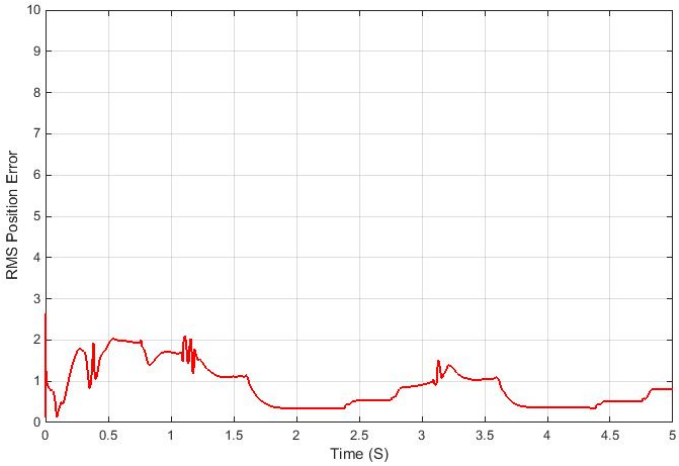

(b) RMS Position Error

Figure 4.6: Dynamic observer & static wall-targets: Error comparisons for Constant Acceleration Bearing-Doppler filter

4.3 Indoor Localization of Walls & Doors

We now turn to a more realistic situation of localizing walls as well as a door in the room and design filters that can better handle the nonlinearities in this case. Observer could move in any pattern inside the room to localize the walls and figure out the position of walls and door, as precisely as possible. A Doppler radar provides radial velocity depending upon relative dynamics between observer and target. In classical case, Doppler radar is stationary at a point, whereas, target being scanned moves towards or away from radar. On the other hand, in our case, walls and furniture in room is stationary whereas, radar moves around to create a relative motion between them. Now if radar moves in such pattern so that order of this relative dynamics meets the observability conditions, then true range of targets can be estimated just from Doppler-only measurements.

4.3.1 Constant-Acceleration Tracker Design

Consider the scenario of a $(5 \times 5)m^2$ room with a 1 m wide door that opens up into a long gallery, as shown in 4.7b. In this scenario, observer consists of a radar on a drone and pointing towards north-east corner of the room, whereas, target obviously consists of stationary walls surrounding the observer. The radar keeps on scanning and collecting measurements as the drone flies around. We know from our previous discussion that frequency measurements obtained from a circular moving Doppler radar meets all observability conditions. Therefore, in this scenario again we move radar in the circular pattern. Now as radar moves and scans from point A to B on the wall, it receives and detects Doppler velocity from the wall because of the relative motion between the two. Then at point B target would appear to make a sharp 90^o maneuver towards point C and so on.

With Bearings and Doppler measurements together, target is observable as long as LOS angle between observer and target doesn't remain constant. In our case, when radar starts scanning the walls, say in counter clockwise pattern, then obviously LOS angle keeps on changing. Moreover, since we know how radar is rotating, we can also find the relative bearing with high accuracy. In this case, it would be simply the bearing at which

the radar is pointing. This means that we could design a filter based on this inverse bearing and Doppler measurements, which would meet all observability requirements and we don't have to worry about target's dynamics order as well.

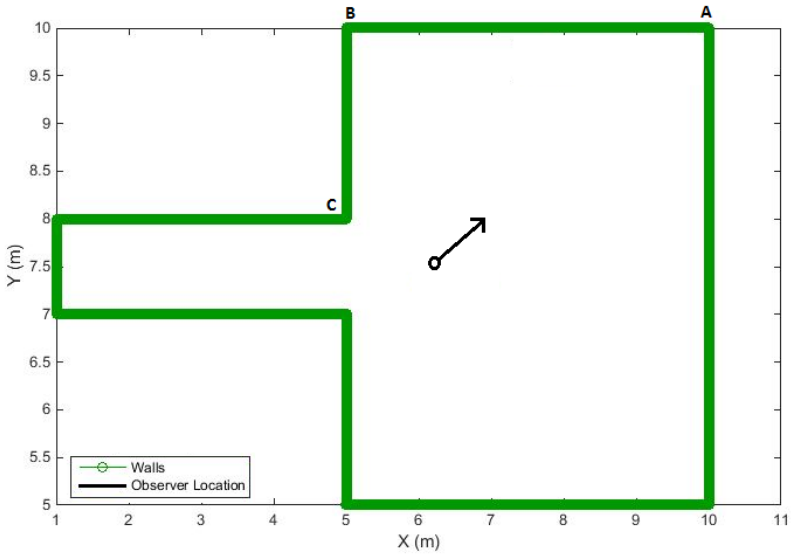

(a) Simulated room with door leading to a gallery on left side

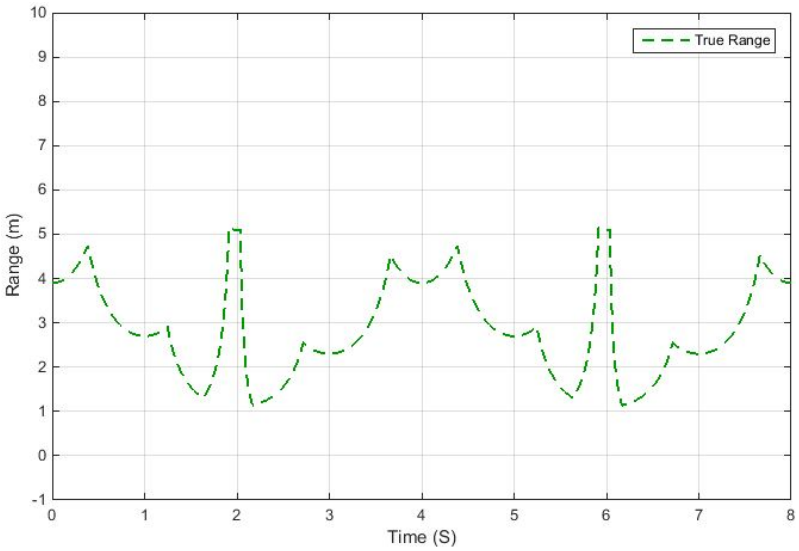

(b) True range of walls w.r.t observer as it moves around in the room

Figure 4.7: Dynamic observer & static wall-targets scenario

In simulations, we assume that a radar with a narrow beam scans the room in counter clockwise direction, starting at 0^o with respect to X-axis. Room's geometry for this case is shown in Figure 4.7a. It contains three walls on top, bottom and right hand side. A door leading into a gallery is assumed on left hand side. Arrow at observer's location indicates the direction in which radar is currently pointing. Figure 4.7b shows the true relative range of walls from radar as its beam scans in counter clockwise direction.

As before, angle is measured from positive x-axis. Note that in circular room's case, walls might appear as constant acceleration target and we could use either **Piecewise-Constant-Accelration Model** Eq. (3.8) or **Coordinated Turn Model** Eq. (3.21), as described in previous chapter. However, since in general rooms are rectangular, therefore, wall-targets would appear to maneuver at corners. To track such highly maneuvering targets, we could incorporate higher derivatives in system's state space model such as '**acceleration** $= \frac{d^2\bar{r}(t)}{dt^2}$' [70,92] or '**jerk** $= \frac{d^3\bar{r}(t)}{dt^3}$' [92,98,99].

One commonly used model for maneuvering targets is **Wiener-sequence acceleration model**. It assumes that target moves with some acceleration, where increments in this acceleration are modeled as independent white noise process. The state space model remains same as in Eq. (3.7), which is repeated here for convenience ,

$$X[k+1] = F_a X[k] + G_a v[k] \tag{4.9}$$

where, F_a is state transition matrix. It is defined as,

$$F_a = \begin{bmatrix} F_{aa} & 0_{3\times3} & 0_{3\times3} \\ 0_{3\times3} & F_{aa} & 0_{3\times3} \\ 0_{3\times3} & 0_{3\times3} & F_{aa} \end{bmatrix}, \qquad F_{aa} = \begin{bmatrix} 1 & T & \frac{T^2}{2} \\ 0 & 1 & T \\ 0 & 0 & 1 \end{bmatrix} \tag{4.10}$$

where $0_{n\times n}$ is a $n \times n$ all zeros matrix. The Gain matrix G_a is

$$G_a = \begin{bmatrix} G_{aa} & 0_{3\times1} \\ 0_{3\times1} & G_{aa} \end{bmatrix} \qquad G_{aa} = \begin{bmatrix} \frac{T^2}{2} \\ T \\ 1 \end{bmatrix} \tag{4.11}$$

v(k) is zero-mean white Gaussian process noise with variance σ_v. The covariance of process noise multiplied by gain G is given as,

$$\begin{aligned} Q_a &= E[G_a v(k) v(k) G_a'] \\ &= \sigma_v^2 G_a G_a' \\ &= \sigma_v^2 \begin{bmatrix} Q_{aa} & 0_{3\times3} & 0_{3\times3} \\ 0_{3\times3} & Q_{aa} & 0_{3\times3} \\ 0_{3\times3} & 0_{3\times3} & Q_{aa} \end{bmatrix} \end{aligned} \tag{4.12}$$

$$Q_{aa} = \begin{bmatrix} \frac{T^4}{4} & \frac{T^3}{2} & \frac{T^2}{2} \\ \frac{T^3}{2} & \frac{T^2}{2} & T \\ \frac{T^2}{2} & T & 1 \end{bmatrix} \tag{4.13}$$

In order to compare the two filters, namely Doppler-only measurements based and Bearing-Doppler measurements based, initial conditions for both filters were kept same. System is initialized with range along X and Y coordinates as 10m with Std. Dev. of 5m, velocity of 2m/s with Std. Dev. 2m/s, acceleration of $1m/s^2$ with standard deviation (Std. Dev.) $2m/s^2$. Process noise Std. Dev. is 5×10^{-2}. Bearing and Doppler measurement noise Std. Dev is 0.5^o and 0.01m/s, respectively.

Figure 4.8a shows the results for Doppler-only tracking. In the figure, broken-green line shows the true range where as solid-blue line shows the estimated range. Figure 4.8b shows RMS position errors. As expected, the range error reduces to less than a meter within 1 second as filter converges. RMS results were obtained for 100 MC runs. There were zero divergent tracks in 100 MC runs, where divergence threshold was selected as $10m$.

Figure 4.9a shows the results for Bearing-Doppler filter as radar scans the room. In this case, Bearing-Doppler tracker converges to within 1 meter of true range in about $1s$, as well. Results for RMS position errors computed using 100 MC runs are shown in Figure 4.9b. There were zero divergent tracks in 100 MC runs, where divergence threshold was selected as $10m$.

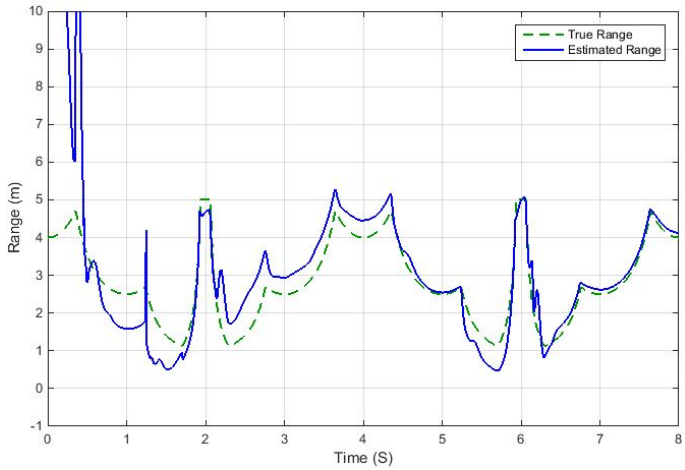

(a) Estimated range compared to true range

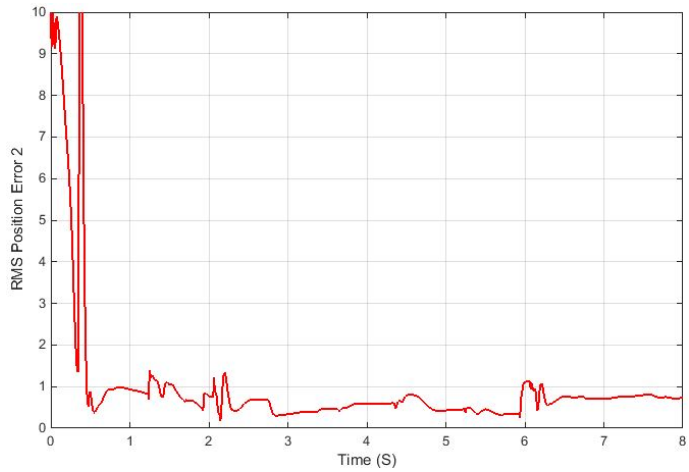

(b) RMS Position Error

Figure 4.8: Indoor Walls & Door Localization: Error Comparisons for Constant Acceleration Doppler-only filter

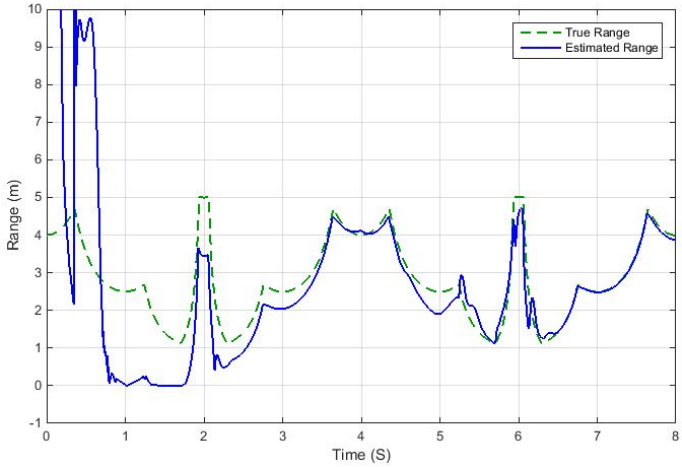

(a) Estimated range compared to true range

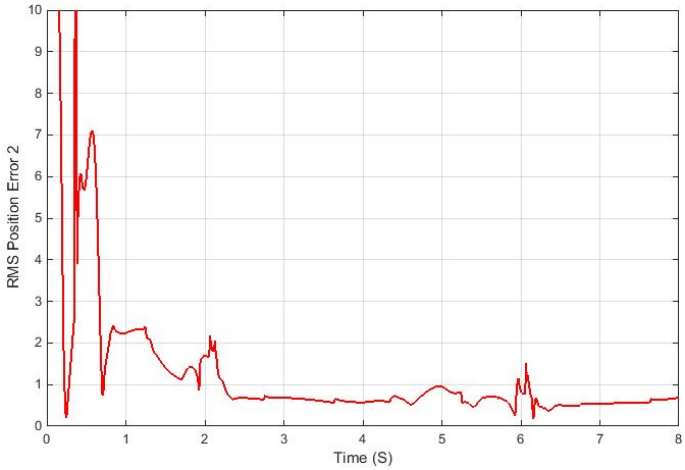

(b) RMS Position Error

Figure 4.9: Indoor Walls & Door Localization: Error Comparisons for Constant Acceleration Bearing-Doppler filter

4.3.2 Constant-Jerk Tracker Design

As we noted in previous section, corners in the room present themselves as highly maneuvering targets. This adds severe higher order derivatives in relative dynamics which can't be ignored. In previous design, we only considered dynamics model uptill 2 degrees i.e. velocity and acceleration. Although, we tried to handle the higher order effects as noise in the state space model, it appears that errors can only be reduced so much. In this section, we design another tracker that incorporates one more derivative of motion i.e. jerk. The model so obtained is referred to as constant jerk model in literature [92][98][99] and has been tried in some applications of tracking highly maneuvering targets.

State transition matrix for this model is given as,

$$F_j = \begin{bmatrix} F_{jj} & 0_{4\times4} & 0_{4\times4} \\ 0_{4\times4} & F_{jj} & 0_{4\times4} \\ 0_{4\times4} & 0_{4\times4} & F_{jj} \end{bmatrix}, \qquad F_{jj} = \begin{bmatrix} 1 & T & \frac{T^2}{2} & \frac{T^3}{6} \\ 0 & 1 & T & \frac{T^2}{2} \\ 0 & 0 & 1 & T \\ 0 & 0 & 0 & 1 \end{bmatrix} \tag{4.14}$$

where $0_{4\times4}$ is 4×4 matrix of all zeros. Covariance matrix equivalently now becomes,

$$Q_j = \sigma_v^2 \begin{bmatrix} Q_{jj} & 0_{4\times4} & 0_{4\times4} \\ 0_{4\times4} & Q_{jj} & 0_{4\times4} \\ 0_{4\times4} & 0_{4\times4} & Q_{jj} \end{bmatrix} \tag{4.15}$$

$$Q_{jj} = \begin{bmatrix} \frac{T^7}{252} & \frac{T^6}{72} & \frac{T^5}{30} & \frac{T^4}{24} \\ \frac{T^6}{72} & \frac{T^5}{20} & \frac{T^4}{8} & \frac{T^3}{6} \\ \frac{T^5}{30} & \frac{T^4}{8} & \frac{T^3}{3} & \frac{T^2}{2} \\ \frac{T^4}{24} & \frac{T^3}{6} & \frac{T^2}{2} & T \end{bmatrix} \tag{4.16}$$

Rest of the design and conditions remains same as mentioned in previous tracker's case. Simulation results of tracking wall position relative to observer are shown in Figure

4.10a, where estimated range (solid-blue line) is compared with true range (broken-green line). RMS position errors are shown in Fig. 4.10b. As expected, errors are considerably smaller with constant jerk model. In this case, range error even reduces to less than 100 cm. Results were averaged after 100 MC runs. Moreover, there were zero divergent tracks out of the 100 MC runs.

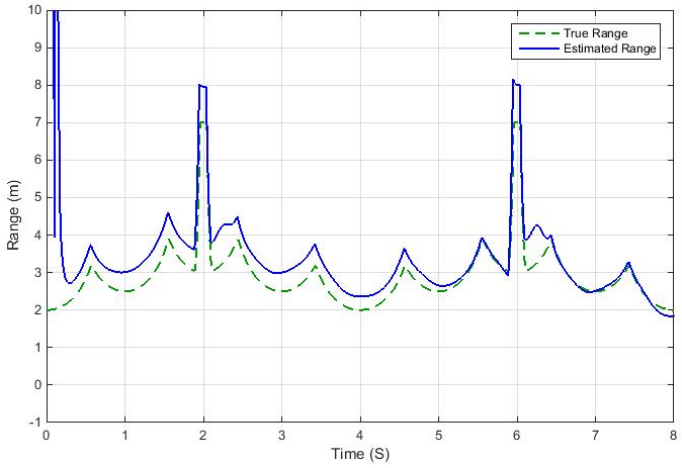

(a) Estimated range compared to true range

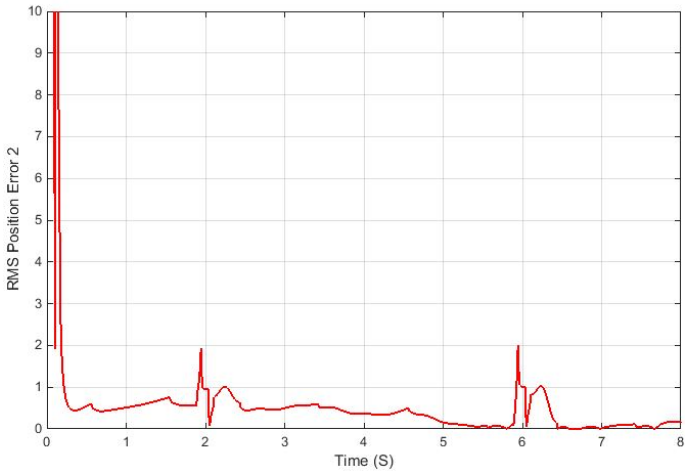

(b) RMS Position Error

Figure 4.10: Indoor Walls & Door Localization: Error Comparisons for Constant Jerk Bearing-Doppler filter

4.3.3 Coordinated-Turn Tracker Design

Upon close observation of true relative range profile in Figure 4.7b, curves and arcs are obvious. In traditional target tracking, this type of range profile is obtained when target is under coordinated turn maneuver [92]. Many dynamic models have been proposed to track such targets. Out of these models, ones that have survived the test of time are Coordinated turn models with either known or unknown target-turn rates[92][96][97]. These can be further classified as in Cartesian or Polar form. Thorough research on these models have enabled the deep understanding of their applicability and usage.

We can model our system using Coordinated turn model. For problem at hand, since turn rate is unknown therefore we can augment it as another parameter to be estimated in the state space model. Let x and y denote target's position in Cartesian coordinates; V_x and V_y denote velocity components along x and y axis; h denote the heading angle and ω denote the turn rate.

$$h = atan2(V_y, V_x) \tag{4.17}$$

$$\omega = \frac{dh}{dt} \tag{4.18}$$

State vector in this model now becomes,

$$X[k] = \begin{bmatrix} \text{x position} \\ \text{y position} \\ \text{speed} \\ \text{heading angle} \\ \text{turn rate} \end{bmatrix} = \begin{bmatrix} x \\ y \\ v \\ h \\ \omega \end{bmatrix} \tag{4.19}$$

Corresponding differential equation for this case is given as,

$$X[k+1] = f_p(X[k]) + G(X[k])v[k] \tag{4.20}$$

$$Z[k] = h(X[k]) + w(k) \tag{4.21}$$

where $f_p(x)$ is,

$$f_p(x) = \begin{bmatrix} x + \frac{2v}{\omega}\sin(\frac{\omega T}{2})\cos(h = \frac{\omega T}{2}) \\ y + \frac{2v}{\omega}\sin(\frac{\omega T}{2})\sin(h = \frac{\omega T}{2}) \\ v \\ h + \omega T \\ \omega \end{bmatrix} \tag{4.22}$$

Equation (4.19) and (4.22) are described in much detail in [70][92][96][97]. Rest of the design and conditions remains the same as mentioned in previous case studies. Simulation results of tracking walls relative to observer are shown in Figure 4.11a, where estimated range (solid-blue line) is compared with true range (broken-green line). RMS position errors are shown in Fig. 4.11b. As expected, errors are considerably smaller with this model. Results were averaged after 100 MC runs. Moreover, there were zero divergent tracks out of the 100 MC runs.

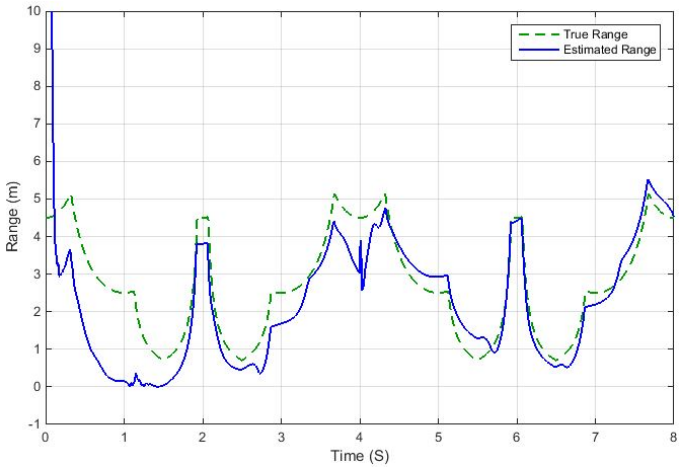

(a) Estimated range compared to true range

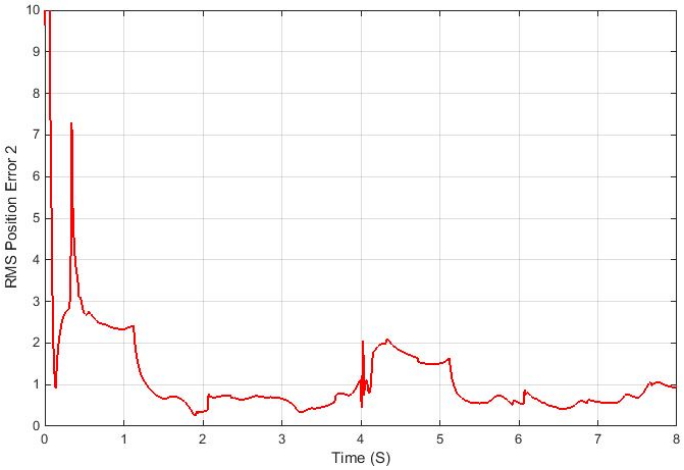

(b) RMS Position Error

Figure 4.11: Indoor Walls & Door Localization: Error Comparisons for Coordinated-Turn Bearing-Doppler filter

Chapter 5
Smart Helmets: Sensing for Safety

5.1 Introduction

Information and communication technologies have entered every aspect of our daily lives - changing forever the way people interact, communicate and work. With stakes being invested everyday, much has been accomplished in increasing the productivity and quantity of work. However, unfortunately little has been done in improving a worker's safety. The importance of following work procedures and regulations at such places cannot be over stressed. Nevertheless accidents, injuries and claims are rampant, resulting in ever increasing compensations and work delays.

All the statistics and analysis point out an important fact that manual implementation of OHS rules and regulations is not enough. ICT technologies must be involved and integrated into a worker's daily life specifically targeting their safety. According to Occupational Health and Safety (OHS) regulations [100–103], workers must wear specialized personal protective equipment (PPE) whenever they are on work sites. Aim of this research is to figure out a way to integrate specialized sensors in this safety equipment - enhancing workers' situational awareness. Since PPE is already heavy enough, therefore, one target is that these sensors should be light enough so as not to add any more weight. Moreover, these should be robust enough to handle the different rough and rugged work conditions.

In this chapter, we look at challenges of developing such sensors and possibilities of integrating them into safety equipment. We perform various simulations, to check out the localization performance of our framework. In previous chapters, we have de-

rived the observability conditions for Nth-order dynamics systems in case of Bearings and Doppler measurements. Then we designed different filters meeting the observability criteria and developed case studies to gauge their performance. Simulation analysis verified the theoretical claims about observability. Moreover, Unscented Kalman Filter consistently performed better, in sense of lower RMS error and lesser divergent tracks. In this chapter, we now turn to our attention towards a more practical application of sensing for workers' safety in dangerous work environments.

Requirements of Sensing for Safety

Personal Protective Equipment (PPE) refers to the safety clothing, helmet, goggles, ear muffins or other protective gear that workers must wear on dangerous work environments. Some examples of PPE include high visibility reflective clothing such as vests, wide brimmed hats and hard hats to minimize bodily damage. Ear plugs or ear muffs are commonly used to minimize the risk of exposure to excessive noise. These are the lowest order control steps in the hierarchy of safety measures and are used as increased protection from the hazard. However, PPE relies only on the awareness and proper fit of the user and does nothing to minimize the danger or hazard itself. This means that the users require thorough training and active supervision to ensure compliance and effectiveness.

Hazard localization

As mentioned earlier that some of the main reasons of injuries and fatalities are

- Collision with a moving object (Vehicle, crane, etc)
- Falling from heights (marked, monitored or unmonitored)

Regardless of being in use for decades, PPEs are not smartly designed. For example, consider the scenario of a construction site, where a dumper is reversing with workers working nearby, Figure [5.1]. Although heavy machinery like a dumper or excavator uses high pitched beeping tone when moving around but then OHS regulations requires

workers to wear ear muffs when working in a noisy environment. Contradiction like this leads to numerous fatalities each year.

Figure 5.1: Unaware worker in blind spot of a reversing dumper

To minimize a hazard, first step is to localize it accurately & precisely. In previous chapters, we successfully localized surrounding walls and targets using CW Doppler radars. To this end, a drone carrying the radar had to fly around to create relative Doppler frequency, between itself and targets. Our aim in this research is to add and integrate these tiny CW Doppler radars on the already used PPEs so that,

- it can enhance a Workers' situational awareness
- it should only add negligible weight to PPE
- it should only add negligible cost to overall PPE cost
- it can provide feedback to a worker in face of eminent danger
- it used should be rugged enough to withstand rough condition of dangerous working environments

First logical question should be as where on a worker to put this miniature radar? According to OHS regulations, everyone on the dangerous work sites must wear a hard

hat. At the moment, these hats are only made up of hard plastic, with sole purpose to avoid an injury to head in case of an accident. Our idea is to make these helmets smart by adding radars to sense the surrounding environment and providing feedback to user in case of danger. Being lightweight, these CW radars won't add any significant weight to these hats. Moreover, being cheap, they won't add any significant cost for mass production.

5.2 Smart Helmets

Target localization using CW radar placed on a worker's hard hat has two main challenges,

- How to place Doppler radar on a hard hat to localize objects surrounding the user?
- How to provide feedback to the user in case of imminent danger?

After localizing the targets, providing feedback to the user is also a major research and design problem. One possible way could be play a beeping sound in left ear if something is approaching at high speed from left. In case of rescue operations in low visibility, a rescue worker could be handed a smartphone which shows the sensed environment. However, providing feedback and related work will be handled in future. In this chapter, we focus our attention to localizing targets by assuming that radar is fixed on a hardhat. This means that a person wearing the hardhat can randomly move around, wobbling his head. The question is that under such random movements is it still possible to localize targets? We already know that if observer moves around in circular pattern, obtaining Doppler frequency measurements from stationary surrounding targets then, we can estimate true range. However, that would not be a very feasible situation for workers. In next section we propose a method of obtaining instantaneous frequency measurements from changing phase of the returned waveforms in a CW radar.

5.3 Radar Phase Rate

Consider a continuous wave radar that's transmitting towards and receiving back echoes from a room wall, as shown in the Figure 5.2.

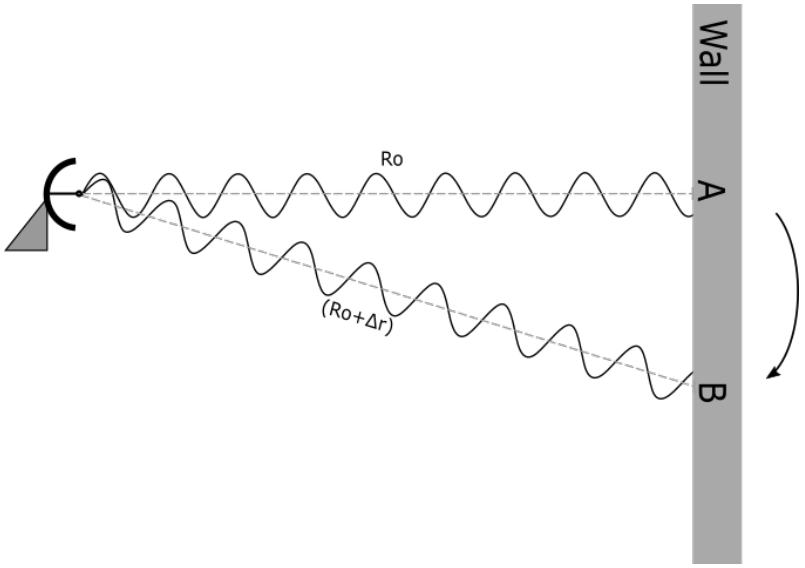

Figure 5.2: Radar transmitting towards a wall and receiving back echoes.

If R is the distance from radar to a point A on the wall then total number of wavelengths λ contained in the two-way path is given as,

$$\text{Total wavelengths between radar and wall} = N = \frac{2R}{\lambda} \tag{5.1}$$

One wavelength corresponds to an angular distance of 2π radians. Now as electromagnetic wave moves during its transit to and from the wall, it covers a total of $2\pi N$ radians. Therefore,

$$\text{Phase} = \phi = 2\pi\left(\frac{2R}{\lambda}\right) \tag{5.2}$$

Now as in classical case, if target is moving then its distance R from radar and phase ϕ are continuously changing. A change in phase with respect to time is called angular

frequency. In case of moving target it is the well-known Doppler angular frequency. However, in our case wall is not moving.

On the other hand, if the radar rotates and focuses now on point B then total distance between radar and target has changed again, as shown in Figure 5.2. This in turn leads to a change in phase. As before when considered with respect to time, it gives us instantaneous angular frequency ω_ϕ,

$$\begin{aligned} \omega_\phi &= \frac{d\phi}{dt} \\ \omega_\phi &= \frac{4\pi}{\lambda}\frac{dR}{dt} \\ \omega_\phi &= \frac{4\pi}{\lambda}V_\phi \\ 2\pi f_\phi &= \frac{4\pi}{\lambda}V_\phi \\ f_\phi &= \frac{2V_\phi}{\lambda} \end{aligned} \tag{5.3}$$

where V_ϕ represents range rate and f_ϕ represents the frequency obtained because of rate of change of phase.

Figure 5.3a shows a simulation of a CW radar inside a 5x5 meter room. Arrow head depicts the direction in which radar is currently pointing. As radar beam sweeps around, the phase of the returned wave keeps on changing, generating a frequency f_ϕ and phase velocity v_ϕ. Although similar in expression to Doppler frequency-velocity relation, here we obtained a frequency-velocity relation that is dependent upon radar's rotation rate. Figure 5.3b shows the range profile obtained with respect to radar as its antenna rotates, whereas, figure 5.3c shows the corresponding phase velocity profile.

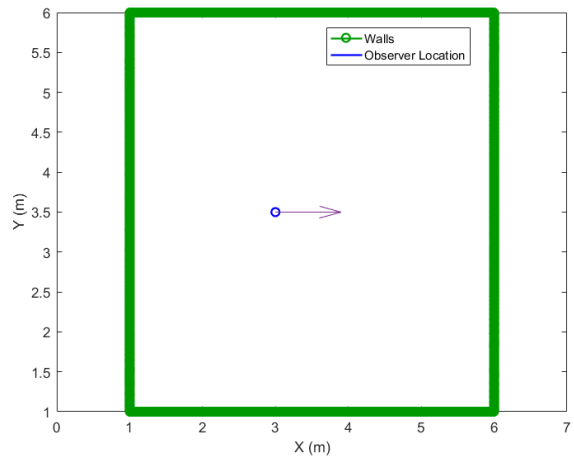

(a) Estimated Range Comparison

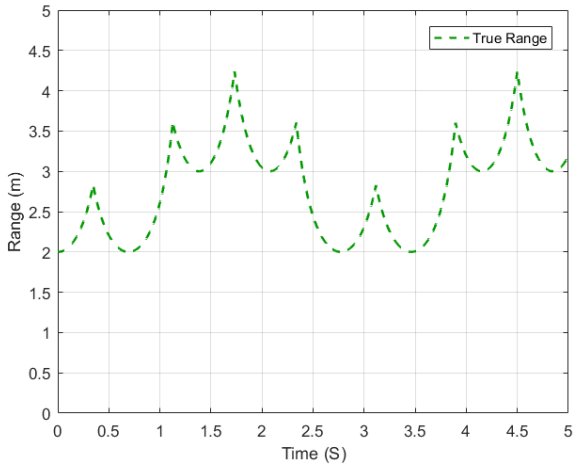

(b) RMS Position Error

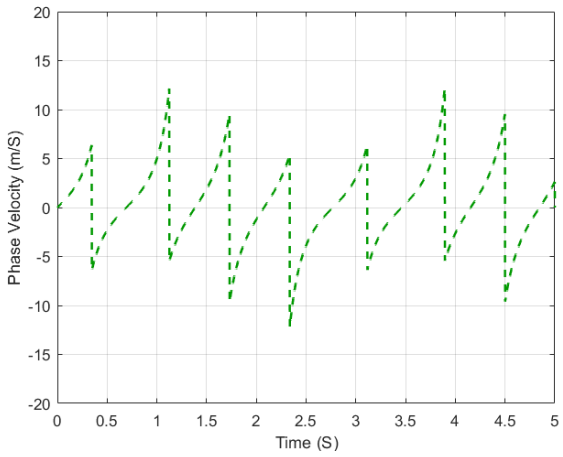

(c) RMS Velocity Error

Figure 5.3

Note that we not only have frequency measurements of the target but also the bearing measurements. It's because in this case target bearing at a given instant would be the angle at which radar antenna is pointing. Figure 5.4 shows the corresponding bearing profile that we obtain from our simulation of the rotating radar.

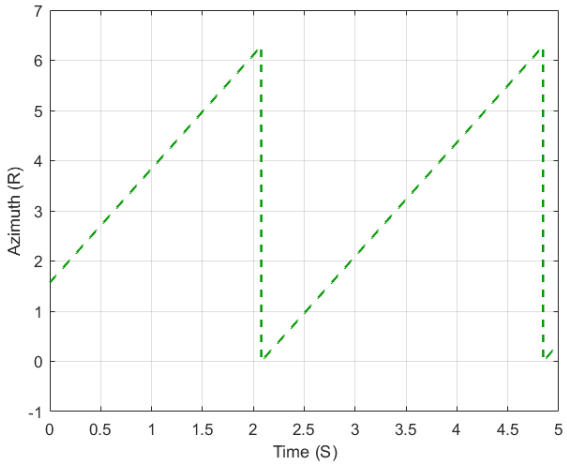

Figure 5.4: Radar transmitting towards a wall and receiving back echoes.

Now that we have frequency and bearing measurements, we can use this information to estimate a target's true range.

5.4 Design of Smart Helmet

Sensing the environment using a light-weight & inexpensive CW radar, by attaching it to a worker's hard hat, has some very intriguing issues. For example, instead of putting one rotating antenna on top of the hat, one can use a phased-array antenna with elements around the hat's brim, as shown in Figure 5.5. Then we can trigger each antenna element sequentially one after the other. This way we can get 360^0 measurements easily without any moving part plus we can easily control the rate of rotation.

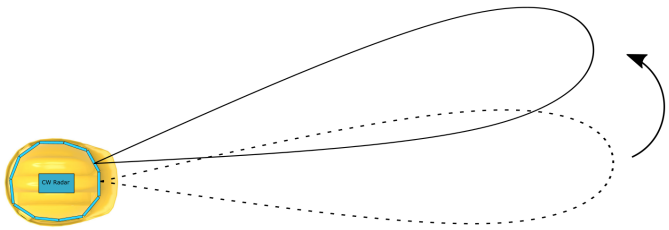

Figure 5.5: Example of a CW radar mounted on a worker's hat with phased array antenna elements around the brim of the hat

Human head movements could act as a potential source of noise during phase comparison of the returned waveform. However, we have assumed that such movements would not effect our phase measurements. It is because during normal movements, human head typically can move about 2-3 cm in any direction. If we consider a typical indoor distance of say 10m, then an electromagnetic radar wave would take only about 66.67 ns to return to the radar after reflection from wall. Now even if the radar spends say 150ns at one point measuring the phase and then 150 ns at next point, then in 300 ns human head could only have moved negligible distance. Hence we can ignore such movements at this stage.

5.5 Indoor localization with CW Radar

Without the loss of generality, assume a point-like observer 'O' and target 'T'. We assume observer to be located inside a room of size 5×5 m, having a door leading to a hallway on left hand side. It is assumed that radar is fixed on top of a worker's hard hat. The worker itself moves around randomly, whereas, the radar on top of observer takes 360^o measurements (Bearings and Doppler Frequency) of its surroundings. This means that we now have to consider the following movements as well,

- user's head movements and wobbliness
- user's walking or running movements

Everything surrounding the observer would be a potential target. From the observability conditions and filters designed in previous chapters, we now have a framework of

localizing the walls and objects around an observer. Measurement vector Z[k] is related to state X[k] through nonlinear function h() as,

$$Z[k] = h(X[k]) + w(k) \tag{5.4}$$

where $w(k)$ is zero mean white Gaussian observation noise with variance σ_w. h(.) is a nonlinear function of the state and for bearing & phase velocity measurements, it is given as,

$$h(x[k]) = [\theta, \bar{V}_\phi]^T \tag{5.5}$$

Simulation Results: Randomly moving worker with CW radar

Average walking speed of humans is about $3mph$ or $5kmph$. However, we should note that a worker can randomly start moving from anywhere between standing-still at one second to running at the next. Therefore, the idea in this simulation is to allow observer to move randomly at average human speed with variance of about $5kmph$. We use the **Constant-Acceleration Tracker** [4.3.1] designed in previous chapter, based on **Wiener-sequence acceleration model**. Observer is also moving randomly with velocity standard deviation of $5kmph$. Rest of the simulation settings and parameters remains the same as in previous chapter.

Figure [5.6a] shows result of one of the possible worker's trajectories. In the figure, blue line depicts worker's trajectory whereas, surrounding walls are depicted in green. As the worker moves around, CW radar rotates 360^o obtaining bearing and phase measurements simultaneously.

Figure [5.6b] shows the actual distance of walls from observer at each point compared with estimated distance. We can see that the range error is quite large at start but it starts decreasing - reaching within few cms after 2-3 seconds. Figure [5.6c] shows RMS position errors for 100 MC runs. We can also notice some estimation errors around door. It's

because the door appears as high maneuvering target to the tracker, but given that we are meeting observability conditions, filter converges to the original range quickly.

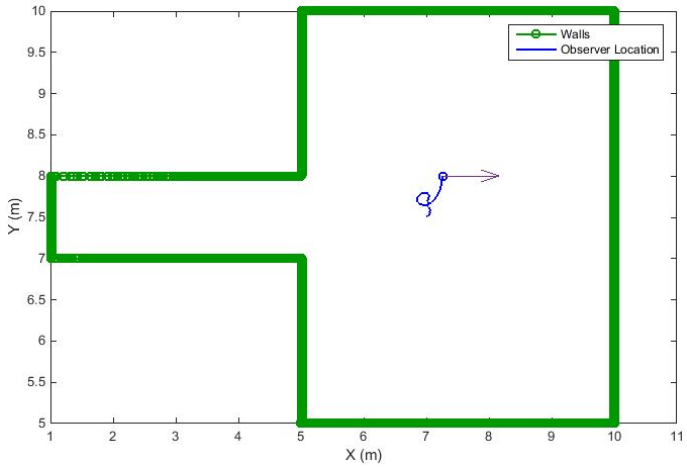

(a) Worker (Blue) wearing smarthat and randomly moving inside a room (Green)

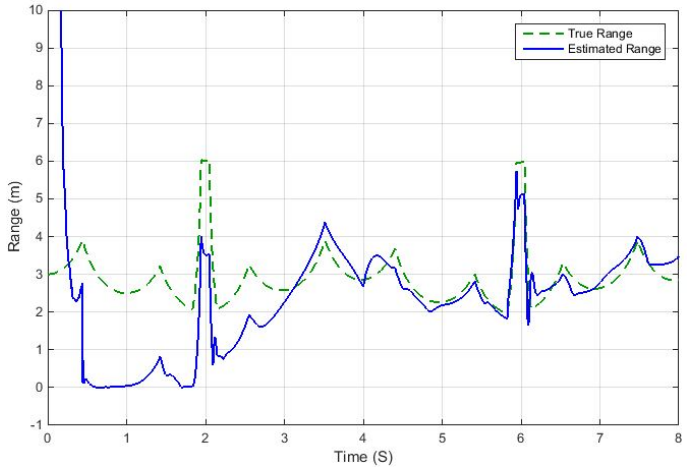

(b) Estimated range compared to true range

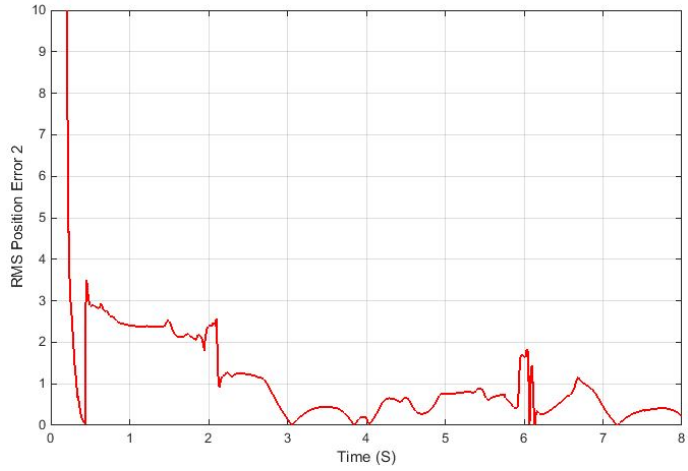

(c) RMS Position Error

Figure 5.6: Error Comparisons for randomly moving worker using Tracker-1 (Section-4.3.1)

By looking range profile of walls with respect to radar, it appears that surrounding walls present themselves as highly maneuvering targets to a dynamic observer whose head is also randomly moving. In section [4.3.2], we derived a **Constant-Jerk model** to handle such nonlinearities in target motion and to get better range estimation - lowering RMS errors. Observer and target's state space equation and simulation parameters remain same as before. However, tracker's state space model now incorporates 3rd derivative of position, as shown in Eq. 4.14. Remaining simulation parameters and setting are same as in previous simulation. Fig. 5.7 below shows the results, where Figure [5.7a] is just another example of possible random movements in the room. However, looking at RMS Position Error plot in Figure [5.7b], the improvement in estimation by including the Jerk parameter is pretty obvious. Not only the filter converges to within few cms of actual range in less than a second but also it remains low even after high nonlinearities near doorways.

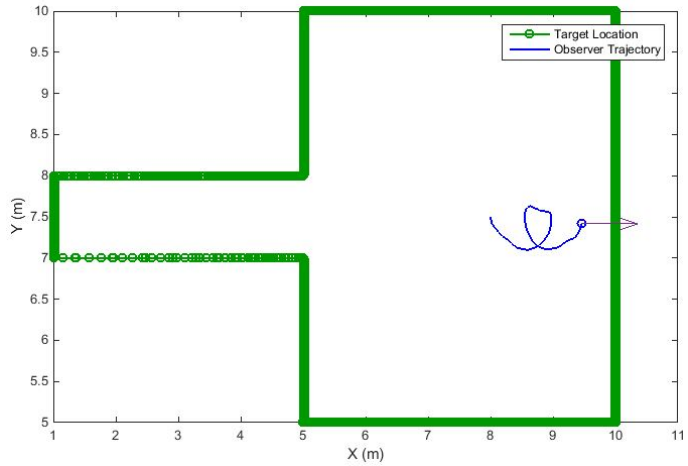

(a) Worker (Blue) wearing smarthat and randomly moving inside a room (Green)

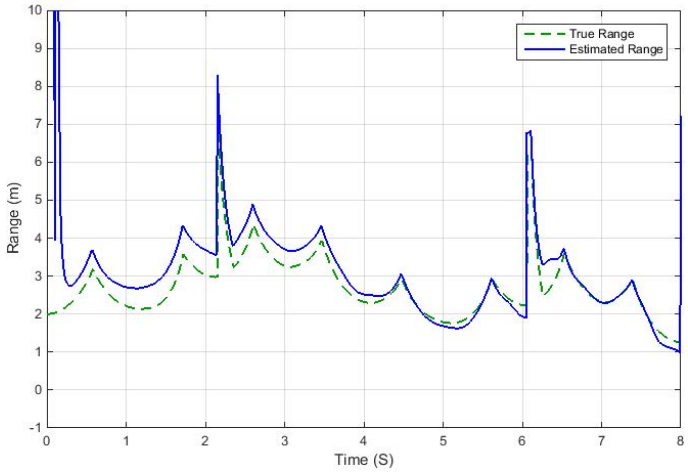

(b) Estimated range compared to true range

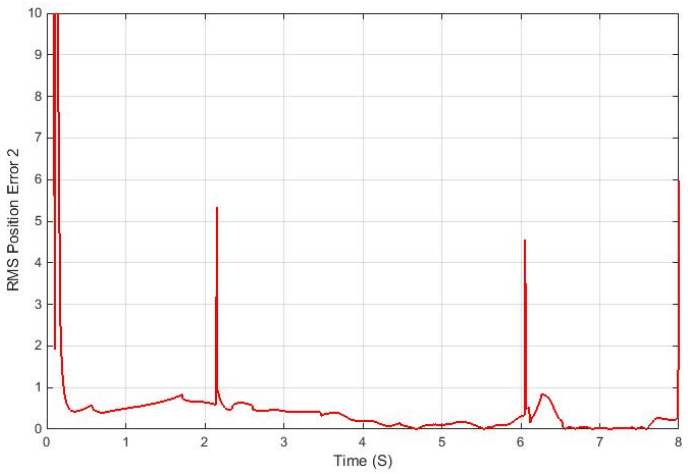

(c) RMS Position Error

Figure 5.7: Error Comparisons for randomly moving worker using Tracker-2 (Section-4.3.2)

Although random human motions and movements add vulnerabilities to our trackers but simulations verify that such random movements can be handled easily through added noise in system, therefore filters converge to true values. Just as before Constant-Jerk filter outperforms the Constant-Acceleration filter. However, former also has more computations and added complexity. It then depends upon the final system and it's application as to prefer accuracy vs computational complexity. One point to note is that constant jerk filter also converges much faster than the constant acceleration filter, where the former takes less than a second whereas, later takes 3 seconds on average in our case studies.

5.6 Performance Improvement using Amplitude of Received Signal

As Kalman filter based algorithms are recursive, so they need a starting point to initiate the recurrence. If estimation errors of such filtering algorithm are compatible with those represented by covariance matrix then filter is said to be *consistent* [70]. Consistency as defined here also implies that the mean and covariance estimate of the posterior PDF satisfy [73],

$$trace\left[P_{XX} - E\left[(X-\hat{X})(X-\hat{X})^T\right]\right] \geq 0 \tag{5.6}$$

where $(X - \hat{X})$ represents the state estimation error. Therefore, at initialization it is just as important that filter's covariance associated with the initial estimate efficiently reflects its accuracy. In Bayesian estimation, initial state is a random variable and it is assumed to have Gaussian distribution with known mean and covariance. In case of linear systems with Gaussian noise, initial conditions doesn't really effect stability of the filter, other than that it delays the convergence. This initialization can be achieved in a variety of different ways, for example, through geometric or probabilistic approaches. In its original implementation Kalman assumed that mean and covariance of initial state are known. In case where true initial state parameters are not known and one randomly makes the initial variance too large then filter would take a large time to converge. Espe-

cially if observations are themselves noisy and are not frequently available.

Unlike their linear counterparts, convergence and stability of nonlinear filters is quite sensitive to proper initialization. If covariance matrix is initialized with large values than nonlinear filters in general and Extended Kalman filter in specific easily diverges or converge to a wrong estimate. One remedy to this divergence issue is to restart the algorithm as soon as covariance matrix values becomes too large, but obviously this is not a solution. In many application, filters are initialized using a different sensor which provides a good enough starting point. Or in some cases, algorithms use first few measurements to get an estimate of starting point. In most cases, researchers derive the initial conditions depending upon geometry of the problem. As mentioned earlier, in our case we assumed that observer and target are located in a 5x5 m room. Therefore, we initialized the filters with a range variance of about 9 m. Results with this initialization were discussed in previous section. Of all the Gaussian approximate methods that we implemented, EKF diverged about 20%, whereas, UKF and CKF only diverged only about 0.4% of all runs.

Although our initialization strategy worked pretty well, but obviously one assumption about a general room size would not suit all environments. Therefore, we need another strategy to initialize the filter. As mentioned earlier, now a days with advancement in electronics and fabrication technology, one can easily get a CW Doppler radar for few dollars, either online or off the counter. In our system, we are already using one radar to obtain radial velocity information. The power of the signal received by the radar is inversely proportional to the range of the target as follows [90]

$$P_{R_1} = \frac{P_T G^2 \lambda^2 \sigma}{(4\pi)^3 R_1^4} \tag{5.7}$$

where,

- P_{R_1} is Power received at the radar,
- P_T is Power transmitted by the radar,
- G is the antenna gain

- λ is the radar operating wavelength
- σ is the radar cross section of the target
- R_1 is the range of target from radar

Now assume another CW radar placed side by side with our first radar and displaced by a small distance Δr. If we assume that two Doppler radars are identical, then the power received at this second Doppler radar from the same target at the same instant could be obtained as,

$$P_{R_2} = \frac{P_T G^2 \lambda^2 \sigma}{(4\pi)^3 R_2^4} = \frac{P_T G^2 \lambda^2 \sigma}{(4\pi)^3 (R_1 + \Delta r)^4} \tag{5.8}$$

where,

- P_{R_2} is Power received at radar 2,
- R_2 is the range of target from radar

From equations 5.7 and 5.8 we can write that,

$$\frac{P_{R_1}}{P_{R_2}} = \frac{P_T G^2 \lambda^2 \sigma (4\pi)^3 (R_1 + \Delta r)^4}{P_T G^2 \lambda^2 \sigma (4\pi)^3 R_1^4} = \frac{(R_1 + \Delta r)^4}{R_1^4} \tag{5.9}$$

We can use Binomial theorem to expand the powered Binomial term in equation 5.6. The formal expression for Binomial theorem is given as,

$$(a+b)^n = \sum_{k=0}^{n} \binom{n}{k} a^{n-k} b^k \tag{5.10}$$

$$\binom{n}{k} = \frac{n!}{(n-k)!k!} \tag{5.11}$$

Using Binomial theorem to expand the fourth powered term in numerator, we can

write,

$$\begin{aligned}
\frac{P_{R_1}}{P_{R_2}} &= \frac{\sum_{k=0}^{4} \binom{4}{k} R_1^{4-k} (\Delta r)^k}{R_1^4} \\
\frac{P_{R_1}}{P_{R_2}} &= \frac{R_1^4 + 4R_1^3(\Delta r) + 6R_1^2(\Delta r)^2 + 4R_1(\Delta r)^3 + (\Delta r)^4}{R_1^4} \\
\frac{P_{R_1}}{P_{R_2}} &= 1 + \frac{4}{R_1} + \frac{6}{R_1^2} + \frac{4}{R_1^3} + \frac{1}{R_1^4}
\end{aligned} \tag{5.12}$$

Ignoring 2nd and higher order terms and rearranging the above equation, we can obtain R_1 as follows,

$$R_1 = \frac{4\Delta r}{\frac{P_{R_1}}{P_{R_2}} - 1} \tag{5.13}$$

This shows that we can use the amplitude information in the returned radar signals to derive pretty close estimate about initial range by using only one additional radar. This rough estimate when used to initialize the filters to begin the recursion, reduces the convergence time significantly. Figures [5.8] & [5.9] shows the tracking results after incorporating the above method of initialing the trackers. Looking at the range and velocity RMS error plots in Figures [5.8a] & [5.8b], we can easily see the effect of proper initialization in case of Constant Acceleration Model based trackers. Previously tracker was taking 3 seconds on average to converge within 100 cms of true range. Now it is only taking a fraction of the first second. Similar is the case for Constant-Jerk model based trackers as shown in Figure [5.9]

.

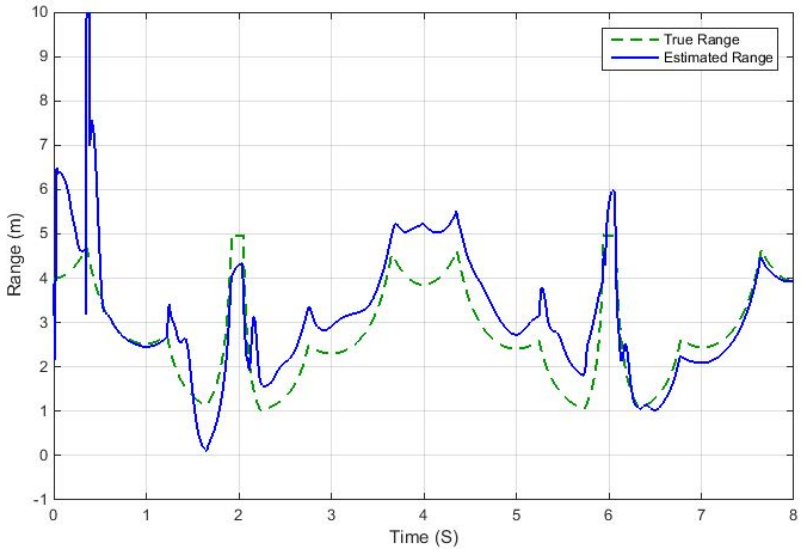

(a) Estimated Range Comparison

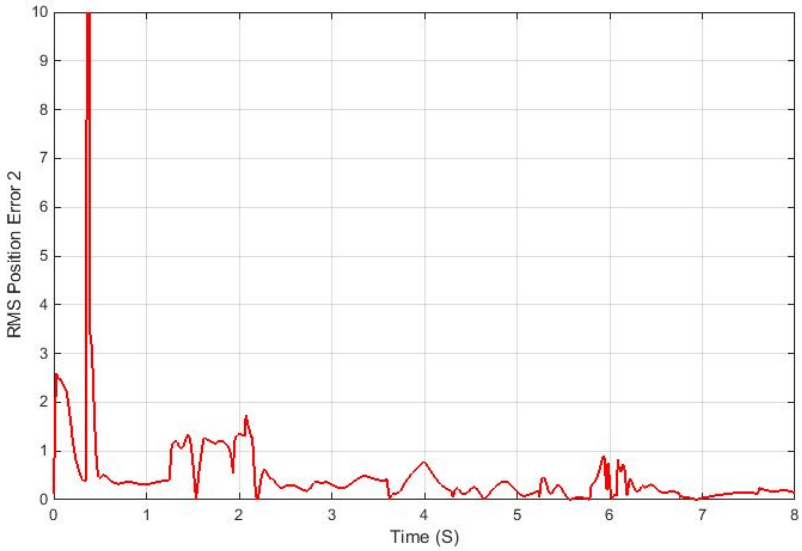

(b) RMS Position Error

Figure 5.8: Errors Comparisons for 100 MC runs of a randomly moving worker using Tracker-1 (Section-4.3.1) with Initialization

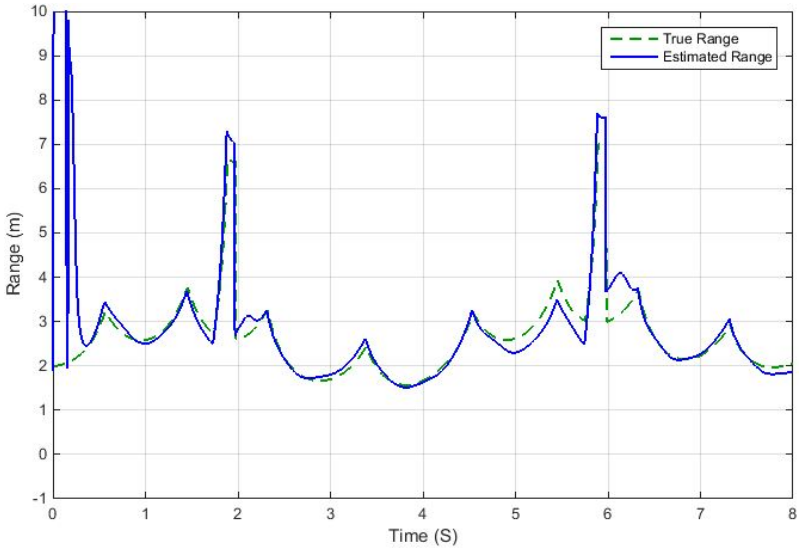

(a) Estimated Range Comparison

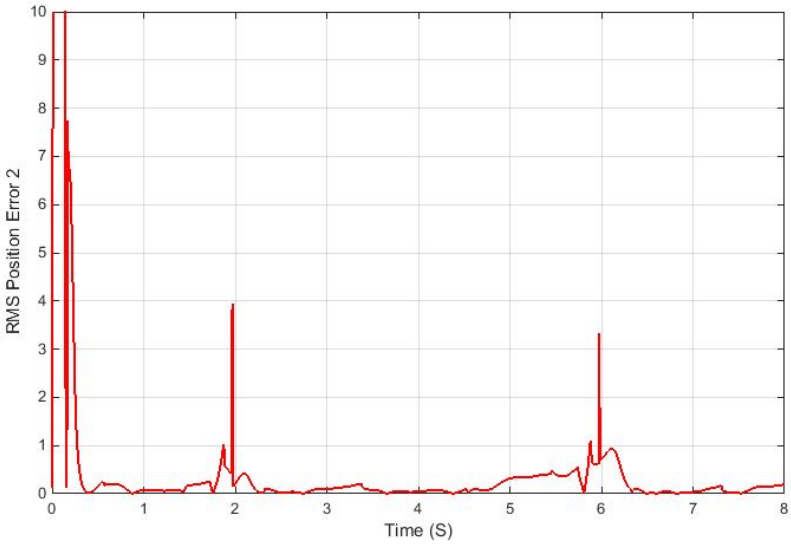

(b) RMS Position Error

Figure 5.9: Errors Comparisons for 100 MC runs of a randomly moving worker using Tracker-2 (Section-4.3.2) with Initialization

Chapter 6
Conclusions

6.1 Summary of Results

THIS thesis has addressed the problem of improving the safety of workers in unsafe work environments such as construction and mining. By looking at all the requirements and constraints, we noted the significant weight of the safety gear already worn by workers. This means any new safety proposal needs be innovative in adding only negligible weight to a workers uniform, having low power consumption and being robust under harsh treatment. We addressed these issues by proposing the design of a smart helmet for workers using cheap radars.

To this end, we have proposed the idea of using CW Doppler radars for sensing the environment. With advancement in technology and microelectronics, CW radars are available for a couple of dollars off the shelf. As mentioned earlier, a Doppler radar can only provide relative radial velocity information of targets. So, the first issue to tackle was figuring out if the range is observable from Doppler measurements or not. While working on this issue we realized that environment sensing is the same problem faced by the drone community in designing its navigation system.

For the target to be observable with either or both bearing and frequency measurements, LOS angle between the observer and the target must not remain constant. And with frequency-only measurements, the range is observable if and only if the dynamics order of the observers motion is of two or more degrees higher than the targets motion.

To verify this observability analysis, we designed an estimation framework using Kalman filters with nonlinear frequency and bearing measurements. Simulation results

verified that RMS range and velocity errors decreased with each 900 maneuvers that the observer made. However, such sudden maneuvers are not practical in real life with drones or UAVs. Therefore, we suggested the idea of circular motion by the observer, as all observability conditions are met with such motion. Simulation results further verified this and range estimates converged to actual values within a couple of the observers rotations. Unscented Kalman filters consistently performed better in terms of lower RMS errors and fewer divergent tracks. Then we extended our idea from localizing single point-like targets to detecting walls and doors of a room. Our assumption was that the radar would be fixed on a drone flying in a pattern, attempting to localize the surroundings so it can find its way. To this end, we showed that if a drone/UAV, equipped with a simple CW radar, flies in a circle within a closed room it can accurately localize surrounding walls. One main difference between localizing targets with drones and with workers is that, while a drone can move in any pattern, we cannot ask a worker to move in a pattern to localize his surroundings. To tackle this issue, we developed the idea of obtaining frequency measurements from rate of change of phase of reflected radar waves. This way even if person is stationary at a point, the radar can simply sweep the room, measure rate of phase change and calculate frequency. We presented the design of a smart helmet based on this idea using CW radars and phased array antennas with its antenna-elements around the hats brim. This way a worker wearing the smart helmet would not have to move around, and using a rotating beam we could obtain frequency and bearing measurements of surrounding targets. We designed various simulations with filters of varying model complexities and results showed that we can successfully localize walls within a few cm of the actual location.

One of the main research questions in using CW radars on helmets was how random human head movements would affect estimation results. We showed in our research and simulations that random human head movements and walking do not pose much threat to estimation accuracy, as they could easily be handled through added noise in the system. This is because the range and distances under consideration are quite small compared to the velocity of EM waves. These can leave the radar and return after reflection before a person can move significantly.

Kalman filter based algorithms are recursive and need a good starting point to initialize the system. Since our system is highly non-linear, initializations significantly effect the estimations results. Poor and improper initializations also lead to filter divergence. In our work, we introduced the idea of placing two CW radars, side by side, and showed how we can leverage the power of returned waveform to estimate initial target range. Simulations further showed that this methodology decreased the filter convergence time significantly.

6.2 Future Research Direction

The design of a smart helmet consists of two parts. The first is understanding the environment and localizing targets around the user. The second is updating the user by providing feedback about the location and nature of events. In this thesis, we have tackled the first issue. One important research direction is to figure out ways to provide feedback to the inattentive worker. Should this be audial or visual? One idea is to sound a beep in either ear depending on the location of the target, but only if it approaches at high speed or if the worker himself is about to hit an obstacle. How to alarm the worker in such a way that the beep appears to come from the actual geospatial location of the target is itself an interesting research problem.

If only a single target is present in the environment it can be localized based on delay measurements at receivers. However, the radars accuracy in indoor environments is effected by reflections (multi-path) from multiple moving targets. In some cases, a direct path between the radar and the target might be blocked, but an indirect path arising from multiple propagations and reflections might be available. If a targets directional information is available this problem becomes easier. In this case, multiple targets can be separated based on their associated angle information. A plethora of research has been done on this multi target separation issue, producing many useful algorithms. An important research issue is to tackle this in our smart helmet use case. We have proposed a system utilizing phased array antennas around the helmets brim. Then a targets angle is the direction in which the antennas beam is directed. This information needs to

be further investigated to differentiate between direct and indirect path reflection and separating multiple targets.

The ambition to build an autonomous car, seamlessly guiding itself towards its destination, has inspired the automotive industry for decades. The progress in millimeter wave semiconductor technology along with sophisticated waveform designs and signal processing techniques have led to many breakthroughs in the last few years. Now self driving cars use a multitude of sensors like radars, lidars, cameras, GPS, Ultrasound, etc. to implement Advance Driving Assistance Systems (ADAS). An ADAS can increase drivers capabilities in many ways, including assisting in parking, generating cross traffic alerts, lane changing alerts, blind spot detections and rear collision warnings. Radars are being used for estimating range, velocity and direction of moving objects. Over time the automotive industry has developed solutions based mostly on Pulsed Continuous Wave or Frequency Modulated Continuous Wave (FMCW) radars. Although range observability is not an issue with these radars, they have complex mathematics which require more processing power as well as sophisticated waveform designs to obtain range-velocity profiles. When we started this research, integrated FMCW radar chips were not available. However, with high demand from the automotive industry these chips have started to appear in the last 1-2 years. Compared to humans, cars can carry more weight and have stronger batteries that can easily run powerful computer processors to implement mathematics required for FMCW radars. But in our safety and drones case, we are limited by the radars weight, the power required and the harsh treatment it has to withstand. Although FMCW radars chips now available on the market can provide much accurate range and velocity information, they are also expensive, require more processing power and have waveform design issues. One important research area is to check the feasibility of mounting these new FMCW radar chips on a workers helmet. Ultimately, we must compare the two competing radar technologies (CW and FMCW) to figure out which is better suited for drones and helmets: the expensive and sophisticated FMCW radar, which would avoid observability issues, or the cheaper and simpler CW radar, with its observability difficulties. The problem is designing a radar that is optimized to our particular workers safety use case: i.e. a light weight, single chip, low power radar, using

fewer computations and having a special waveforms library optimized for indoor measurements.

Another interesting future research direction would be to create an Internet-of-Helmets and connect it with a central database which updates the map of the construction site in real time. Supervisors could view the location of each worker and/or machine to manage them properly. By capturing the relative positive of each radar in the network, the central database could run sophisticated and more powerful Machine Learning and Graph algorithms to analyze this network, predicting accidents and threats.

Bibliography

[1] "Safe work australia annual report 2015-16," Safe Work Australia, Statistical report, 2016. [Online]. Available: http://www.safeworkaustralia.gov.au/sites/swa/about/publications/pages/annual-report-2015-16

[2] H. Liu, H. Darabi, P. Banerjee, and J. Liu, "Survey of wireless indoor positioning techniques and systems," *IEEE Transactions on Systems, Man, and Cybernetics, Part C (Applications and Reviews)*, vol. 37, no. 6, pp. 1067–1080, Nov 2007.

[3] G. Deak, K. Curran, and J. Condell, "A survey of active and passive indoor localisation systems," *Computer Communications*, vol. 35, no. 16, pp. 1939 – 1954, 2012. [Online]. Available: http://www.sciencedirect.com/science/article/pii/S014036641200196X

[4] J. Hightower, R. Want, and G. Borriello, "Spoton: An indoor 3d location sensing technology based on rf signal strength," *UW CSE 00-02-02,*, 2000. [Online]. Available: http://seattle.intel-research.net/people/hightower/pubs/hightower2000indoor/hightower2000indoor.pdf

[5] L. M. Ni, Y. Liu, Y. C. Lau, and A. P. Patil, "Landmarc: indoor location sensing using active rfid," pp. 407–415, March 2003.

[6] P. Steggles and S. Gschwind, "The ubisense smart space platform."

[7] P. Bahl and V. N. Padmanabhan, "Radar: an in-building rf-based user location and tracking system," in *Proceedings IEEE INFOCOM 2000. Conference on Computer Communications. Nineteenth Annual Joint Conference of the IEEE Computer and Communications Societies (Cat. No.00CH37064)*, vol. 2, 2000, pp. 775–784 vol.2.

[8] V. Bahl and V. Padmanabhan, "Enhancements to the radar user location and tracking system," Tech. Rep., February 2000. [Online]. Available: https://www.microsoft.com/en-us/research/publication/enhancements-to-the-radar-user-location-and-tracking-system/

[9] M. A. Youssef, A. Agrawala, and A. U. Shankar, "Wlan location determination via clustering and probability distributions," in *Proceedings of the First IEEE International Conference on Pervasive Computing and Communications*, ser. PERCOM '03. Washington, DC, USA: IEEE Computer Society, 2003, pp. 143–. [Online]. Available: http://dl.acm.org/citation.cfm?id=826025.826335

[10] T. Roos, P. Myllymäki, H. Tirri, P. Misikangas, and J. Sievänen, "A probabilistic approach to wlan user location estimation," *International Journal of Wireless Information Networks*, vol. 9, no. 3, pp. 155–164, Jul 2002. [Online]. Available: https://doi.org/10.1023/A:1016003126882

[11] "Ekahau positioning engine." [Online]. Available: https://www.ekahau.com/

[12] L. Ma, Z. Zhang, and X. Tan, "A novel through-wall imaging method using ultra wideband pulse system," in *2006 International Conference on Intelligent Information Hiding and Multimedia*, Dec 2006, pp. 147–150.

[13] L.-P. Song, C. Yu, and Q. H. Liu, "Through-wall imaging (twi) by radar: 2-d tomographic results and analyses," *IEEE Transactions on Geoscience and Remote Sensing*, vol. 43, no. 12, pp. 2793–2798, Dec 2005.

[14] Y. K. Cho, J. H. Youn, and D. Martinez, "Error modeling for an untethered ultra-wideband system for construction indoor asset tracking," *Automation in Construction*, vol. 19, no. 1, pp. 43 – 54, 2010. [Online]. Available: http://www.sciencedirect.com/science/article/pii/S0926580509001253

[15] R. Zetik, J. Sachs, and R. Thoma, "Uwb localization - active and passive approach [ultra wideband radar]," in *Instrumentation and Measurement Technology Conference, 2004. IMTC 04. Proceedings of the 21st IEEE*, vol. 2, 2004, pp. 1005–1009 Vol.2.

[16] M. V. Jochen Teizer and A. Walia, "Ultrawideband for automated real-time three-dimensional location sensing for workforce, equipment, and material positioning and tracking," vol. 2081, pp. 56–64, 2008.

[17] T. Cheng, M. Venugopal, J. Teizer, and P. Vela, "Performance evaluation of ultra wideband technology for construction resource location tracking in harsh environments," *Automation in Construction*, vol. 20, no. 8, pp. 1173 – 1184, 2011. [Online]. Available: http://www.sciencedirect.com/science/article/pii/S0926580511000732

[18] "Place lab, a privacy-observant location system," 2011. [Online]. Available: http://placelab.org

[19] "Wifi based rtls aeroscout," 2011. [Online]. Available: http://www.aeroscout.com

[20] S. Woo, S. Jeong, E. Mok, L. Xia, C. Choi, M. Pyeon, and J. Heo, "Application of wifi-based indoor positioning system for labor tracking at construction sites: A case study in guangzhou {MTR}," *Automation in Construction*, vol. 20, no. 1, pp. 3 – 13, 2011, ¡ce:title¿Global convergence in construction¡/ce:title¿. [Online]. Available: http://www.sciencedirect.com/science/article/pii/S092658051000107X

[21] A. Carbonari, A. Giretti, and B. Naticchia, "A proactive system for real-time safety management in construction sites," *Automation in Construction*, vol. 20, no. 6, pp. 686 – 698, 2011, ¡ce:title¿Selected papers from the 26th {ISARC} 2009¡/ce:title¿. [Online]. Available: http://www.sciencedirect.com/science/article/pii/S0926580511000756

[22] M. Addlesee, R. Curwen, S. Hodges, J. Newman, P. Steggles, A. Ward, and A. Hopper, "Implementing a sentient computing system," *Computer*, vol. 34, no. 8, pp. 50–56, Aug 2001.

[23] S. Chae and T. Yoshida, "Application of rfid technology to prevention of collision accident with heavy equipment," *Automation in Construction*, vol. 19, no. 3, pp. 368 – 374, 2010, ¡ce:title¿25th International Symposium

on Automation and Robotics in Construction¡/ce:title¿. [Online]. Available: http://www.sciencedirect.com/science/article/pii/S0926580509001976

[24] H. Yang, D. A. Chew, W. Wu, Z. Zhou, and Q. Li, "Design and implementation of an identification system in construction site safety for proactive accident prevention," *Accident Analysis & Prevention*, vol. 48, no. 0, pp. 193 – 203, 2012, ¡ce:title¿Intelligent Speed Adaptation + Construction Projects¡/ce:title¿. [Online]. Available: http://www.sciencedirect.com/science/article/pii/S0001457511001837

[25] J. Teizer, B. S. Allread, C. E. Fullerton, and J. Hinze, "Autonomous pro-active real-time construction worker and equipment operator proximity safety alert system," *Automation in Construction*, vol. 19, no. 5, pp. 630 – 640, 2010, ¡ce:title¿Building Information Modeling and Collaborative Working Environments¡/ce:title¿. [Online]. Available: http://www.sciencedirect.com/science/article/pii/S0926580510000361

[26] W. Wu, A. G. Gibb, and Q. Li, "Accident precursors and near misses on construction sites: An investigative tool to derive information from accident databases," *Safety Science*, vol. 48, no. 7, pp. 845 – 858, 2010. [Online]. Available: http://www.sciencedirect.com/science/article/pii/S0925753510001098

[27] W. Wu, H. Yang, D. A. Chew, S. hua Yang, A. G. Gibb, and Q. Li, "Towards an autonomous real-time tracking system of near-miss accidents on construction sites," *Automation in Construction*, vol. 19, no. 2, pp. 134 – 141, 2010. [Online]. Available: http://www.sciencedirect.com/science/article/pii/S0926580509001873

[28] W. Lu, G. Q. Huang, and H. Li, "Scenarios for applying rfid technology in construction project management," *Automation in Construction*, vol. 20, no. 2, pp. 101 – 106, 2011, ¡ce:title¿Building Information Modeling and Changing Construction Practices¡/ce:title¿. [Online]. Available: http://www.sciencedirect.com/science/article/pii/S0926580510001366

[29] R. Bostelman, J. Teizer, S. J. Ray, M. Agronin, and D. Albanese, "Methods for improving visibility measurement standards of powered industrial vehicles," *Safety Science*, vol. 62, no. 0, pp. 257 – 270, 2014. [Online]. Available: http://www.sciencedirect.com/science/article/pii/S092575351300204X

[30] S. J. Ray and J. Teizer, "Computing 3d blind spots of construction equipment: Implementation and evaluation of an automated measurement and visualization method utilizing range point cloud data," *Automation in Construction*, vol. 36, no. 0, pp. 95 – 107, 2013. [Online]. Available: http://www.sciencedirect.com/science/article/pii/S0926580513001210

[31] J. Teizer, B. S. Allread, and U. Mantripragada, "Automating the blind spot measurement of construction equipment," *Automation in Construction*, vol. 19, no. 4, pp. 491 – 501, 2010, ¡ce:title¿Building information modeling and interoperability¡/ce:title¿. [Online]. Available: http://www.sciencedirect.com/science/article/pii/S0926580509002015

[32] E. Trucco and A. Kaka, "A framework for automatic progress assessment on construction sites using computer vision," vol. 2, no. 2, pp. 147–164, 2004.

[33] Y. M. Ibrahim, T. C. Lukins, X. Zhang, E. Trucco, and A. P. Kaka, "Towards automated progress assessment of workpackage components in construction projects using computer vision," *Adv. Eng. Inform.*, vol. 23, no. 1, pp. 93–103, Jan. 2009. [Online]. Available: http://dx.doi.org/10.1016/j.aei.2008.07.002

[34] S. S. Mani Golparvar-Fard and F. Pea-Mora, "Interactive visual construction progress monitoring with d4 ar - 4d augmented reality - models," pp. 41–50, 2009.

[35] M. Golparvar-Fard, J. Bohn, J. Teizer, S. Savarese, and F. Pea-Mora, "Evaluation of image-based modeling and laser scanning accuracy for emerging automated performance monitoring techniques," *Automation in Construction*, vol. 20, no. 8, pp. 1143 – 1155, 2011. [Online]. Available: http://www.sciencedirect.com/science/article/pii/S0926580511000707

[36] C. Kim, B. Kim, and H. Kim, "4d cad model updating using image processing-based construction progress monitoring," *Automation in Construction*, vol. 35, no. 0, pp. 44 – 52, 2013. [Online]. Available: http://www.sciencedirect.com/science/article/pii/S0926580513000332

[37] C. Kim, H. Son, and C. Kim, "Automated construction progress measurement using a 4d building information model and 3d data," *Automation in Construction*, vol. 31, no. 0, pp. 75 – 82, 2013. [Online]. Available: http://www.sciencedirect.com/science/article/pii/S0926580512002361

[38] J. Yang, T. Cheng, J. Teizer, P. Vela, and Z. Shi, "A performance evaluation of vision and radio frequency tracking methods for interacting workforce," *Advanced Engineering Informatics*, vol. 25, no. 4, pp. 736 – 747, 2011, ¡ce:title¿Special Section: Advances and Challenges in Computing in Civil and Building Engineering¡/ce:title¿. [Online]. Available: http://www.sciencedirect.com/science/article/pii/S1474034611000309

[39] M. Memarzadeh, M. Golparvar-Fard, and J. C. Niebles, "Automated 2d detection of construction equipment and workers from site video streams using histograms of oriented gradients and colors," *Automation in Construction*, vol. 32, no. 0, pp. 24 – 37, 2013. [Online]. Available: http://www.sciencedirect.com/science/article/pii/S0926580512002403

[40] M.-W. Park and I. Brilakis, "Construction worker detection in video frames for initializing vision trackers," *Automation in Construction*, vol. 28, no. 0, pp. 15 – 25, 2012. [Online]. Available: http://www.sciencedirect.com/science/article/pii/S0926580512001136

[41] S. Han and S. Lee, "A vision-based motion capture and recognition framework for behavior-based safety management," *Automation in Construction*, vol. 35, no. 0, pp. 131 – 141, 2013. [Online]. Available: http://www.sciencedirect.com/science/article/pii/S0926580513000514

[42] A. Peddi, L. Huan, Y. Bai, and S. Kim, *Development of Human Pose Analyzing Algorithms for the Determination of Construction Productivity in Real-Time*, ch. 1, pp. 11–20. [Online]. Available: http://ascelibrary.org/doi/abs/10.1061/41020%28339%292

[43] J. Gong and C. Caldas, *Learning and Classifying Motions of Construction Workers and Equipment Using Bag of Video Feature Words and Bayesian Learning Methods*, ch. 34, pp. 274–281. [Online]. Available: http://ascelibrary.org/doi/abs/10.1061/41182%28416%2934

[44] Y. Li and C. Liu, "Integrating field data and 3d simulation for tower crane activity monitoring and alarming," *Automation in Construction*, vol. 27, no. 0, pp. 111 – 119, 2012. [Online]. Available: http://www.sciencedirect.com/science/article/pii/S092658051200074X

[45] S. Davies, "Watching out for the workers [safety workstations]," *Manufacturing, IET*, vol. 86, no. 4, pp. 32–34, 2007.

[46] R. Cucchiara, A. Prati, and R. Vezzani, "A multi-camera vision system for fall detection and alarm generation," *Expert Systems*, vol. 24, no. 5, pp. 334–345, 2007. [Online]. Available: http://dx.doi.org/10.1111/j.1468-0394.2007.00438.x

[47] S. J. Ray and J. Teizer, "Real-time construction worker posture analysis for ergonomics training," *Advanced Engineering Informatics*, vol. 26, no. 2, pp. 439 – 455, 2012, ¡ce:title¿Knowledge based engineering to support complex product design¡/ce:title¿. [Online]. Available: http://www.sciencedirect.com/science/article/pii/S1474034612000183

[48] J. Yang, O. Arif, P. Vela, J. Teizer, and Z. Shi, "Tracking multiple workers on construction sites using video cameras," *Advanced Engineering Informatics*, vol. 24, no. 4, pp. 428 – 434, 2010, ¡ce:title¿Construction Informatics¡/ce:title¿. [Online]. Available: http://www.sciencedirect.com/science/article/pii/S1474034610000522

[49] J. Teizer and P. Vela, "Personnel tracking on construction sites using video cameras," *Advanced Engineering Informatics*, vol. 23, no. 4, pp. 452 – 462,

2009, ¡ce:title¿Civil Engineering Informatics¡/ce:title¿. [Online]. Available: http://www.sciencedirect.com/science/article/pii/S147403460900038X

[50] K. M. T. K. M. Sulankivi, Kristiina; Khknen, "4d-bim for construction safety planning," 2010. [Online]. Available: http://www.cib2010.org/post/files/papers/1167.pdf

[51] K. K. K. M. T. M. M.-L. Kiviniemi, Markku; Sulankivi, "Bim-based safety management and communication for building construction," 2011. [Online]. Available: http://www.vtt.fi/inf/pdf/tiedotteet/2011/T2597.pdf

[52] B. Mayton, G. Dublon, S. Palacios, and J. Paradiso, "Truss: Tracking risk with ubiquitous smart sensing," in *Sensors, 2012 IEEE*, 2012, pp. 1–4.

[53] S. Corbellini, F. Ferraris, and M. Parvis, "A system for monitoring workers' safety in an unhealthy environment by means of wearable sensors," in *Instrumentation and Measurement Technology Conference Proceedings, 2008. IMTC 2008. IEEE*, 2008, pp. 951–955.

[54] U.-K. Lee, J.-H. Kim, H. Cho, and K.-I. Kang, "Development of a mobile safety monitoring system for construction sites," *Automation in Construction*, vol. 18, no. 3, pp. 258 – 264, 2009. [Online]. Available: http://www.sciencedirect.com/science/article/pii/S0926580508001441

[55] P. Lukowicz, J. Ward, H. Junker, M. Stger, G. Trster, A. Atrash, and T. Starner, "Recognizing workshop activity using body worn microphones and accelerometers," vol. 3001, pp. 18–32, 2004. [Online]. Available: http://dx.doi.org/10.1007/978-3-540-24646-6_2

[56] J. Ward, P. Lukowicz, G. Troster, and T. Starner, "Activity recognition of assembly tasks using body-worn microphones and accelerometers," *Pattern Analysis and Machine Intelligence, IEEE Transactions on*, vol. 28, no. 10, pp. 1553–1567, 2006.

[57] D. Hudgens and J. McDermott, "Construction hard hat having electronic circuitry," Sep. 22 2009, uS Patent 7,592,911. [Online]. Available: http://www.google.sc/patents/US7592911

[58] C. Qiang, S. Ji-ping, Z. Zhe, and Z. Fan, "Zigbee based intelligent helmet for coal miners," in *Computer Science and Information Engineering, 2009 WRI World Congress on*, vol. 3, 2009, pp. 433–435.

[59] S. Barro-Torres, T. M. Fernndez-Carams, H. J. Prez-Iglesias, and C. J. Escudero, "Real-time personal protective equipment monitoring system," *Computer Communications*, vol. 36, no. 1, pp. 42 – 50, 2012. [Online]. Available: http://www.sciencedirect.com/science/article/pii/S0140366412000060

[60] R.-J. Dzeng, Y.-C. Fang, and I.-C. Chen, "A feasibility study of using smartphone built-in accelerometers to detect fall portents," *Automation in Construction*, vol. 38, no. 0, pp. 74 – 86, 2014. [Online]. Available: http://www.sciencedirect.com/science/article/pii/S0926580513002070

[61] D. Torrent and C. Caldas, "Methodology for automating the identification and localization of construction components on industrial projects," *Journal of Computing in Civil Engineering*, vol. 23, no. 1, pp. 3–13, 2009. [Online]. Available: http://ascelibrary.org/doi/abs/10.1061/%28ASCE%290887-3801%282009%2923%3A1%283%29

[62] S. N. Razavi and C. T. Haas, "Multisensor data fusion for on-site materials tracking in construction," *Automation in Construction*, vol. 19, no. 8, pp. 1037 – 1046, 2010, ¡ce:title¿The role of {VR} and {BIM} to manage the construction and design processes¡/ce:title¿. [Online]. Available: http://www.sciencedirect.com/science/article/pii/S0926580510001159

[63] M.-W. Park, A. Makhmalbaf, and I. Brilakis, "Comparative study of vision tracking methods for tracking of construction site resources," *Automation in Construction*, vol. 20, no. 7, pp. 905 – 915, 2011. [Online]. Available: http://www.sciencedirect.com/science/article/pii/S0926580511000343

[64] A. Shahi, J. S. West, and C. T. Haas, "Onsite 3d marking for construction activity tracking," *Automation in Construction*, vol. 30, no. 0, pp. 136 – 143, 2013. [Online]. Available: http://www.sciencedirect.com/science/article/pii/S0926580512002221

[65] A. H. Behzadan, Z. Aziz, C. J. Anumba, and V. R. Kamat, "Ubiquitous location tracking for context-specific information delivery on construction sites," *Automation in Construction*, vol. 17, no. 6, pp. 737 – 748, 2008. [Online]. Available: http://www.sciencedirect.com/science/article/pii/S0926580508000186

[66] V. Hinkka and J. Ttil, "Rfid tracking implementation model for the technical trade and construction supply chains," *Automation in Construction*, vol. 35, no. 0, pp. 405 – 414, 2013. [Online]. Available: http://www.sciencedirect.com/science/article/pii/S0926580513000915

[67] R. Maalek and F. Sadeghpour, "Accuracy assessment of ultra-wide band technology in tracking static resources in indoor construction scenarios," *Automation in Construction*, vol. 30, no. 0, pp. 170 – 183, 2013. [Online]. Available: http://www.sciencedirect.com/science/article/pii/S0926580512001720

[68] S. M. Kay, *Fundamentals of Statistical Signal Processing: Estimation Theory*, ser. Prentice Hall Signal Processing Series. Upper Saddle River, NJ, USA: Prentice-Hall, Inc., 1993.

[69] S. Blackman and R. Popoli, *Design and Analysis of Modern Tracking Systems*, ser. Artech House radar library. Artech House, 1999. [Online]. Available: https://books.google.com.au/books?id=lTIfAQAAIAAJ

[70] Y. Bar-Shalom, X. Li, and T. Kirubarajan, *Estimation with Applications to Tracking and Navigation: Theory Algorithms and Software*. Wiley, 2004. [Online]. Available: https://books.google.com.au/books?id=xz9nQ4wdXG4C

[71] R. E. Kalman and R. S. Bucy, "New results in linear filtering and prediction theory," *Trans. ASME, Ser. D, J. Basic Eng*, p. 109, 1961.

[72] S. J. Julier, J. K. Uhlmann, and H. F. Durrant-Whyte, "A new approach for filtering nonlinear systems," in *American Control Conference, Proceedings of the 1995*, vol. 3, Jun 1995, pp. 1628–1632 vol.3.

[73] S. J. Julier and J. K. Uhlmann, "Unscented filtering and nonlinear estimation," *Proceedings of the IEEE*, vol. 92, no. 3, pp. 401–422, Mar 2004.

[74] I. Arasaratnam and S. Haykin, "Square-root quadrature kalman filtering," *IEEE Transactions on Signal Processing*, vol. 56, no. 6, pp. 2589–2593, 2008.

[75] ——, "Cubature kalman filters," *IEEE Transactions on Automatic Control*, vol. 54, no. 6, pp. 1254–1269, June 2009.

[76] M. S. Arulampalam, S. Maskell, N. Gordon, and T. Clapp, "A tutorial on particle filters for online nonlinear/non-gaussian bayesian tracking," *IEEE Transactions on Signal Processing*, vol. 50, no. 2, pp. 174–188, Feb 2002.

[77] R. E. Kalman, "A new approach to linear filtering and prediction problems," *Transactions of the ASME–Journal of Basic Engineering*, vol. 82, no. Series D, pp. 35–45, 1960.

[78] R. Kalman, *Lectures on Controllability and Observability*. Berlin, Heidelberg: Springer Berlin Heidelberg, 2011, pp. 1–149. [Online]. Available: http://dx.doi.org/10.1007/978-3-642-11063-4_1

[79] M. S. Grewal, *Kalman Filtering: Theory and Practice Using MATLAB*. Hoboken, New Jersey: John Wiley & Sons, Inc, 2014. [Online]. Available: http://au.wiley.com/WileyCDA/WileyTitle/productCd-1118851218.html

[80] T. Kailath, *Linear Systems*, ser. Information and System Sciences Series. Prentice-Hall, 1980. [Online]. Available: https://books.google.com.au/books?id=ggYqAQAAMAAJ

[81] S. C. Nardone and V. J. Aidala, "Observability criteria for bearings-only target motion analysis," *IEEE Transactions on Aerospace and Electronic Systems*, vol. AES-17, no. 2, pp. 162–166, March 1981.

[82] S. E. Hammel and V. J. Aidala, "Observability requirements for three-dimensional tracking via angle measurements," *IEEE Transactions on Aerospace and Electronic Systems*, vol. AES-21, no. 2, pp. 200–207, March 1985.

[83] E. Fogel and M. Gavish, "Nth-order dynamics target observability from angle measurements," *IEEE Transactions on Aerospace and Electronic Systems*, vol. 24, no. 3, pp. 305–308, May 1988.

[84] K. Becker, "Simple linear theory approach to TMA observability," *IEEE Transactions on Aerospace and Electronic Systems*, vol. 29, no. 2, pp. 575–578, Apr 1993.

[85] ——, "A general approach to TMA observability from angle and frequency measurements," *IEEE Transactions on Aerospace and Electronic Systems*, vol. 32, no. 1, pp. 487–494, Jan 1996.

[86] A. N. Payne, "Observability problem for bearings-only tracking," *International Journal of Control*, vol. 49, no. 3, pp. 761–768, 1989. [Online]. Available: http://www.tandfonline.com/doi/abs/10.1080/00207178908559665

[87] C. Jauffret and D. Pillon, *New Observability Criterion in Target Motion Analysis*. Dordrecht: Springer Netherlands, 1989, pp. 479–484. [Online]. Available: http://dx.doi.org/10.1007/978-94-009-2289-1_53

[88] M. J. Shensa, "On the uniqueness of doppler tracking," *The Journal of the Acoustical Society of America*, vol. 70, no. 4, pp. 1062–1064, 1981. [Online]. Available: http://scitation.aip.org/content/asa/journal/jasa/70/4/10.1121/1.386550

[89] J. M. Passerieux, D. Pillon, P. Blanc-Benon, and C. Jaufret, "Target motion analysis with bearings and frequencies measurements," in *Signals, Systems and Computers, 1988. Twenty-Second Asilomar Conference on*, vol. 1, 1988, pp. 458–462.

[90] M. Skolnik, *Introduction to Radar Systems*, ser. Electrical engineering series. McGraw-Hill, 2001. [Online]. Available: https://books.google.com.au/books?id=Y6-APwAACAAJ

[91] S. Arulampalam, "A comparison of recursive style angle-only target motion analysis algorithms," DSTO Electronics and Surveillance Research Laboratory Salisbury, S. Aust, Book, Online, 2000. [Online]. Available: http://www.dsto.defence.gov.au/corporate/reports/DSTO-TR-0917.pdfhttp://www.dsto.defence.gov.au

[92] X. R. Li and V. P. Jilkov, "Survey of maneuvering target tracking. part i. dynamic models," *IEEE Transactions on Aerospace and Electronic Systems*, vol. 39, no. 4, pp. 1333–1364, Oct 2003.

[93] B. Ristic, S. Arulampalm, and N. Gordon, *Beyond the Kalman filter : particle filters for tracking applications*. Artech House Boston, Ma. ; London, 2004.

[94] B. Ristic, S. Arulampalam, and J. McCarthy, "Target motion analysis using range-only measurements: algorithms, performance and application to {ISAR} data," *Signal Processing*, vol. 82, no. 2, pp. 273 – 296, 2002. [Online]. Available: http://www.sciencedirect.com/science/article/pii/S0165168401001876

[95] B. Ristic and M. Arulampalam, "Tracking a manoeuvring target using angle-only measurements: algorithms and performance," *Signal Processing*, vol. 83, no. 6, pp. 1223 – 1238, 2003. [Online]. Available: http://www.sciencedirect.com/science/article/pii/S0165168403000422

[96] D. Laneuville, "Polar versus cartesian velocity models for maneuvering target tracking with imm," in *Aerospace Conference, 2013 IEEE*, March 2013, pp. 1–15.

[97] M. Roth, G. Hendeby, and F. Gustafsson, "Ekf/ukf maneuvering target tracking using coordinated turn models with polar/cartesian velocity," in *Information Fusion (FUSION), 2014 17th International Conference on*, July 2014, pp. 1–8.

[98] K. Mehrotra and P. R. Mahapatra, "A jerk model for tracking highly maneuvering targets," *IEEE Transactions on Aerospace and Electronic Systems*, vol. 33, no. 4, pp. 1094–1105, Oct 1997.

[99] P. R. Mahapatra and K. Mehrotra, "Mixed coordinate tracking of generalized maneuvering targets using acceleration and jerk models," *IEEE Transactions on Aerospace and Electronic Systems*, vol. 36, no. 3, pp. 992–1000, Jul 2000.

[100] *Occupational Health and Safety Regulations*, WorkSafe Victoria, 2017. [Online]. Available: https://www.worksafe.vic.gov.au/news/notices/ohs-regulations-reform-2017

[101] *Model Code of Practice for Construction Work*, Safe Work Australia, 2013. [Online]. Available: https://www.safeworkaustralia.gov.au/construction#model-codes-of-practice

[102] *Model Work Health and Safety Regulations*, Safe Work Australia, 2016. [Online]. Available: https://www.safeworkaustralia.gov.au/doc/model-work-health-and-safety-regulations

[103] *Working Safely In The General Construction Industry - A Handbook For The Construction Regulations*, Work Safe Victoria, July 2014. [Online]. Available: http://www.worksafe.vic.gov.au/pages/forms-and-publications/forms-and-publications/